

รายงานการวิจัยฉบับสมบูรณ์

“Development of Ni-W-B alloy composite coatings with high hardness and
good wear resistance”

จัดทำโดย

Dr.Jiaqian Qin	หัวหน้าโครงการ
Assoc. Prof. Dr.Yuttanant Boonyongmaneerat	นักวิจัย
Dr.Sarintorn Limpanart	นักวิจัย
Mr.Adisak Thueploy	นักวิจัย
Mr.Jumpot Wanichsampan	นักวิจัย

บทคัดย่อและแฟ้มข้อมูลฉบับเต็มของวิทยานิพนธ์ตั้งแต่ปีการศึกษา 2554 ที่ให้บริการในคลังปัญญาจุฬาฯ (CUIR)

เป็นแฟ้มข้อมูลของนิสิตเจ้าของวิทยานิพนธ์ที่ส่งผ่านทางบัณฑิตวิทยาลัย

The abstract and full text of theses from the academic year 2011 in Chulalongkorn University Intellectual Repository(CUIR)
are the thesis authors' files submitted through the Graduate School.

Development of Ni-W-B alloy composite coatings with high hardness and good wear resistance

รายงานการวิจัยฉบับสมบูรณ์

รายงานช่วงระยะเวลาตั้งแต่วันที่ 1 October 2558 ถึงวันที่ 30 September 2559

ชื่อหัวหน้าโครงการ Dr. Jiaqian Qin

ผู้ร่วมโครงการ Assoc. Prof. Dr. Yuttanant Boonyongmaneerat

Dr. Sarintorn Limpanart

Mr. Adisak Thueploy

Mr. Jumpot Warinchsampan

หน่วยงาน สถาบันวิจัยโลหะและวัสดุ จุฬาลงกรณ์มหาวิทยาลัย

1. การดำเนินงาน : ได้ดำเนินงานตามแผนงานที่ได้วางไว้ทุกประการ

ได้ปรับเปลี่ยนแผนงานที่ได้วางไว้ดังนี้ คือ

โครงการวิจัยนี้ มีแผนงานวิจัย และความก้าวหน้าของการดำเนินงาน ดังแสดงในตารางที่ 1

ตารางที่ 1 แผนงานวิจัย และความก้าวหน้าของการดำเนินโครงการ

กิจกรรม	ปีที่ 1												
	ต.ค. 58	พ.ย. 58	ธ.ค. 58	ม.ค. 59	ก.พ. 59	มี.ค. 59	เม.ย. 59	พ.ค. 59	มิ.ย. 59	ก.ค. 59	ส.ค. 59	ก.ย. 59	
1) literature searching, experimental design, purchasing chemical and glassware	←												
2) Deposition of NI-W-B, Ni-W/B coatings			←										
3) Characterization of microstructure, morphology, and cross section, SEM				←									
4) Phase identify and grain size, XRD				←									
5) Hardness and wear resistance				←									
6) Heat treatment				←									
7) Data analysis			←										
8) Write report and manuscript					↔							↔	

↔ แผนงานวิจัย ความก้าวหน้าของการดำเนินงาน

2. สรุปผลการดำเนินงาน

In this 12 month, we have designed the experimental details and done all Ni-W/B composite coating and Ni-W-B alloy coatings. The present results demonstrate that Ni-W/B composite coating is a good method to prepare the hard composite coating. Now we have published some manuscripts:

- 1) Electrodeposition and mechanical properties of Ni-W matrix composite coatings with embedded amorphous boron particles, International Journal of Electrochemical Science, 11(2016) 9529-9541.
- 2) Effect of sodium dodecyl sulphate and sodium bromide additives on Ni-W nanocoatings, Journal of Nanoscience and Nanotechnology, 17 (2017) 1217-1224.
- 3) Co-electrodeposition of hard Ni-W/diamond nanocomposite coatings, Scientific Reports, 6 (2016) 22285.
- 4) Effect of electrodeposition conditions on structure and mechanical properties of Ni-W/diamond composite coatings, Surface & Coatings Technology, 309 (2017) 337-343.

The experimental details and results are listed as follows.

Experimental details

Substrate and its preparation

In this project, we select low carbon steel as the substrate. Prior to each experiment, the steel plates are pre-treated in alkaline sodium hydroxide solution (60 °C), hydrochloric acid (14%) solution, and then rinsed in distilled water.



Fig. 1. The rectifier of this project

Experimental setup

In this project, the direct current/pulse current is applied to the system by a rectifier (SMD-10P, Dashun, Handan, China), as shown in Fig.1. The deposition setup is shown in Fig. 2. The carbon steel is pretreated and masked with insulated tapes to be 20*20 mm. A Pt mesh is used as counter electrode. The steel plate and Pt mesh are vertically immersed into 200 ml of plating baths. The temperature of the plating bath is controlled with a water bath. Electrodeposition is carried out under constant current density ($0.05-0.2 \text{ A/cm}^2$) at temperature of 40-75 degree Celsius with stirring.



Fig. 2. The deposition setup, 1. Hotplate with magnetic stirrer, 2. Water bath, 3. Electrolyte, 4. Cathode, 5. Anode, 6. Thermocouple

Ni-W/B composite coatings with amorphous boron particles

The Ni-W/B composite coatings are fabricated by a direct current electrodeposition method in a Ni-W plating bath with boron particles suspension. The Ni-W plating bath can be prepared using the following chemicals: 18 g/L $\text{NiSO}_4 \cdot 6\text{H}_2\text{O}$, 53 g/L $\text{Na}_2\text{WO}_4 \cdot 2\text{H}_2\text{O}$, 168 g/L $\text{Na}_3\text{C}_6\text{H}_5\text{O}_7 \cdot 2\text{H}_2\text{O}$, 31 g/L NH_4Cl , 18 g/L NaBr. Amorphous boron particles with particle size of 0.02-1 μm (Changsha, China) and concentration of 1 g/L, 3 g/L, 5 g/L, and 10 g/L, are used. The SEM image is shown in [Fig. 3](#).

Ni-W-B alloy coatings

The Ni-W-B alloy coatings are fabricated by a direct current electrodeposition method in a Ni-W plating bath with addition of trimethylamine borane (TMAB) as the boron source. The Ni-W-B plating bath can be prepared using the following chemicals: 18 g/L $\text{NiSO}_4 \cdot 6\text{H}_2\text{O}$, 53 g/L $\text{Na}_2\text{WO}_4 \cdot 2\text{H}_2\text{O}$, 168 g/L $\text{Na}_3\text{C}_6\text{H}_5\text{O}_7 \cdot 2\text{H}_2\text{O}$, 31 g/L NH_4Cl , 18 g/L NaBr, TMAB, 3, 5, 10 g/L.

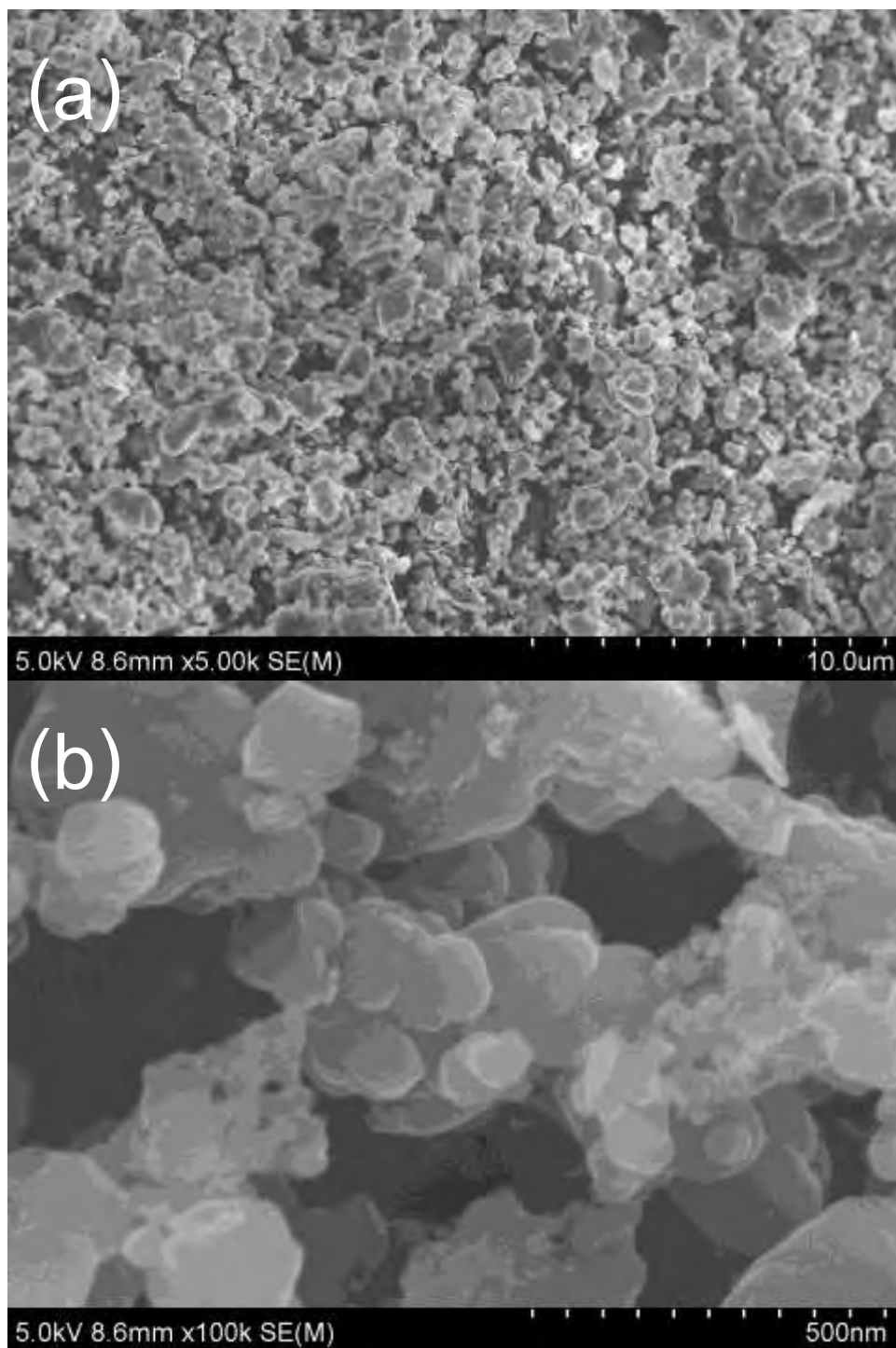


Fig.3. (a) SEM images of amorphous boron, (b) the enlarged SEM image.

Characterization

X-ray diffraction (XRD)

X-Ray diffraction (XRD) technique is employed to analyze the phases of the deposits along identification and analysis of the crystalline structure of the coatings. Brooker D8 advance X-ray diffractometer (Fig. 4) operated at Cu $K\alpha$ radiation at a rating of 40 kV, 20 mA. The scan rate was 0.02° per step and the measuring time 0.5 second/step. Scherer's equation is employed for the calculation of the grain size of the electrodeposited nanocoatings.

$$D = \frac{0.9 \lambda}{\beta \cos \theta} \quad (1)$$

where, D is the grain size, λ is the X-ray wavelength (1.5418 Å), β is the corrected peak width at half maximum intensity (FWHM) and θ is Bragg angle.



Fig. 4. X-ray diffractometer

Scanning electron microscopy (SEM)

The surface morphology and the composition (Ni and W contents) are studied by scanning electron microscopy (SEM, Hitachi, S4800, Fig.5) and energy-dispersive spectroscopy (EDS), respectively.



Fig. 5. Scanning electron microscopy

Inductively coupled plasma mass spectrometry (ICP-MS)

To determine the boron content in the deposits, the samples are measured using an inductively coupled plasma emission spectrometer (ICP-MS, Thermo Scientific) as shown in Fig.6.



Fig. 6. Inductively coupled plasma mass spectrometry

Surface profilometer

The surface profilometer (Gauges, Ambs, US) is carried out to measure the surface roughness. Fig. 7 shows the surface profilometer.

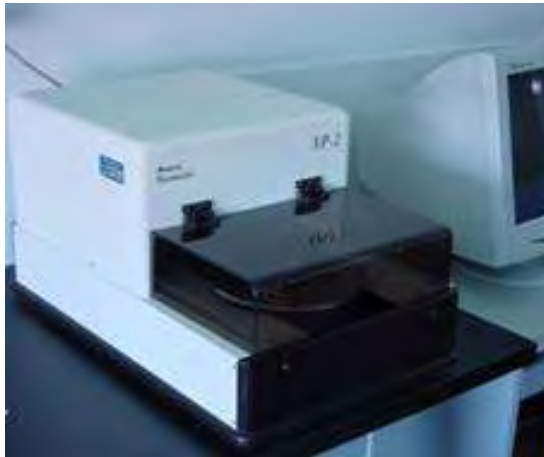


Fig. 7. Surface profilometer

Hardness tester

Knoop microhardness for the surface of coatings is calculated by using a microhardness tester under an indentation load of 100 gf for 15 s after seven different measurement points.

Vickers microhardness for the surface and cross-section of coatings is measured by using a microhardness tester under an indentation load of 50 gf for 15 s after seven different measurement points. Fig. 8 shows the microhardness tester.



Fig. 8. Microhardness tester

Wear testing

The tribological property of the deposits was analyzed by wear test (Fig. 9). The wear test was carried out at an air humidity of 45 ± 10 RH% and a temperature of 24 ± 1 °C using a ball-on-disc tribometer with the sample placed horizontally on a turntable. The tests were performed by applying a load of 20 N to a zirconium dioxide ball of diameter 6 mm, a linear speed of 9.42 cm/s for a total sliding distance of 300m and. Before each test, both the sample and the ball counter face were ultrasonically cleaned in acetone for 10 min, and dried by hot air.

Wear tests were also performed using a CSM reciprocating-sliding tribometer, connected to a computer monitoring the dynamic coefficient of friction (in both sliding directions), relative humidity and temperature. Tests were performed by applying a normal load of 10 N to a stationary ball of diameter 6 mm. The ball materials used were Si_3N_4 . The ball-on-plate machine was set to run at 100 mm/s with reciprocation amplitude of 10 mm and without lubrication. The tests performed at temperatures between 20 and 25 °C. Before each test, both the sample and the ball counterface were ultrasonically cleaned in acetone for 10 min, and dried by hot air. After the wear tests, the morphology of each wear scar was observed by SEM. Also the SEM and EDS were used to obtain information regarding the morphology and chemical composition of the wear debris.



Fig. 9. Wear tester

Results and Discussion

1) Ni-W/amorphous boron composite coating

Electrodeposition is one of the surface modification methods; the obtained films show excellent functional properties and decorative applications and enhance its operating properties subjected to external hazards. The developed Ni-W coatings exhibit higher hardness, higher heat resistance and also a better corrosion behaviour compared to Ni coatings [1-3]. However, the hardness of Ni-W still can't compare to the traditional chromium coating, which exhibits high hardness of ~ 10 GPa[2]. Incorporation of hard particles to the Ni-W nanocoatings could further enhance their hardness. Examples of the Ni-W/hard particles composite coatings which have been investigated and fabricated successfully include Ni-W/diamond [4-6], Ni-W/WC[7], Ni-W/ Al_2O_3 [8], and Ni-W/ SiO_2 [9]. Boron, the elemental neighbour to carbon in the periodic system of elements, is also known to be superhard material [10, 11]. The high hardness of boron could also improve the nanostructured Ni-W coatings. However, there is no report on the effect of boron on the microstructure and mechanical properties of nanostructured Ni-W coating. Herein, Ni-W/B composite coatings were fabricated by the electrodeposition in a Ni-W plating bath containing amorphous boron particles. The microstructure and hardness of the composite coatings were investigated.

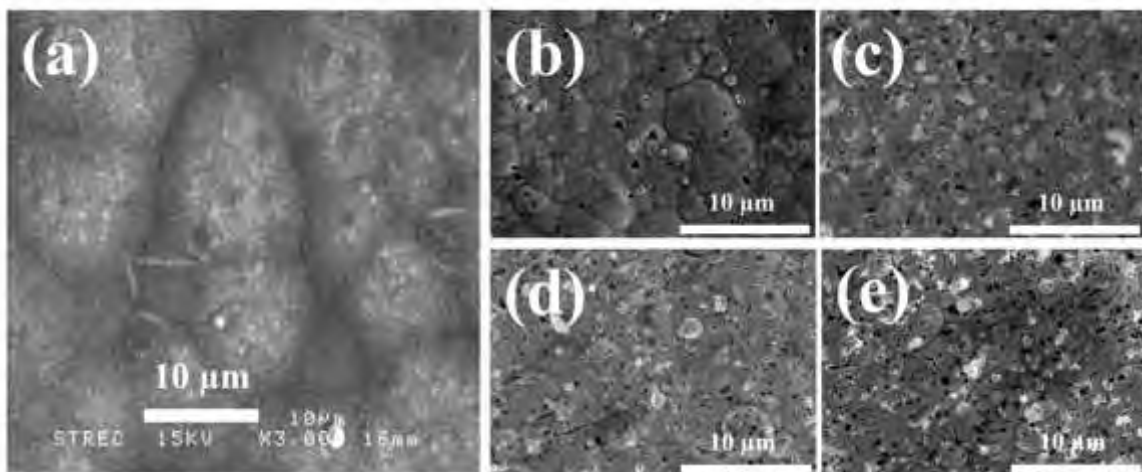


Fig.10. SEM images of Ni-W coating (a), Ni-W/B composite coatings with current density of 0.1 A/cm^2 and different boron concentration in the plating bath, (b) 1 g/L, (c) 3 g/L, (d) 5 g/L, (e) 10 g/L.

1.1) Surface morphology

The Ni-W/B nanocomposite coatings were successfully prepared by co-deposition of boron particles with Ni-W alloy under magnetic stirring. Figure 10 shows the SEM images of the typical surface morphology of the as-deposited Ni-W and Ni-W/B composite coatings prepared at current density of 0.1 A/cm^2 and different boron concentration in the plating bath. It can be seen that all samples exhibit the columnar structure. With the boron incorporation, the columnar size becomes smaller, and the composite coatings show the formation of uniform and fine-grained coatings. Furthermore, the addition of boron particles in the Ni-W matrix decreases the surface roughness and alters the chemical composition. The average surface roughness (Ra) of electrodeposited Ni-W coatings is $1.58 \pm 0.1 \text{ }\mu\text{m}$, while Ra of electrodeposited Ni-W/B composite coatings is $1.26 \pm 0.07 \text{ }\mu\text{m}$, $0.93 \pm 0.04 \text{ }\mu\text{m}$, $1.13 \pm 0.08 \text{ }\mu\text{m}$, and $1.19 \pm 0.06 \text{ }\mu\text{m}$, for boron concentration in the plating bath of 1 g/L, 3 g/L, 5 g/L, and 10 g/L, respectively. The surface roughness further reveals that the addition of boron can smooth the surface. This behavior has been reported by previous researchers for Cu-Si₃N₄ composite coatings [12].

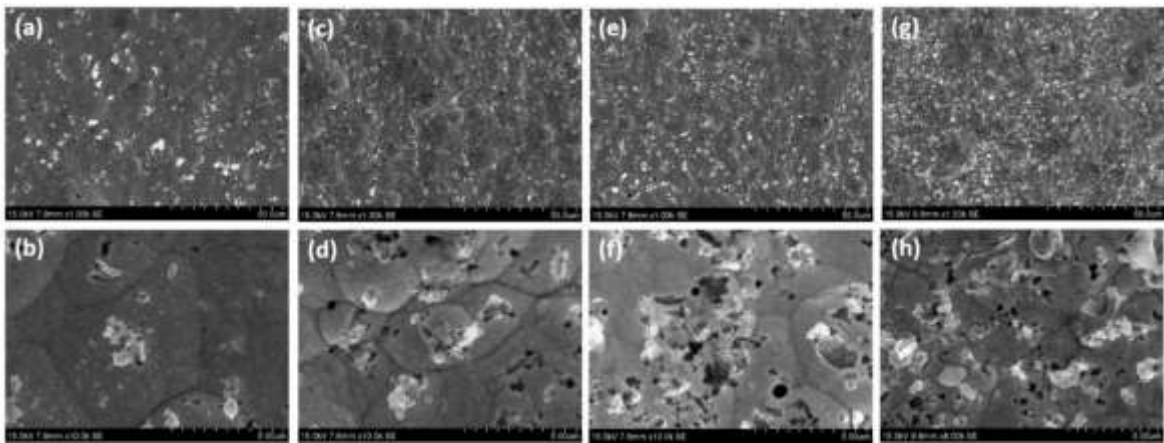


Fig. 11. SEM image of the surface of Ni-W/B coating produced at constant current density of 0.05 A/cm^2 and at boron concentration of (a) 1 g/L (1000x), (b) 1 g/L (10000x), (c) 3 g/L (1000x), (d) 3 g/L (10000x), (e) 5 g/L (1000x), (f) 5 g/L (10000x), (g) 10 g/L (1000x), (h) 10 g/L (8000x).

In addition, the Ni-W/B composite coatings were also prepared at current density of 0.05, 0.15, and 0.2 A/cm^2 and different boron concentration in plating bath, respectively. Fig. 11 shows the SEM images of the Ni-W/B composite coatings prepared at current density of

0.05 A/cm² and different boron concentration in plating bath. Fig. 12 shows the SEM images of the Ni-W/B composite coatings prepared at current density of 0.15 A/cm² and different boron concentration in plating bath. Fig. 13 shows the SEM images of the Ni-W/B composite coatings prepared at current density of 0.2 A/cm² and different boron concentration in plating bath.

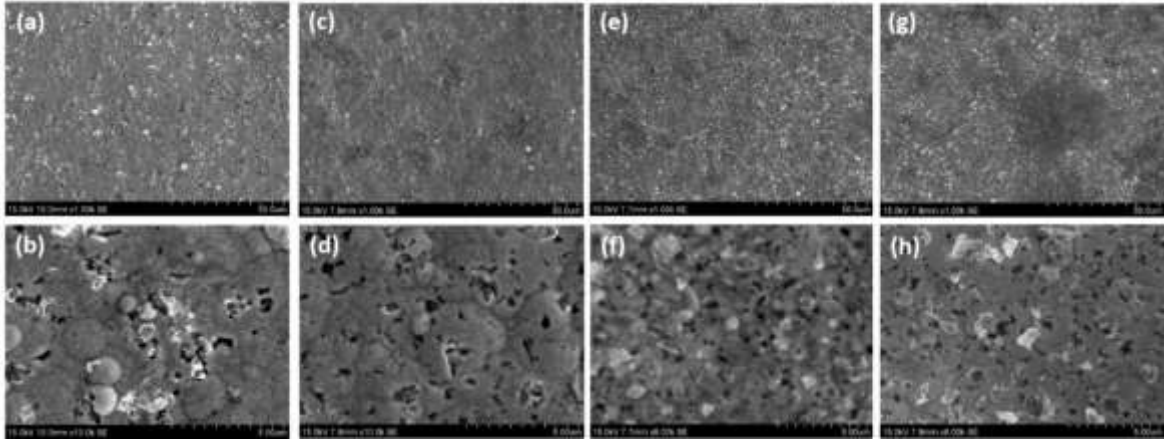


Fig. 12. SEM image of the surface of Ni-W-B coating produced at constant current density of 0.15 A/cm² and at boron concentration of (a) 1 g/L (1000x), (b) 1 g/L (10000x), (c) 3 g/L (1000x), (d) 3 g/L (10000x), (e) 5 g/L (1000x), (f) 5 g/L (8000x), (g) 10 g/L (1000x), (h) 10 g/L (8000x).

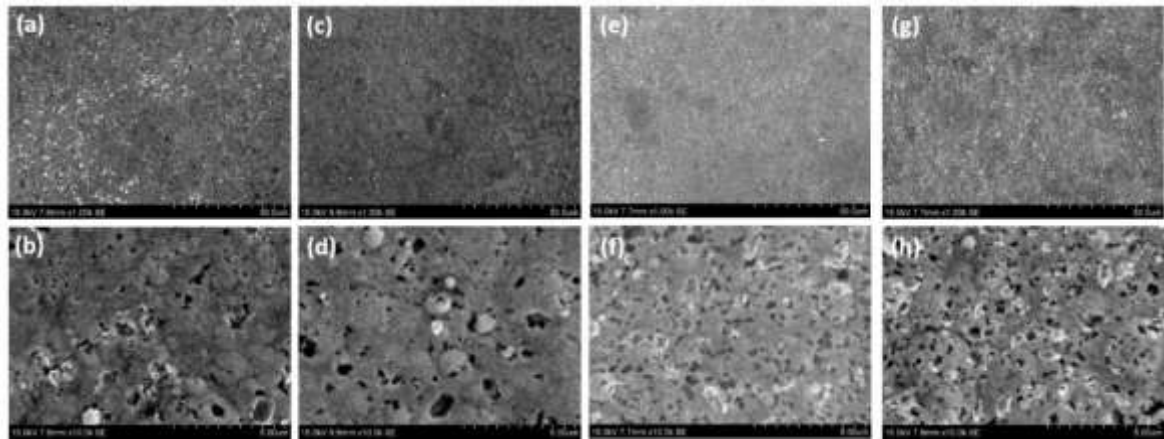


Fig. 13. SEM image of the surface of Ni-W-B coating produced at constant current density of 0.20 A/cm² and at boron concentration of (a) 1 g/L (1000x), (b) 1 g/L (10000x), (c) 3 g/L (1000x), (d) 3 g/L (10000x), (e) 5 g/L (1000x), (f) 5 g/L (10000x), (g) 10 g/L (1000x), (h) 10 g/L (10000x).

Figure 14 shows the cross-sectional SEM images of the Ni-W/B composite coatings fabricated with current density of 0.1 A/cm^2 and different boron concentration in plating bath, 1 g/L, 3 g/L, 5 g/L, and 10 g/L, respectively. Boron particles of sub-micron sizes ($< 1 \mu\text{m}$) were uniformly co-deposited into the Ni-W matrix. It can also be seen that many boron particles were embedded in Ni-W deposition matrix.

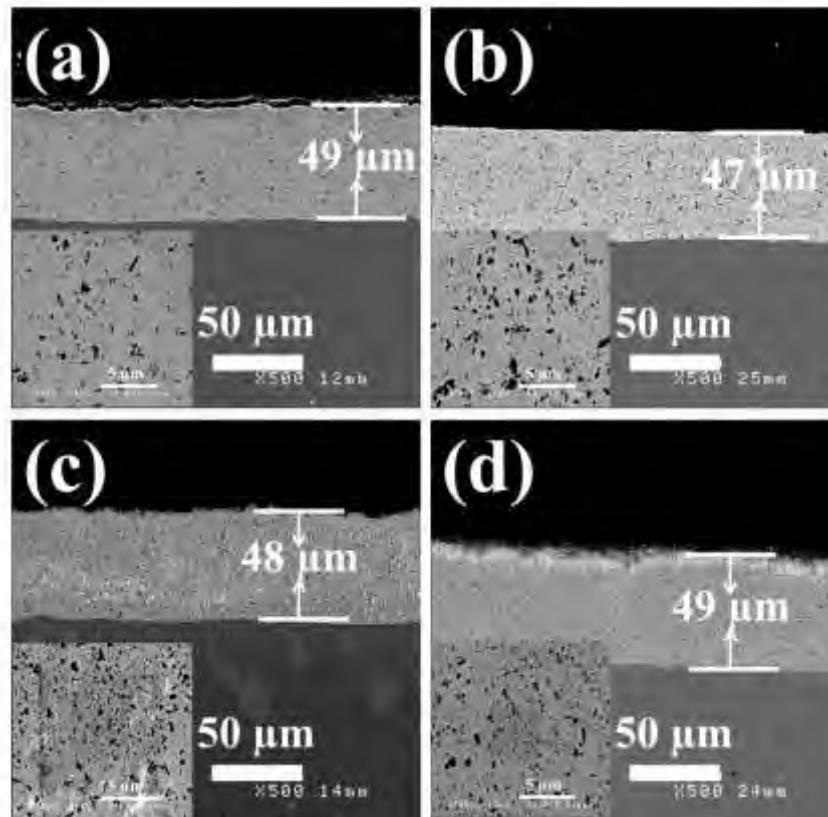


Fig. 14. Cross-sectional SEM images of Ni-W/B composite coatings prepared with current density of 0.1 A/cm^2 and different boron concentration in bath, (a) 1 g/L, (b) 3 g/L, (c) 5 g/L, (d) 10 g/L.

1.2. Cross section

The thickness of Ni-W/B composite coatings was also measured from the cross-sectional SEM images, as shown in Fig. 15. The measured thickness is $\sim 47\text{--}49 \mu\text{m}$ (Fig. 14) for the Ni-W/B composite coatings prepared at current density of 0.1 A/cm^2 and different boron concentration in plating bath. From the Fig. 14 and Fig. 15, it can demonstrate that the incorporated boron does not strongly affect the deposition rate of Ni-W matrix.

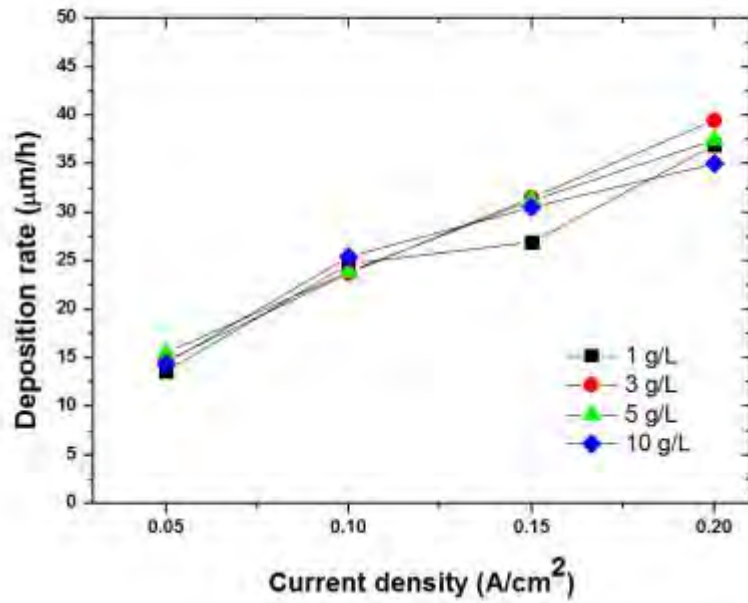


Fig. 15. Relationship between deposition rate ($\mu\text{m/h}$) and current density (A/cm^2) at different boron concentration

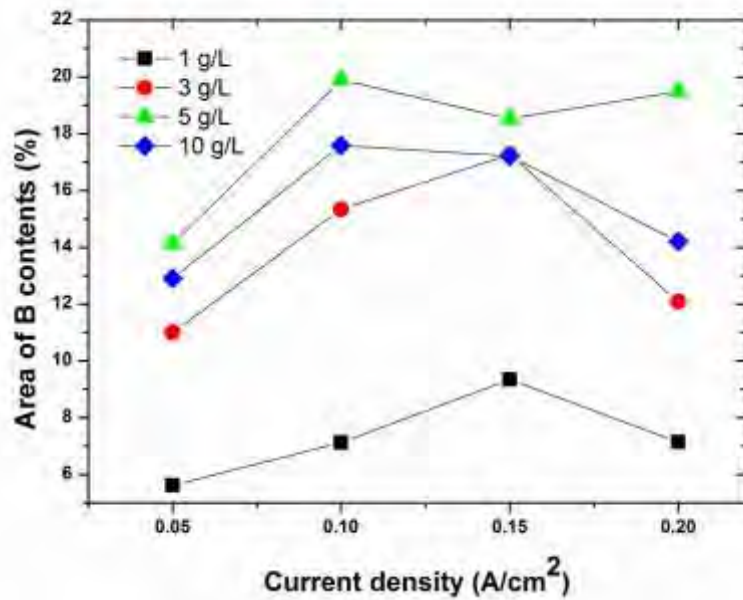


Fig. 16. Effect of current density on B contents of Ni-W/B composite coatings produced at different boron concentration and current density by ImageJ analysis.

1.3. Boron content in the deposits

According to the cross-sectional SEM images, the volume percentages of B particles in coating could be estimated by image analysis software (ImageJ). Fig. 16 shows the estimated boron content in the Ni-W/B composite coatings prepared at different current

density and boron concentration in plating bath. The image analysis results show that the volume percentage of incorporated B particles into Ni-W matrix is 7 vol.%, 15 vol.%, 20 vol.%, and 18 vol.%, for boron concentration in the bath of 1 g/L, 3 g/L, 5 g/L, and 10 g/L, at current density of 0.1 A/cm^2 , respectively.

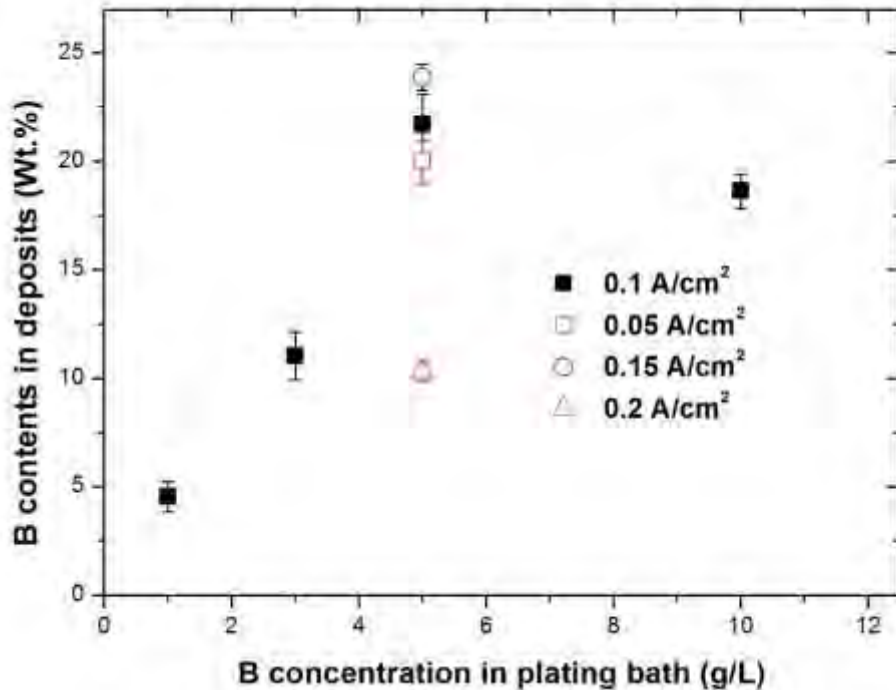


Fig. 17. The effect of boron concentration and current density on boron contents in Ni-W/B composite coatings from ICP analysis.

The B content in the composite coatings was also confirmed by ICP. Fig. 17 shows the relationship between boron concentration in solution and boron content in deposits. From the results presented in Fig. 17, it is interesting to observe that the amount of embedded B particles in the deposits increases sharply with boron concentration in the bath from 1 to 5 g/L, while above 5 g/L, the B content slightly decreases. The maximum B content in deposits (~21.7 wt.%) can be obtained according to the ICP results. Here, we can explain the mechanism of incorporation of B particles in the electrodeposited Ni-W matrix by Guglielmi's model[13]. According to Guglielmi's two step adsorption model, the increase in the B content in the deposits observed up to 5 g/L is due to the increase in the number of particles in the plating bath, which can improve the adsorption rate of boron particles on the growing coatings. Thus, it can incorporate a higher percentage of boron particles in Ni-W matrix according to Yeh and Wan results[13]. While the B concentration in bath reached at 10 g/L,

the B content is lower than that of coating prepared at 5 g/L. Thus it might be caused by the agglomerate of B particles with higher B concentration in the plating bath. Similar results were also reported by the other researchers [5, 14-16]. At this extremely high boron concentration, all boron particles might be not dispersed finely, some of them aggregate. Thus the increase in the boron concentration beyond 5 g/L would cause slight decrease in the level of incorporation of boron particles in Ni-W matrix. In the current study, the boron concentration of 5 g/L is an optimized value in the Ni-W plating bath to prepare the maximum boron content in coating.

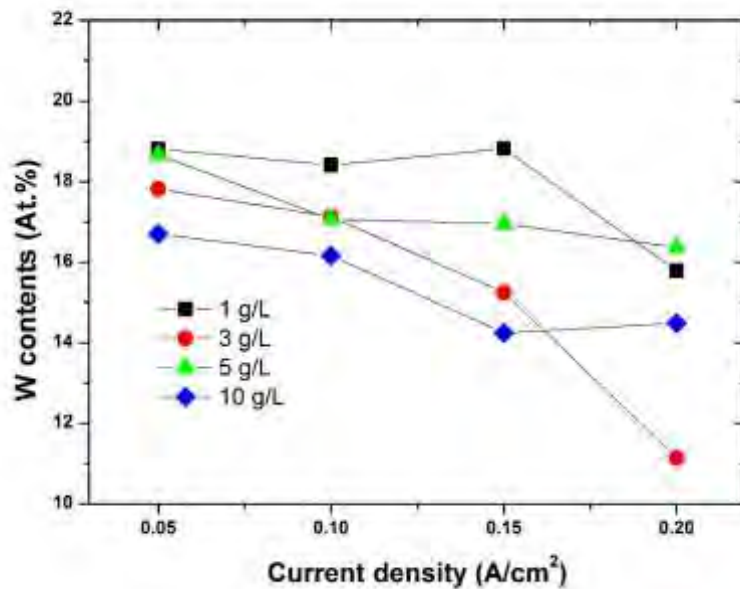


Fig. 18. Effect of current density and boron concentration in plating bath on W contents of Ni-W/B coating from EDS analysis.

1.4. EDS analysis of Ni-W/B composite coatings

The chemical composition was also determined by EDS. The effect of boron concentration in the plating bath on the W content in the deposits is plotted in Fig. 18. The results reveal that the W content in the coatings decreases slightly with boron concentration in the plating bath increasing. From the Fig. 18, the boron concentration in the plating bath was increased from 0 to 10 g/L, the W content in the deposits decreased from ~42 wt.% to ~38 wt.%. Hou et al. [5] also reported a similar tendency in Ni-W/diamond electrodeposition system. The boron particles in the plating bath could absorb hydrogen ions near the cathode and inhibit the reduction reaction of hydrogen ion to hydrogen. The W content in the deposits

decreasing might be caused by the hydrogen ions absorbed by boron particles in the plating bath.

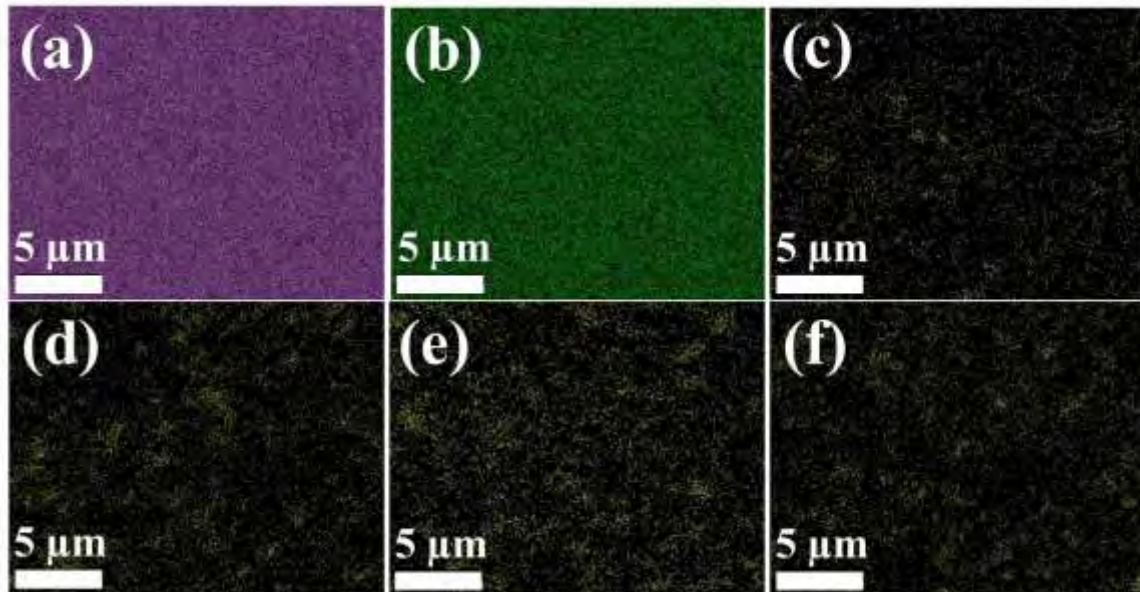


Fig. 19. The EDS elemental mapping of Ni-W/B composite coatings prepared at current density of 0.1 A/cm² and different boron concentration, (a) Ni elemental mapping, (b) W elemental mapping, (c) B elemental mapping at 1 g/L, (d) B elemental mapping at 3 g/L, (e) B elemental mapping at 5 g/L, (f) B elemental mapping at 10 g/L.

The EDS elemental mapping was also carried out to study the element distribution of as-deposited Ni-W/B composite coatings obtained with different concentration of boron in solution. Figure 19 present the B elemental mapping images of Ni-W/B composite coatings prepared with 1g/L, 3 g/L, 5 g/L, and 10 g/L, respectively. The B EDS mapping shows that there is no B particle agglomeration within the coating. This might be due to the fact that B particles are dispersed in solution using sonication dispersion method. The B EDS mapping also indicates that the B content increases with concentration of B particles in bath from 1 to 5 g/L, while above 5 g/L, the B content slightly decreases. The observation of EDS elemental mapping results agree well with the ICP results.

1.5. XRD

The XRD patterns of coatings with different boron concentration in solution as exemplified in Fig. 20, appear to be similar. Ni(W) solid solution can be identified for all the

as-deposited coatings. The incorporation of boron particles to the Ni-W coating does not affect the coatings in terms of phase and their texture. Furthermore, the grain size of Ni-W and Ni-W/B coatings was also estimated from the width of the Ni (111) peaks as shown in Fig. 21. The grain size is 2.8 nm, 2.4 nm, 2.8 nm, 2.8 nm, and 3.1 nm, for Ni-W/B composite coatings prepared at current density of 0.1 A/cm² and boron concentration in bath of 0 g/L, 1 g/L, 3 g/L, 5 g/L, and 10 g/L, respectively. The results further indicate that the incorporation of boron particles also does not strongly change the grain size of electrodeposited Ni-W matrix.

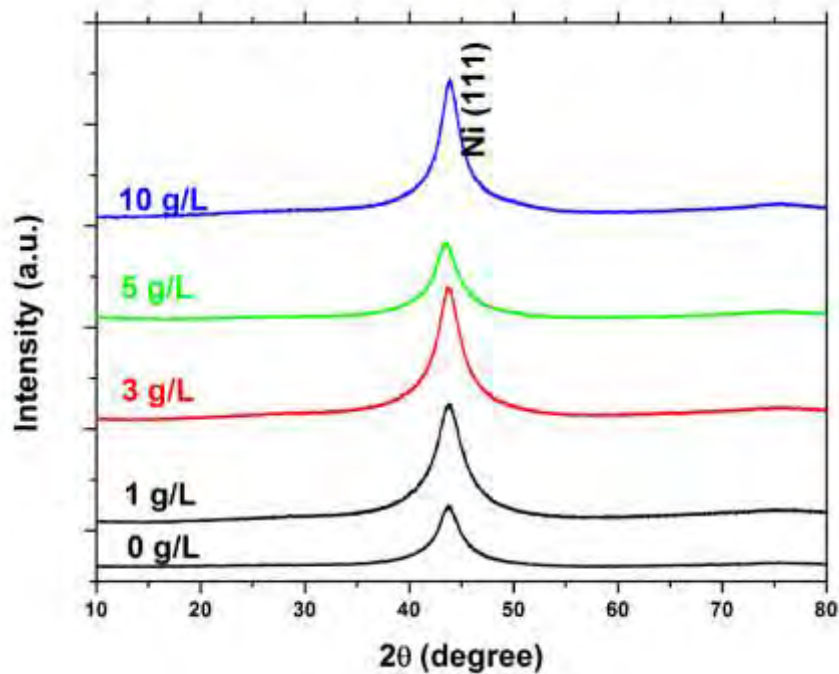


Fig. 20. XRD patterns of coatings with different boron concentration in the plating bath.

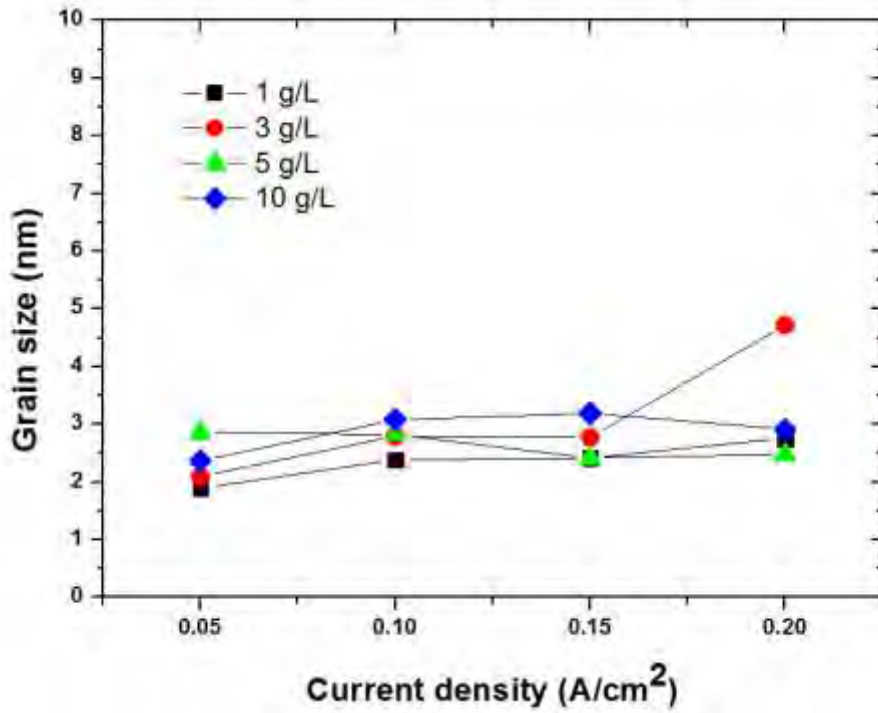


Fig. 21. Effect of current density on grain size of Ni-W/B coating produced at different boron concentration.

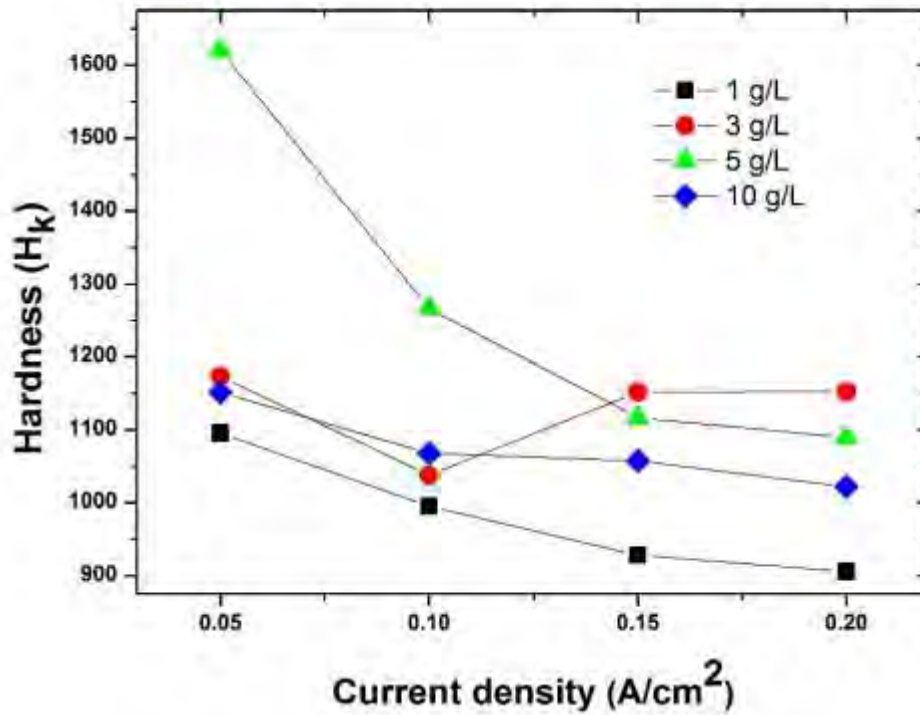


Fig. 22. Effect of current density on hardness of Ni-W/B composite coating produced at different boron concentration.

1.6. Microhardness

The microhardness of Ni-W and Ni-W/B coatings was measured by Knoop Hardness Tester, as shown in Fig. 22. Without incorporation of boron particles, the electrodeposited Ni-W coating exhibits the hardness of 835 HK at current density of 0.1 A cm^{-2} , which is little higher than that of the reported vickers microhardness value[2]. The incorporations of boron particles of 1, 3, 5, and 10 g L^{-1} , have the hardness of 994, 1037, 1266, and 1067 HK, respectively (Fig. 22). The hardness results indicate that the incorporation of boron in coatings can result in a marked enhancement of hardness. The hardness increases with the increase in boron concentration in the plating bath from 1 to 5 g/L , while above 5 g/L , the hardness decreases.

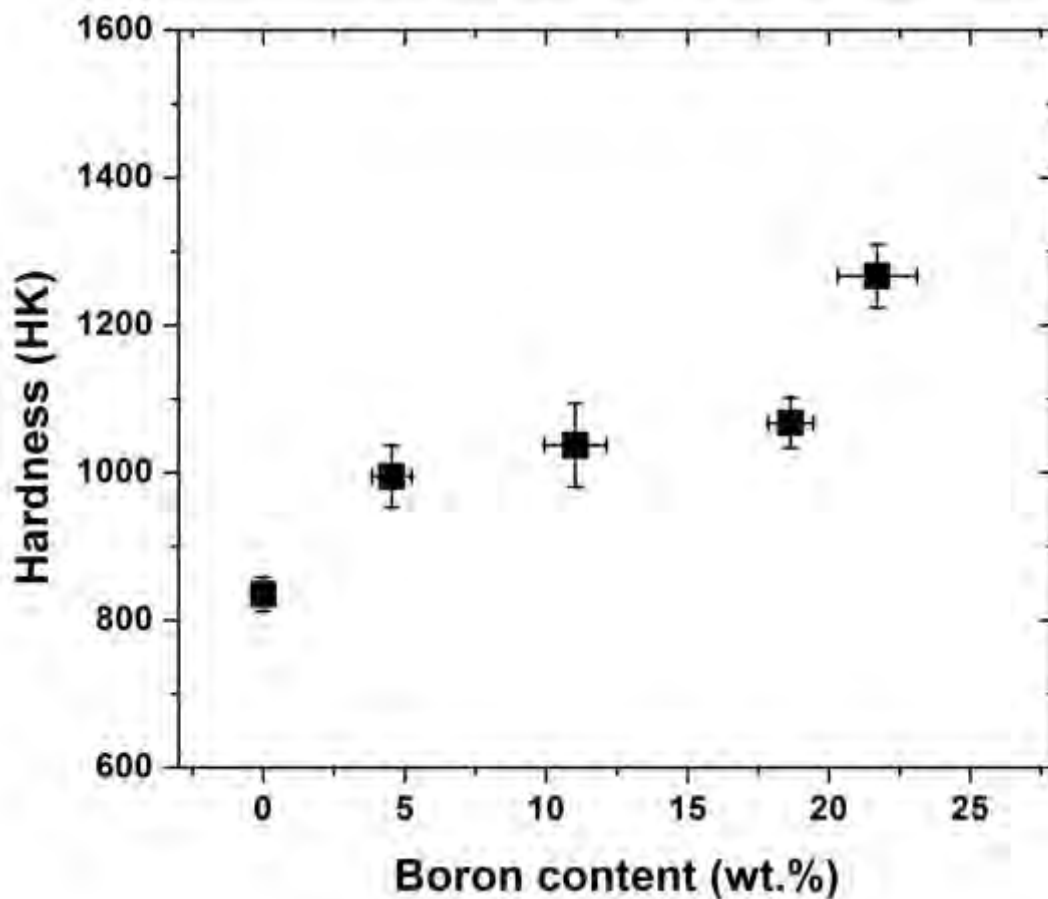


Fig. 23. Hardness of Ni-W coating and Ni-W/B nanocomposite coatings presented as a function of the boron content in the deposits.

To better understand the mechanism of hardness enhanced for the obtained coatings, the relationship between boron content in coatings and hardness is shown in Fig. 23. From

Fig. 23, it can be seen that the hardness depended on the boron content: composite coatings with higher boron content shows higher hardness. For the hardness of composite coatings, it is controlled by the percentage of incorporated particles and hardness of the matrix. In the current study, the incorporation of boron does not strongly affect the grain size and deposition rate of electrodeposited Ni-W matrix. The incorporated boron particles decrease the W content in deposits. As the previous results [2], the W is the grain refining element and can improve the hardness of Ni-W coatings. However, the current results reveal that hardness of composite coatings increase with the decrease in W content in the deposits, and the increase in boron incorporation in the coatings. Therefore, the hardness of Ni-W/B composite coatings is mainly contributed by the amounts of boron incorporation. The improvement mechanism of hardness for composite can be defined two different kinds of hardening mechanism according to the amount and size of particles, i.e., dispersion strengthening and particle strengthening [15, 17]. From the cross-sectional SEM images, the incorporation of boron particles have the sub-micron size ($<1 \mu\text{m}$), both the particle and dispersion strengthening are the mechanism in enhancing the hardness of the Ni-W/B composite coatings.

The current work developed one efficient method to prepare Ni-W/B hard coatings with high B content. The electroplating conditions applied in the present study show that Ni-W/B composite coatings could be deposited from Ni-W plating bath with amorphous boron particles suspension. The higher B content in the deposits can be easily obtained ($\sim 21.7 \text{ wt.}\%$) than those of Ni-W-B coatings prepared from sodium borate ($\sim 1.86 \text{ wt.}\%$) [18, 19] ($\sim 1 \text{ wt.}\%$) [20], and dimethylamino borane ($\sim 1 \text{ wt.}\%$) [21, 22], ($\sim 3 \text{ wt.}\%$) [23]. Several works have also reported the hardness of as-deposited Ni-W-B coatings. For example, Ni-W-B coatings could get a hardness of around 600-875 Hv [18, 19], 600-850 Hv [21-23], prepared from sodium borate, and dimethylamino borane, respectively. While in the present work, the higher hardness (994-1266 HK) of Ni-W/B composite coatings can be easily obtained from Ni-W plating bath with amorphous boron suspension. Furthermore, the previous study also demonstrated that the Ni-W-B coatings contain 1 wt.% B can be chromium replacement alloys [20], the current results are much higher than that of B content. Therefore, the developed method can be potential alternative chromium coatings.

1.7. Wear resistance

The performance of many products and engineering components depends critically on tribological properties of surfaces such as wear and friction. Here the wear testing was also performed by using reciprocating-sliding tribometer for Ni-W (prepared at current density of 0.1 A/cm^2) and Ni-W/B composite coatings (deposited at current density of 0.1 A/cm^2 and boron concentration in plating bath of 1, 3, 5, and 10 g/L). Wear tests were performed using a CSM reciprocating-sliding tribometer, connected to a computer monitoring the dynamic coefficient of friction (in both sliding directions), relative humidity and temperature. Tests were performed by applying a normal load of 10 N to a stationary ball of diameter 6 mm. The ball materials used were Si_3N_4 . The ball-on-plate machine was set to run at 100 mm/s with reciprocation amplitude of 10 mm and without lubrication. The tests performed at temperatures between 20 and 25 °C. Before each test, both the sample and the ball counterface were ultrasonically cleaned in acetone for 10 min, and dried by hot air. The anti-wear performance of the films was estimated from the weight loss of the specimens. After the wear tests, the morphology of each wear scar was observed by SEM. Also the SEM and EDS were used to obtain information regarding the morphology and chemical composition of the wear debris.

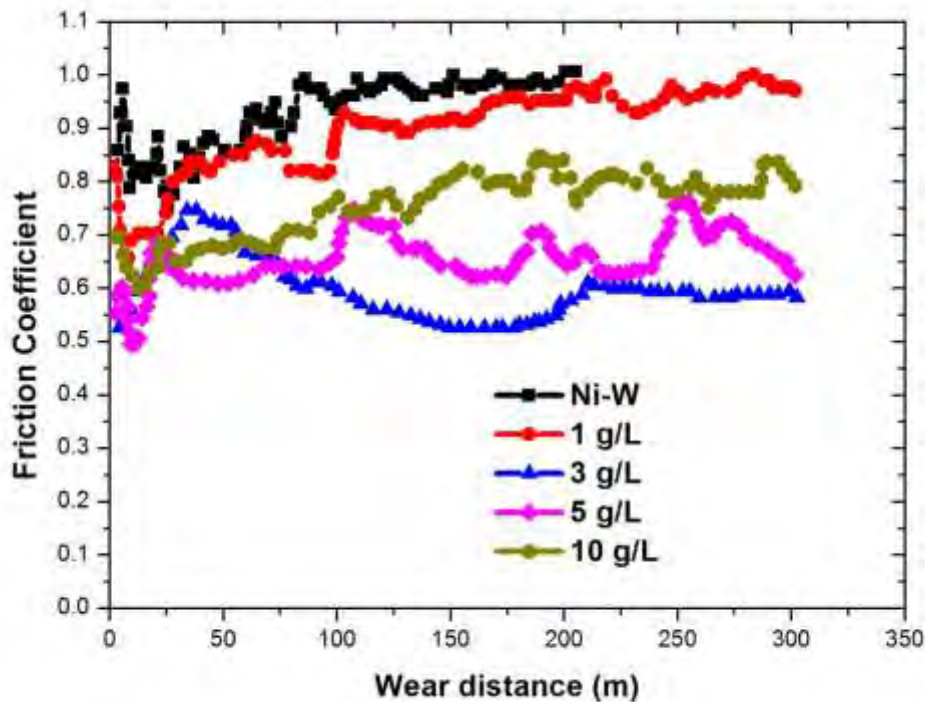


Fig. 24. The friction coefficient during wear testing.

Figure 24 show the corresponding coefficient of friction (CoF) data for Ni-W and Ni-W/B composite coatings, respectively. For Ni-W coating the friction coefficient is always larger than those of Ni-W/B composite coatings. During the wear testing, if the maximum friction force is larger than 10 N, i.e. the CoF is larger than 1 in present case with the load of 10 N, the testing will be stopped by the protection function of the equipment. For Ni-W coatings, one test stopped when the sliding distance reached 200 m because the CoF became larger than 1. For Ni-W/B composite coatings, however, the CoF was kept almost constant ~0.55-0.9 for sliding distance of 300 m or even longer. From the Fig. 24, it can be seen that the boron concentration in plating bath can also affect the friction coefficient. At 1 and 10 g/L of boron concentration in plating bath, the friction coefficient slightly increased with the sliding distance. However, the friction coefficient can keep almost constant ~0.55-0.7 for boron concentration in plating bath of 3 and 5 g/L. Moreover, the Ni-W/B composite coating prepared at the boron concentration in plating bath of 3 g/L exhibited the lowest friction coefficient, and slightly decreased with the sliding distance increasing.

In summary, electrodeposited Ni-W/B nanocomposite coatings were successfully prepared by dispersing the boron particles in the Ni-W bath. With boron incorporation, the W content in the deposits decreases and grain size of coatings slight changes. The boron content in the composite coatings increases with the increase in its concentration in the bath up to 5 g/L, beyond which it decreases. The maximum boron content in the electrodeposited Ni-W matrix is about 21.7 wt.%. The Ni-W/B coatings consist of a hard metal matrix and hard boron particles, and thus exhibit high hardness. The hardness of Ni-W/B composite coatings is mainly contributed by the boron content in deposits. A high hardness of 994-1266 HK was obtained in Ni-W/B composite coatings which is comparable to that of hard chromium plated coatings.

2) Heat treatment of Ni-W/amorphous boron composite coatings

In this part, we are going to study the effect of heat treatment on the structure and mechanical properties of electrodeposited Ni-W/B nanocoating. The influence of temperature and time during heat treatment and boron content during co-electrodeposition on the structure will be discussed. Optical microscope (OM), scanning electron microscopy (SEM) and energy-dispersive X-ray spectroscopy (EDS) are used to study the morphology and

microstructure. Hardness and wear resistance of the composite coatings will be characterized.

The Ni-W/B composite coatings were prepared by co-electrodeposition from a Ni-W bath without any additives. The bath composition and plating conditions are listed in [Table 2-1](#) and [Table 2-2](#).

Table 2-1 Chemical composition of the electrodeposition bath

Chemicals	
Nickel(II) sulphate (NiSO ₄)	18 g/l (3.6 g for 200 ml)
Sodium tungstate	53 g/l (10.6 g for 200 ml)
Tri-Sodium citrate	168 g/l (33.6 g for 200 ml)
Ammonium chloride (NH ₄ Cl)	31 g/l (6.2 g for 200 ml)
Sodium Bromide (NaBr)	18 g/l (3.6 g for 200 ml)
Boron (Amorphous Boron)	1 g/l (0.2 g for 200 ml)
	3 g/l (0.6 g for 200 ml)
	5 g/l (1 g for 200 ml)

Table 2-2 Operating conditions

Parameters	
Temperature	75 °C
Current Density	0.1 A/cm ²
Stirring Speed	100 RPM
pH	~8.6

The deposited samples were further treated under high temperature. The heat treatment conditions are shown in [Table 2-3](#).

Table 2-3 Conditions for heat treatment

Conditions	
Temperature	200-700 °C
Soaking Time	1 – 3 hr
Heating Speed	10 °C/min

2.1 Effect of heat treatment on surface

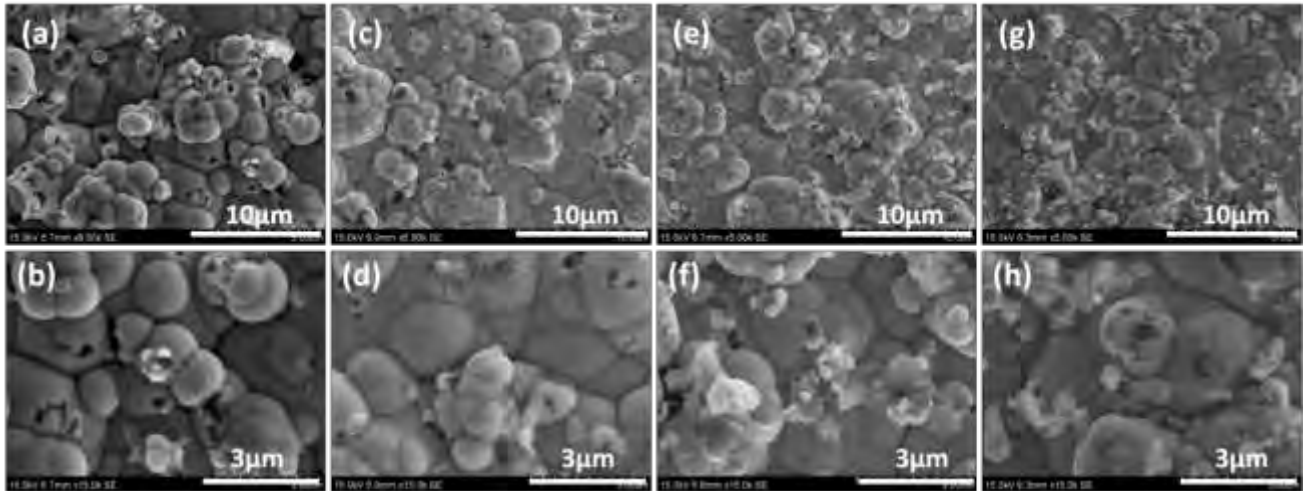


Fig. 2-1 SEM image of the surface of Ni-W-B coating produced at constant boron concentration of 1 g/L and heat treatment at different temperatures (a) without heat treatment (5000x), (b) without heat treatment(15000x), (c) 200°c (5000x), (d) 200°c (15000x), (e) 300°c (5000x), (f) 300°c (15000x), (g) 400°c (5000x), (h) 400°c (15000x).

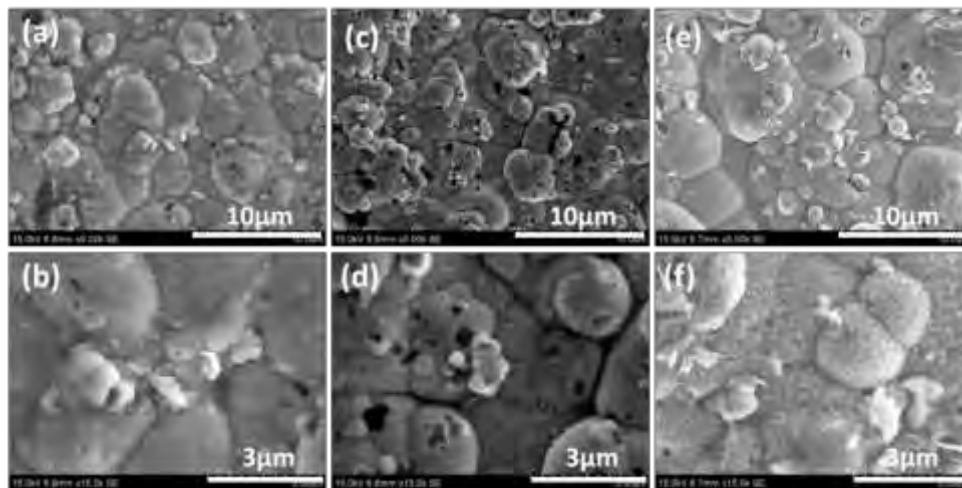


Fig. 2-2 SEM image of the surface of Ni-W-B coating produced at constant boron concentration of 1 g/L and heat treatment at different temperatures (a) 500°c (5000x), (b) 500°c (15000x), (c) 600°c (5000x), (d) 600°c (15000x), (e) 700°c (5000x), (f) 700°c (15000x)

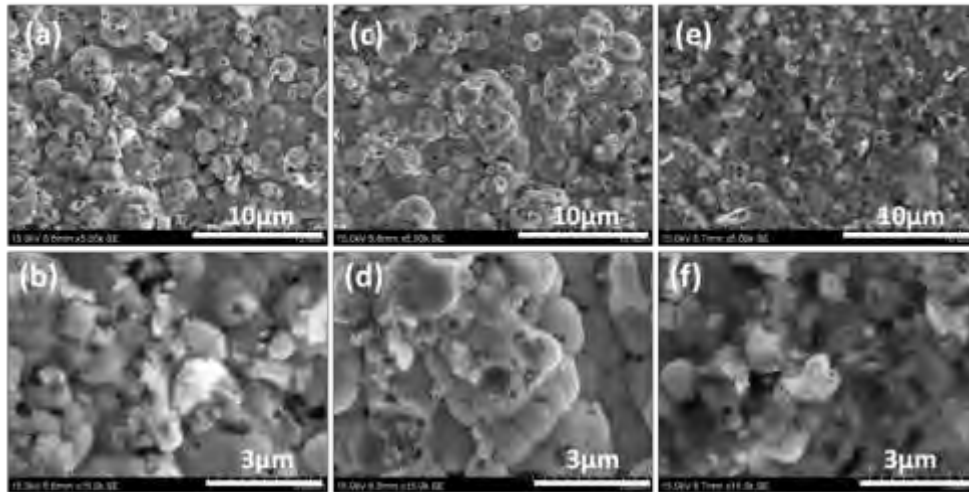


Fig. 2-3 SEM image of the surface of Ni-W-B coating produced at constant boron concentration of 3 g/L and heat treatment at different temperatures (a) without heat treatment (5000x), (b) without heat treatment (15000x), (c) 300°C (5000x), (d) 300°C (15000x), (e) 600°C (5000x), (f) 600°C (15000x)

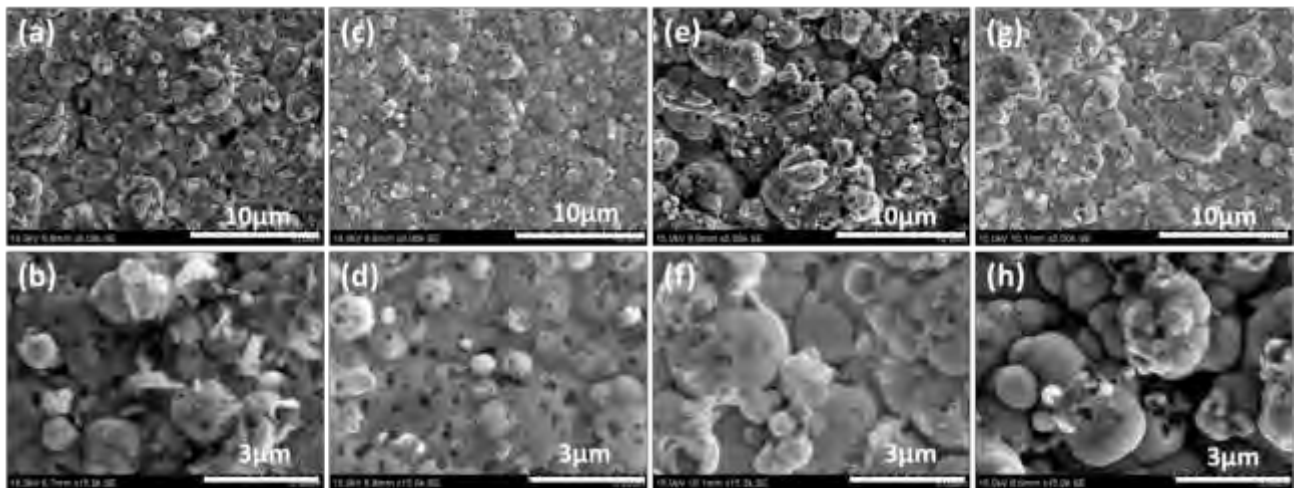


Fig. 2-4 SEM image of the surface of Ni-W-B coating produced at constant boron concentration of 5 g/L and heat treatment at different temperatures (a) without heat treatment (5000x), (b) without heat treatment (15000x), (c) 200°C (5000x), (d) 200°C (15000x), (e) 300°C (5000x), (f) 300°C (15000x), (g) 400°C (5000x), (h) 400°C (15000x).

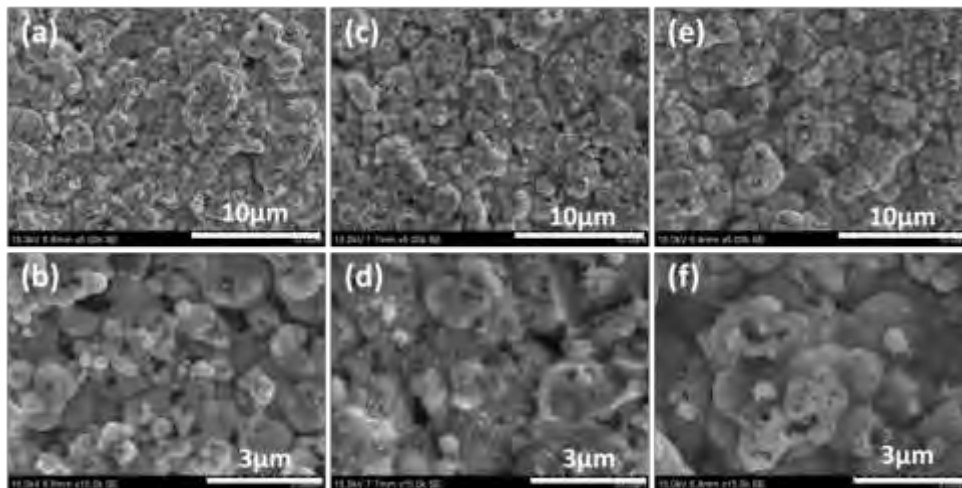


Fig. 2-5 SEM image of the surface of Ni-W-B coating produced at constant boron concentration of 5 g/L and heat treatment at different temperatures (a) 500°C (5000x), (b) 500°C (15000x), (c) 600°C (5000x), (d) 600°C (15000x), (e) 700°C (5000x), (f) 700°C (15000x)

Fig. 2-1-Fig. 2-5 show SEM morphologies of the surface of Ni-W-B composite coatings obtained at different heat treatment temperatures with boron concentration of 1 g/L, 3 g/L and 5 g/L respectively. From SEM observation, the addition of boron particle could strongly affect the microstructure of Ni-W matrix. The granular size is smaller and the boron particle in the metal deposit increases obviously with the increase of boron concentration. For the different heat treatment temperatures, at low temperatures does not affect the morphology obviously, boron particles can be observed clearly and the semispherical shape of nodules look flat and smooth. At high temperatures boron particle is already reacted with the nodules to form some new phases that can confirm from the XRD results, this makes the surface doesn't look flat and smooth. Supported by *Renáta Oriňáková* et al. [16], they found that the shape of nodules in coating heated at 400 °C changed to the rather edginess, protrusive appearance after heating at 875 °C and 1120 °C.

2.2 Effect of the heat treatment on cross-section

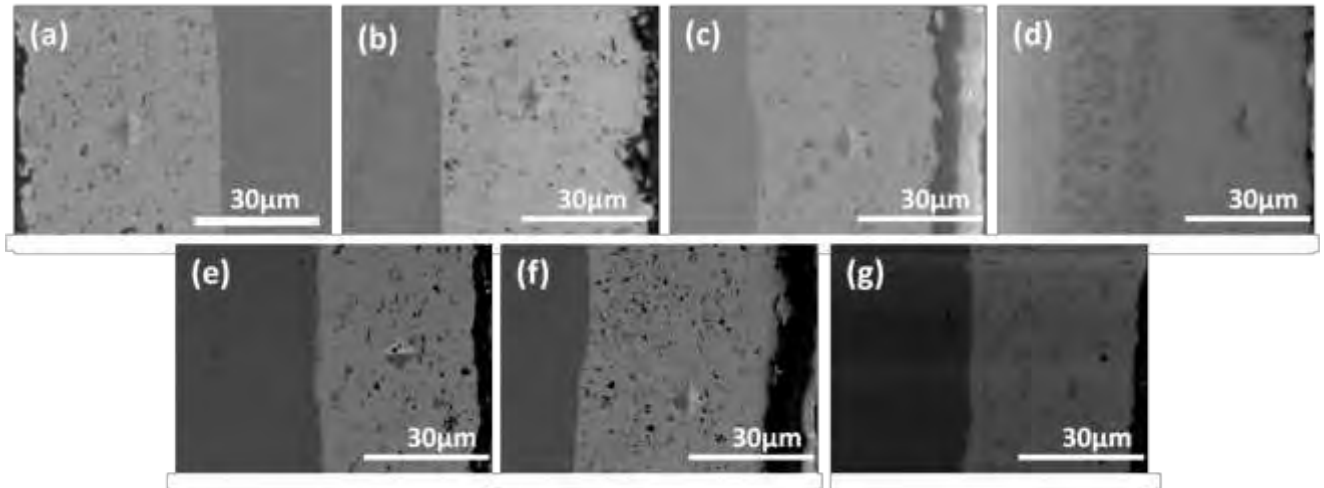


Fig. 1 SEM image of the cross-section of Ni-W-B coating produced at constant boron concentration of 1 g/L and heat treatment at different temperatures (a) without heat treatment (2000x), (b) 200°C (2000x), (c) 300°C (2000x), (d) 400°C (2000x), (e) 500°C (2000x), (f) 600°C (2000x), (g) 700°C (2000x)

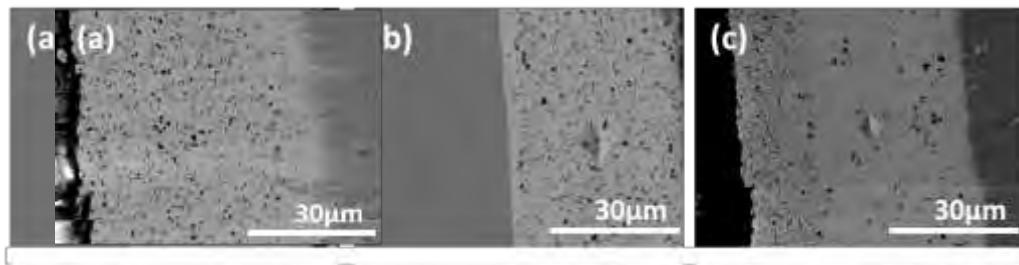


Fig. 2 SEM image of the cross-section of Ni-W-B coating produced at constant boron concentration of 3 g/L and heat treatment at different temperatures (a) without heat treatment (2000x), (b) 300°C (2000x), (c) 600°C (2000x)

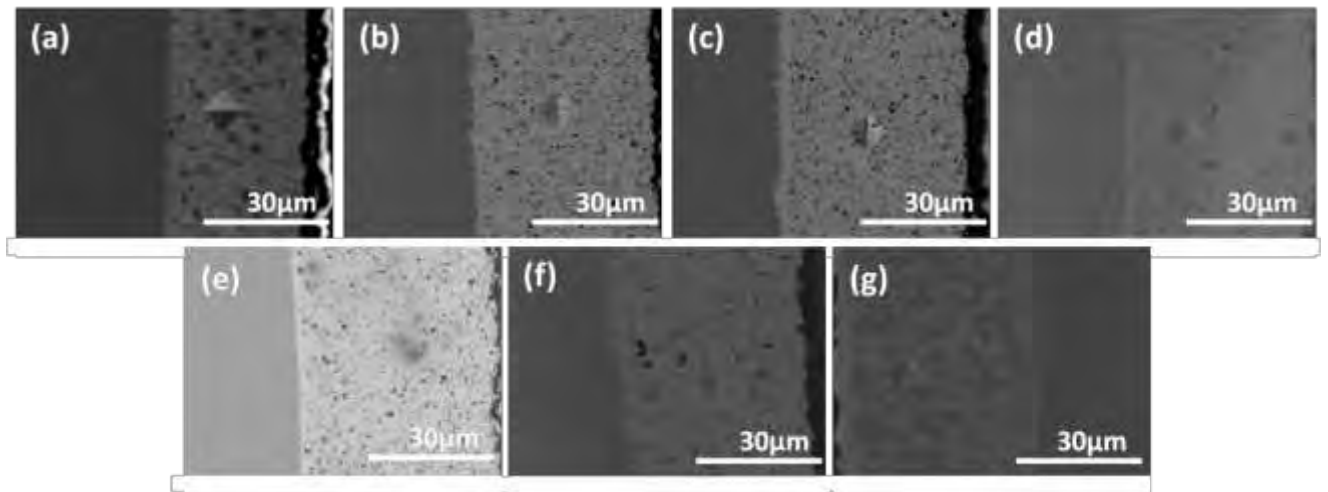


Fig. 2-8 SEM image of the cross-section of Ni-W-B coating produced at constant boron concentration of 5 g/L and heat treatment at different temperatures (a) without heat treatment (2000x), (b) 200°C (2000x), (c) 300°C (2000x), (d) 400°C (2000x), (e) 500°C (2000x), (f) 600°C (2000x), (g) 700°C (2000x)

Fig. 2-6-Fig 2-8 show SEM morphologies of the cross-section of Ni-W-B composite coatings obtained at different heat treatment temperatures with boron concentration of 1 g/L, 3 g/L and 5 g/L respectively. From SEM observation, the different heat treatment temperatures could affect the microstructure of Ni-W matrix, for low heat treatment temperatures you can see boron particle clearly, the particle doesn't disperse into the matrix. For high heat treatment temperature (700°C) boron particles were not observed, the particles are almost inducing into the matrix to form new phases.

2.3 Boron Contents

The percentage of boron content was analyzed by ImageJ program. As shown in Fig.2-9, the boron contents were affected by changing of boron concentration. The Boron contents were increased respectively with the addition of boron concentration.

According to Tetsuo Saji et al. [16], their experiments showed that boron content in the Ni-B films increased in the presence of the boron sources.

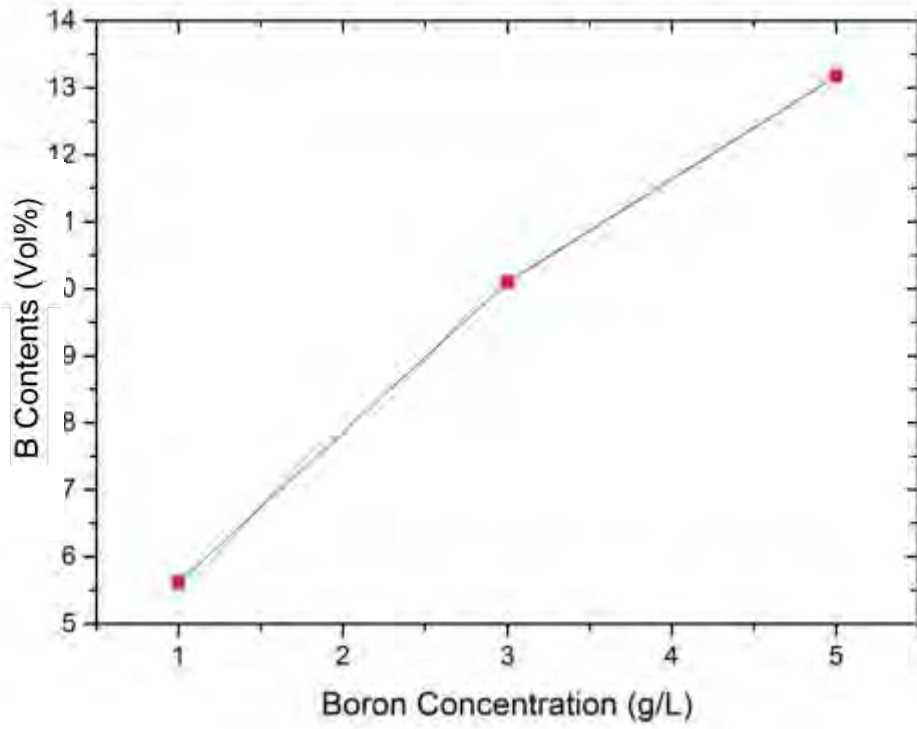


Fig. 2-9 boron contents at different boron concentration

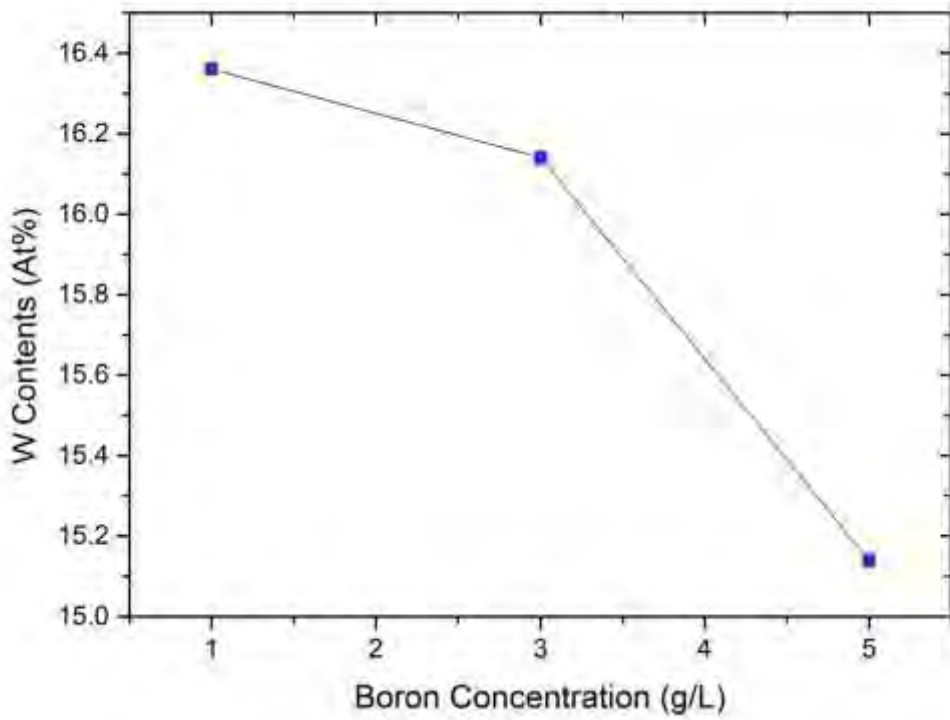


Fig. 2-10 Tungsten contents at different boron concentration

2.4 Tungsten contents

Tungsten contents in a form of the atomic percentage of tungsten were analyzed by Energy dispersive x-ray spectrometry (EDS) technique. According to the Fig.2-10, boron concentration also affect the tungsten contents on the coating by being decreased respectively with increasing boron concentration.

2.5 X-Ray Diffractometer (XRD)

For investigating structural change of Ni-W/B coatings, XRD patterns were measured as shown in Fig.2-11-Fig. 2-13. Considering in the figure of boron concentration 5 g/L in Fig.2-13, diffraction lines assigned to Ni-W alloy were appeared at without heat treatment and low temperature from 200°C to 300°C. From heating at 400°C to 700 °C, diffraction lines assigned to Ni₁₇W₃ and peaks became sharper with increasing heat treatment temperatures that might relate to the grain size and effect on the hardness of this composite coatings.

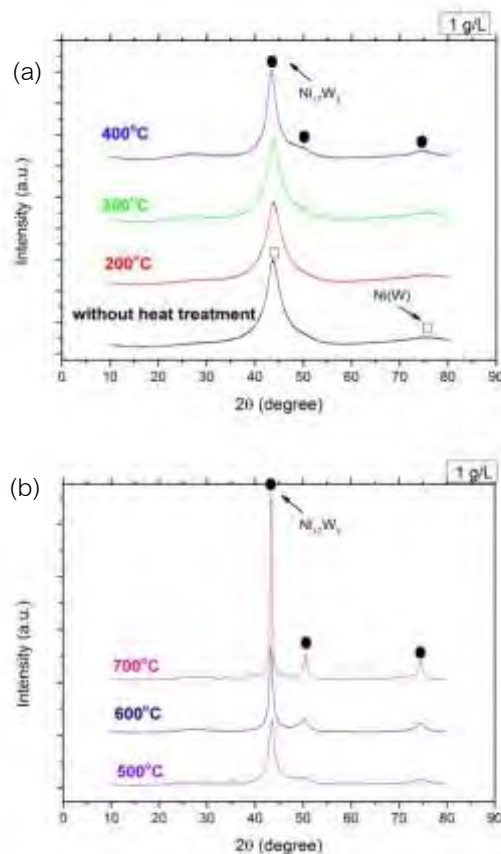


Fig. 2-11 XRD pattern of the Ni-W/B coating produced at boron concentration 1 g/L and doing heat treatment for 1 hour with different temperatures.(a) at without heat treatment and temperature from 200 °C to 400 °C (b) at temperature from 500 °C to 700 °C

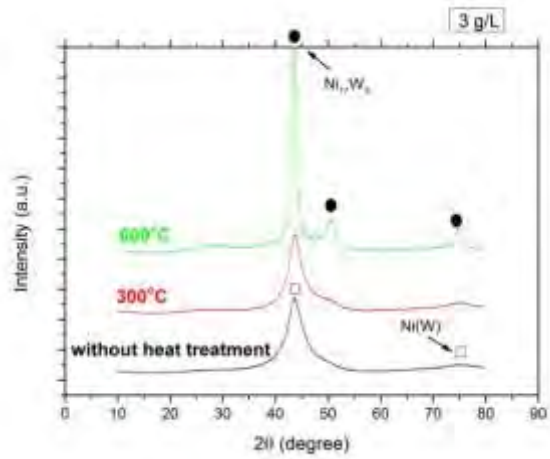


Fig. 2-12 XRD pattern of the Ni-W/B coating produced at boron concentration 3 g/L and doing heat treatment for 1 hour with different temperatures.

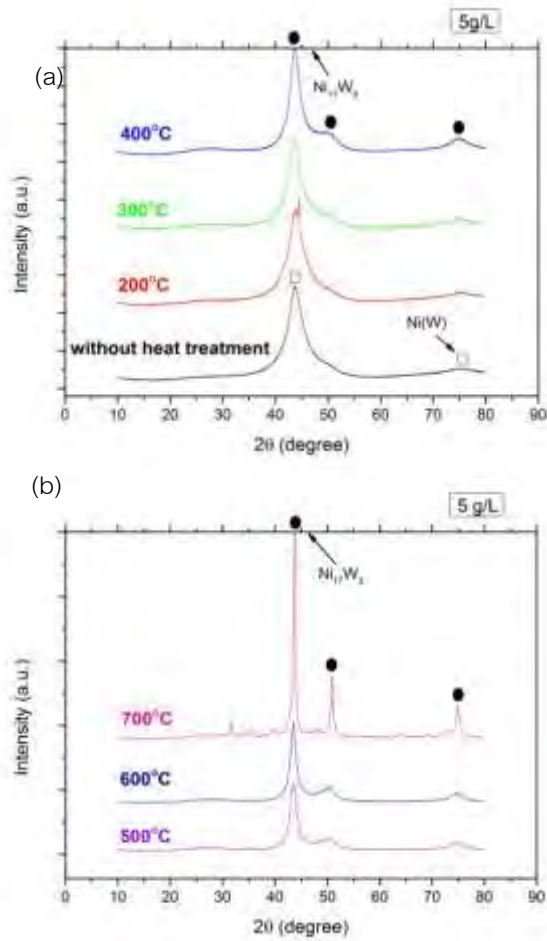


Fig. 2-13 XRD pattern of the Ni-W/B coating produced at boron concentration 5 g/L and doing heat treatment for 1 hour with different temperatures. (a) at without heat treatment and temperature from 200 °C to 400 °C (b) at temperature from 500 °C to 700 °C

2.6 Grain size

The grain size of this coating can be calculated from Scherrer's formulas:

$$\tau = \frac{K\lambda}{\beta \cos \theta} \quad (1)$$

When τ is crystalline size, K is a dimensionless shape factor that has a typical value of about 0.9, λ is the X-ray wavelength and β is the line broadening at half the maximum intensity (FWHM) in radians. As you can see from Fig. 2-14 grain size is nano-sized and when the heat treatment temperature is increased from 0°C or without heat treatment to 700°C, grain size of this coating is very small and also increased respectively, especially at 700°C grain size of Ni-W/B coating produced with different temperature is significantly increased for example, with boron concentration 5 g/L grain size is significantly increased from 6.4 nm to 25.8 nm.

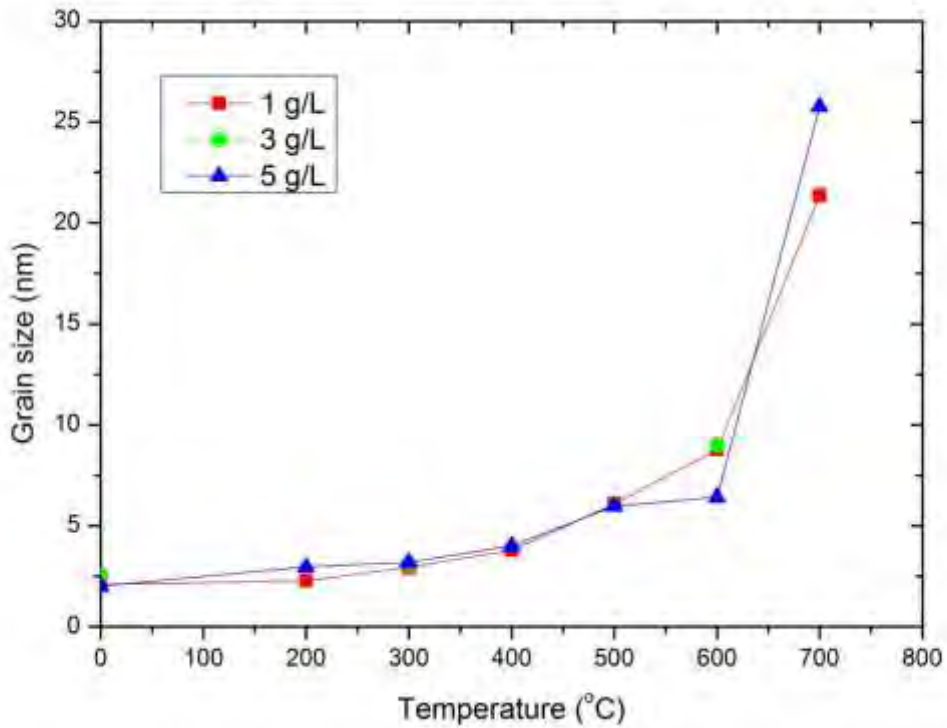


Fig. 3 Effect of heat treatment by varying temperatures on grain size of Ni-W/B coating produced at different boron concentration.

2.7. Hardness

Vickers microhardness for the cross section of coatings was measured using a microhardness tester under an indentation load of 50 gf for 15 s at seven different locations of a specimen, and the average value of the five measurements (except the maximum and minimum values) is quoted as the hardness of the film. Fig. 2-15 shows the effect of heat treatment for 1 hour by varying temperatures on hardness of Ni-W/B composite coatings produced at different boron concentration. The hardness on Ni-W/B coating is slightly increased until the heat treatment temperature is at 600 °C but hardness of this coating is decreased with increasing heat treatment temperature to 700°C. When considering the effect of boron concentration on hardness, with higher boron concentration, the hardness is increased except at 400°C that the hardness with boron concentration 5 g/L is lower than the hardness with boron concentration 1 g/L. According to the Fig.2-16, the maximum hardness is 1199 Hv produced with boron concentration of 5g/L and heat treatment temperature at 600°C for 1 hour.

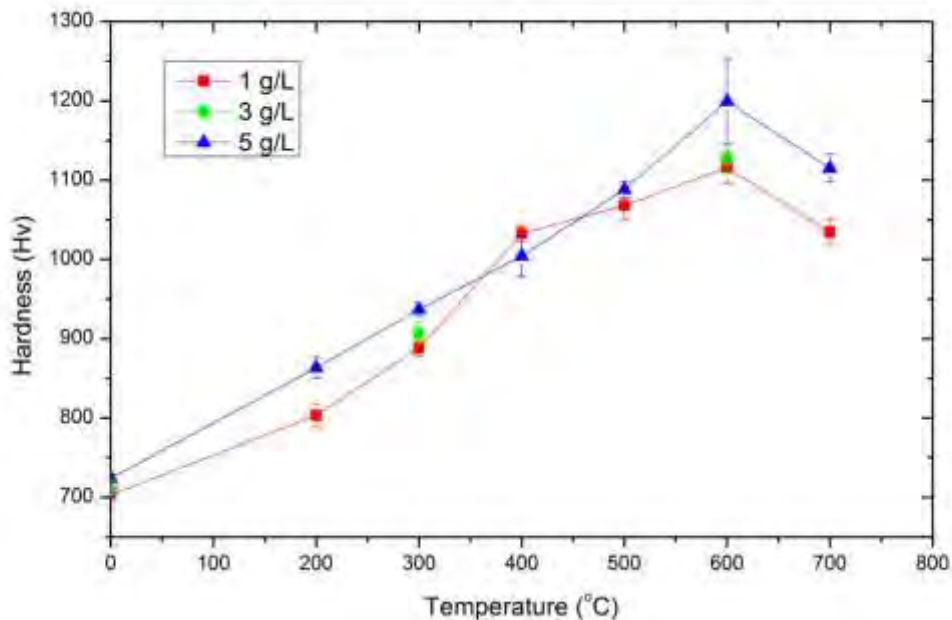


Fig. 2-15. Effect of heat treatment for 1 hour by varying temperatures on the hardness of Ni-W/B composite coatings produced at different boron concentration.

When varying the soaking time of heat treatment process, the hardness is also affected. Fig.2-16 shows the effect of heat treatment by varying soaking times from 1 hour to 3 hours

at 300 °C, 600 °C on the hardness of this composite coating produced at boron concentration 5 g/L. When the soaking time is longer, the hardness is slightly decreased respectively from soaking time 1 hour to 3 hours. The hardness at heat treatment temperature in 600 °C is still higher like previous results.

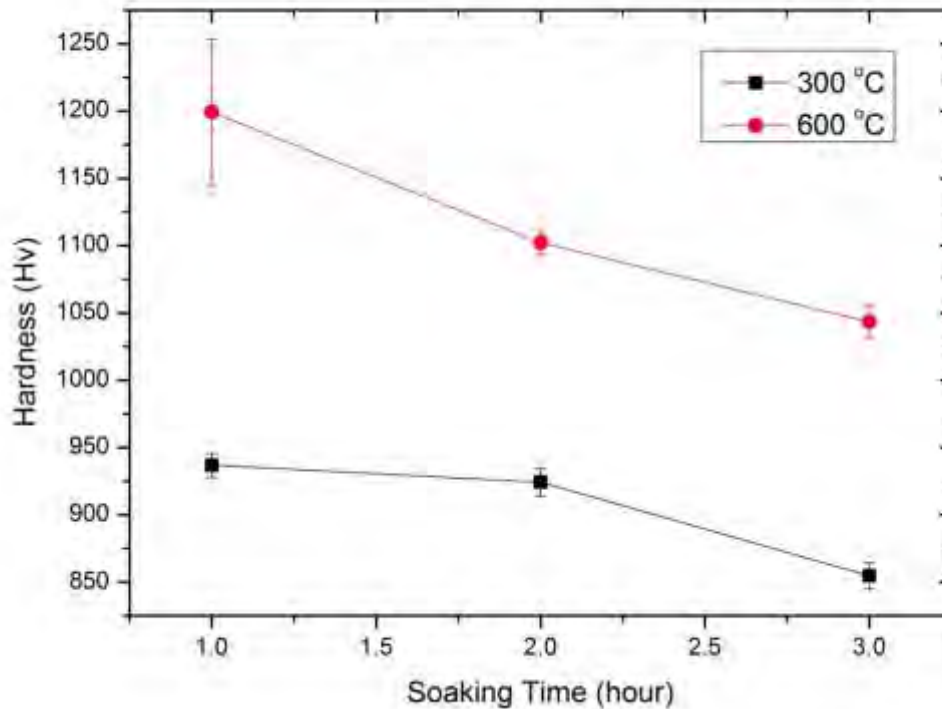


Fig. 2-16 Effect of heat treatment by varying soaking times from 1 hour to 3 hours on the hardness of Ni-W/B composite coatings produced at boron concentration 5 g/L.

Moreover, other factors besides boron concentration, heat treatment temperature and soaking time such as tungsten content, boron content and grain size can be considered as factors that can affect the hardness. The relationship between the effect of tungsten content, boron content and grain size on the hardness as presented in Fig. 2-17 – Fig. 2-19.

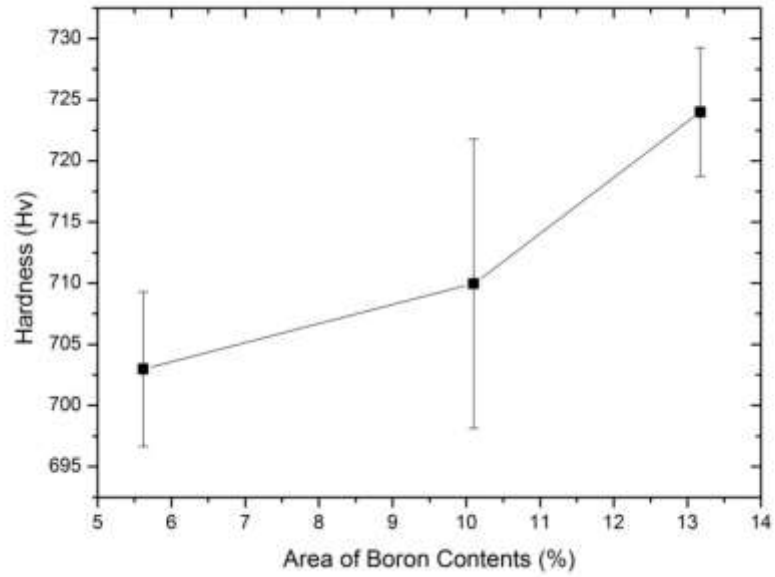


Fig. 2-17 Effect of boron content on the hardness of Ni-W/B coating composite coatings

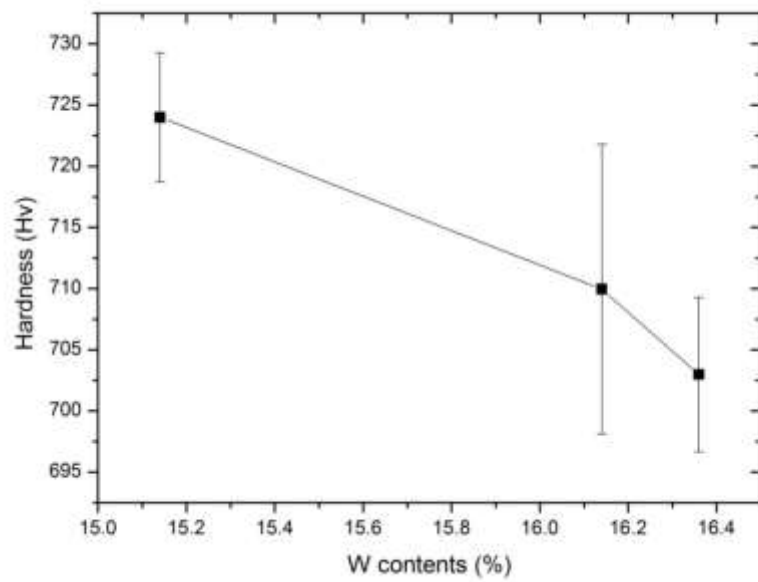


Fig. 2-18 Effect of tungsten content on the hardness of Ni-W/B coating composite coatings

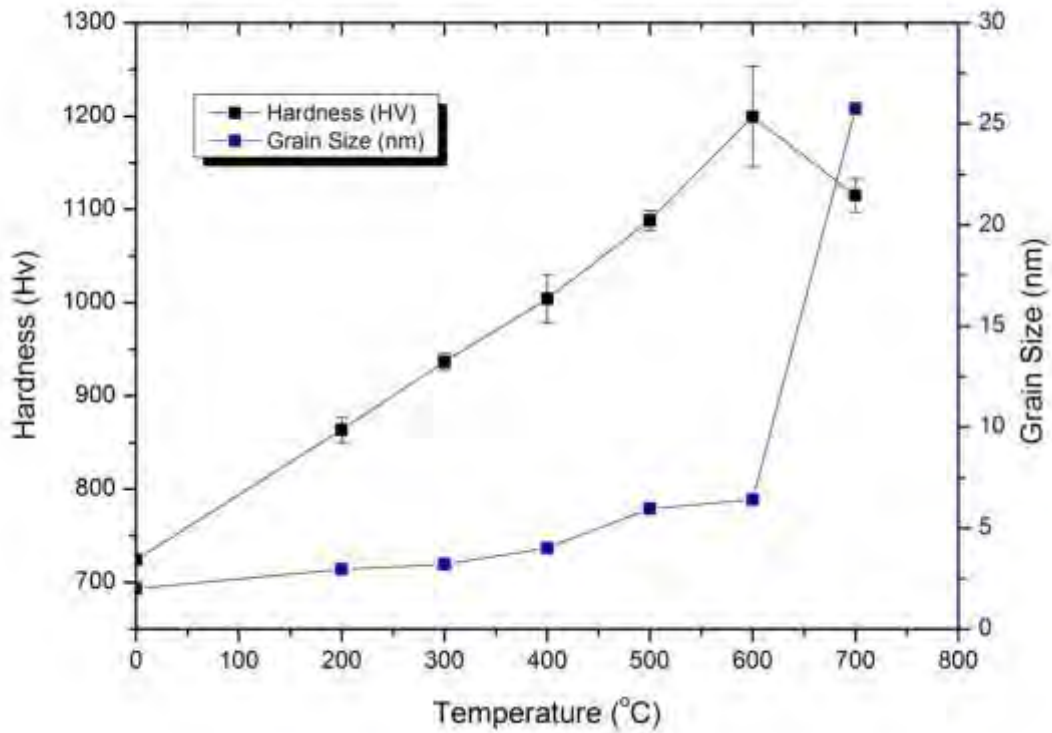


Fig. 2-19 Effect of grain size and heat treatment temperature on the hardness of Ni-W/B coating composite coatings.

2.8 Wear resistance test

Wear resistance can be evaluated by wear resistance test machine. The friction of coefficient was shown in Fig. 2-20. Fig. 2-21 shows the surface area of wear track for as-deposited composite coating and annealed coatings. Because the hardness of composite coating is lower than that of ZrO₂ ball that has the hardness around 12.75 GPa, the ZrO₂ ball will cut the composite coating during the wear process. At 600°C, the surface area of wear track is smaller than those of as-deposited coating and composite coating with annealing temperature 300°C. The results indicate that wear resistance of the coating can be enhanced by the heat treatment.

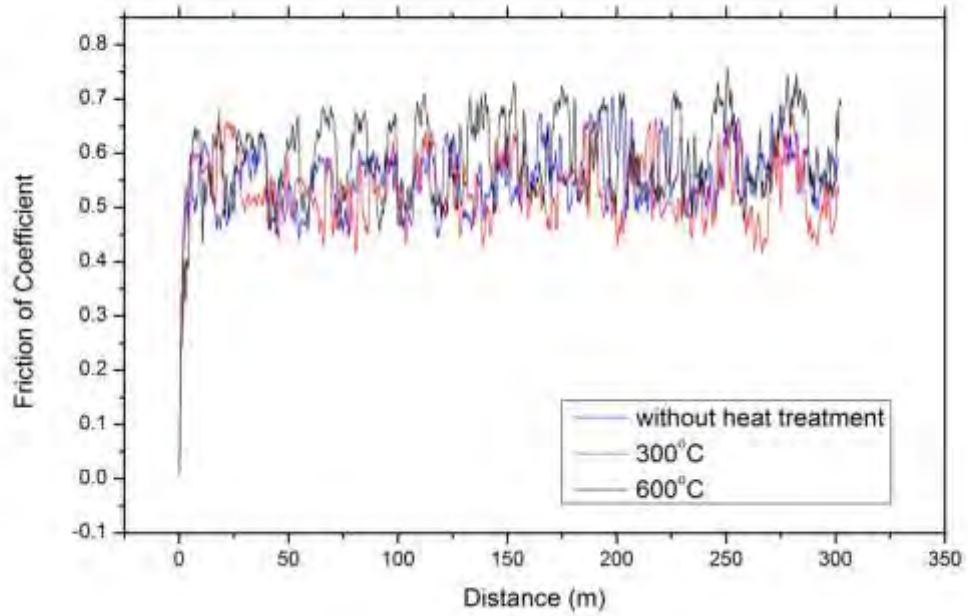


Fig. 2-20 The relation between friction of coefficient and distance.

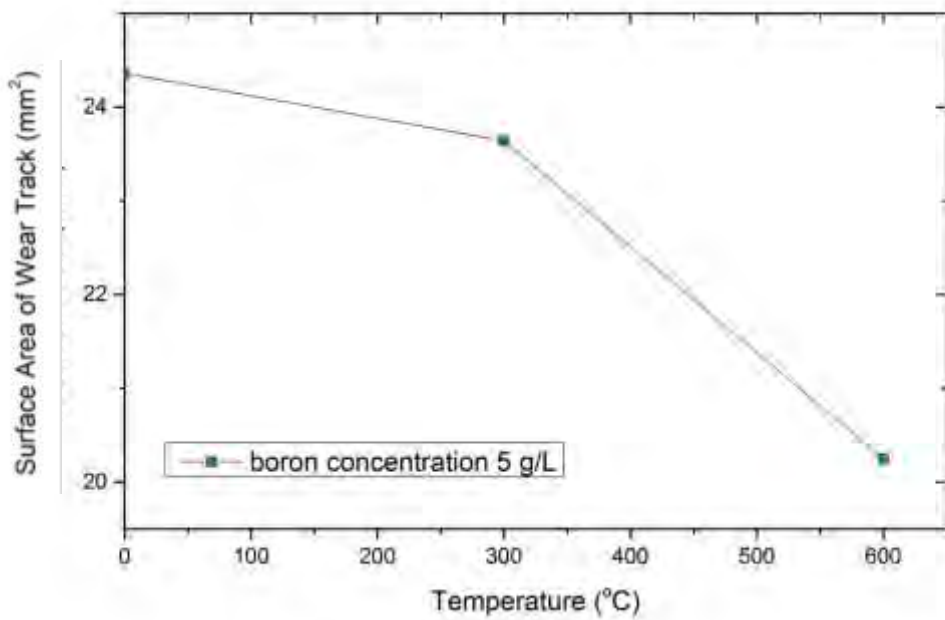


Fig.2-21 Effect of heat treatment temperature on the wear resistance of Ni-W/B coating composite coatings.

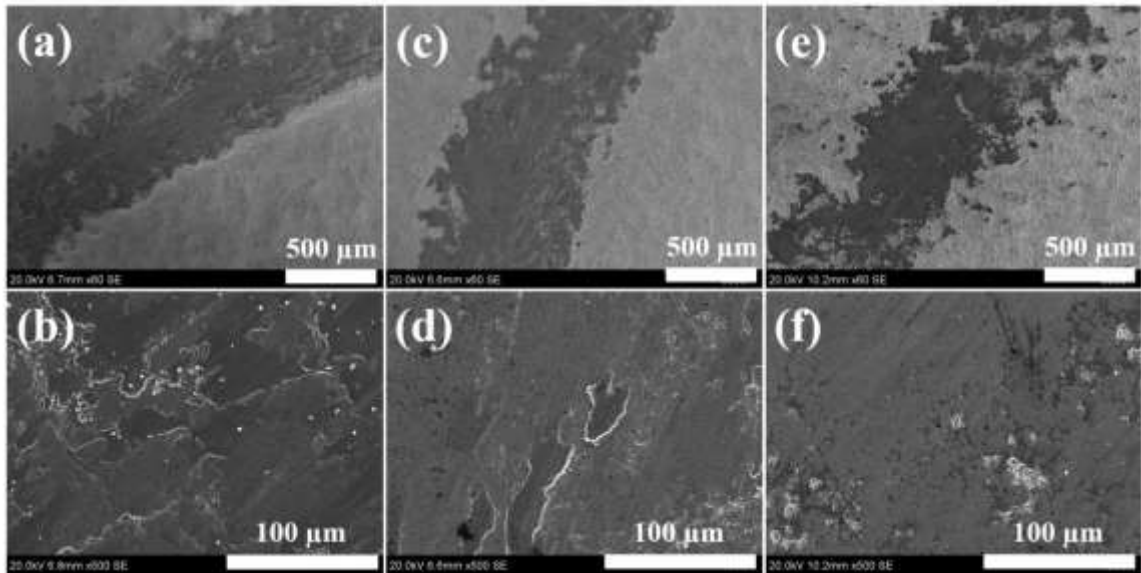


Fig. 2-22. Morphology of the worn surfaces of Ni-W/B composite coatings, (a) and (b) as-deposited, (c) and (d) heat treatment at 300 °C for 1 h, (e) and (f) heat treatment at 600 °C for 1 h.

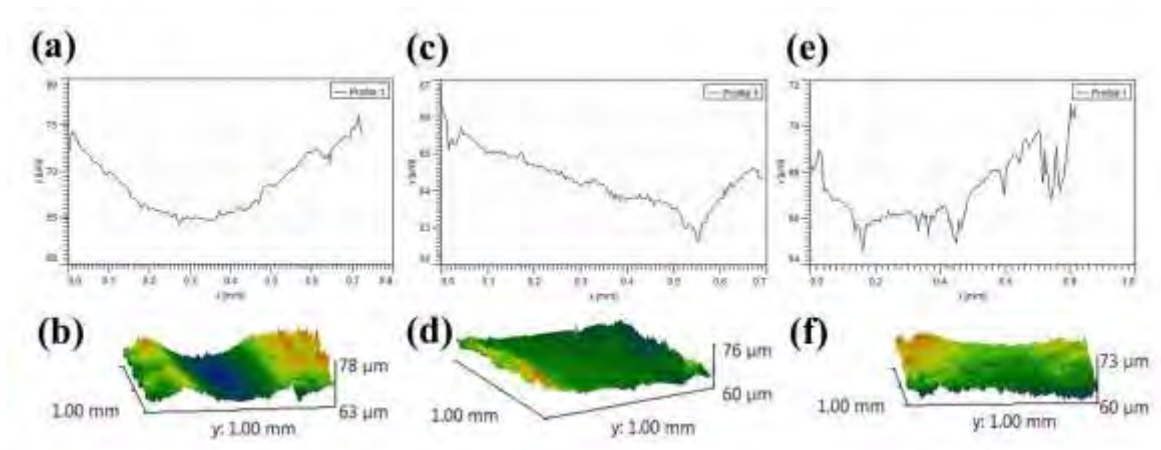


Fig. 2-23. Worn surface observation, 2D (a) and 3D (b) observation of as-deposited Ni-W/B composite coatings, 2D (c) and 3D (d) observation of 300 °C heat treatment of Ni-W/B composite coatings, 2D (e) and 3D (f) observation of 600 °C heat treatment of Ni-W/B composite coatings.

Table 2-4. Variation in micro-hardness, average coefficient of friction, wear rate, wear width and wear depth in Ni-W/B composite coatings affected by heat treatment temperature.

Temperature (°C)	Hardness (Hv)	Average coefficient of friction	Wear rate ($\times 10^{-5}$ mm ³ /Nm)	Wear track width (μ m)	Wear track depth (μ m)
As-deposited	730	0.59	10.63	714	7.76
300	940	0.53	8.51	663	3.42
600	1200	0.55	6.18	596	2.93

The SEM images of wear tracks of Ni-W/B composite coatings under different temperatures are shown in Fig. 2-22. The SEM images indicate that the wear mechanism is mainly contributed by the abrasive and adhesive wear. Furthermore, the SEM images imply that the smoother surface and light abrasive grooves were obtained on the Ni-W/B composite coating with heat treatment temperature of 600 °C. The surface profilometer was further applied to exam the wear track as shown in Fig. 2-23 and Table 2-4. The results clearly demonstrate that the heat treatment can further improve the wear resistance.

3) Corrosion of Ni-W/B composite coatings

According to the environmentally hazardous of hard chromium coating, the alternative way in electrodeposition of nickel-tungsten (Ni-W) alloys has increased in recent years due to their unique combination of corrosion resistance and tribological properties. It was reported from previous research that the corrosion rate of an amorphous Ni-W deposit in hydrochloric acid at 30°C is only 1/40 that of type 304 Stainless steel (UNS S30400) commonly used in industry. Many new method of electrodeposition has invented such as NiW–SiO₂ composite coating. With a various types of composite particle, it will effect differently on corrosion properties.

In this work, the corrosion behavior of Ni-W/B composites coating will be investigated. The main objective of this work is to study the effect of deposition parameters (current density and boron concentration) on the microstructure and corrosion resistance of coating will be determined and discussed.

3.1. Sample preparation

Sample name	Boron concentration (g/L)	Current Density (A/cm ²)
WNE1-5	1	0.1
WNE6-10	3	0.1
WNE11-14	6	0.1
WNE18	10	0.1
WNE17	0	0.1

3.2. Electrochemical characterization

The corrosion resistance of the composite coating was measured by electrochemical impedance spectrum and potentiodynamic polarization curve in 3.5 wt% NaCl solution.

1. Sonification with ethyl alcohol for 3 minutes and check weight before electrochemical testing.
2. OCP (open circuit potential) for 30 minutes. (use last OCP)
3. EIS (electrochemical impedance spectroscopy) with amplitude 10 mV. and frequency from 100 kHz – 10 mHz.
4. OCP for 30 minutes. (use last OCP)
5. Potentiodynamic polarization with the range of 250 mV. above and below the OCP with scan rate 1 mV/s.
6. Sonification with ethyl alcohol for 3 minutes and check the weight after electrochemical testing.
7. Study the surface with SEM.

3.3. Results

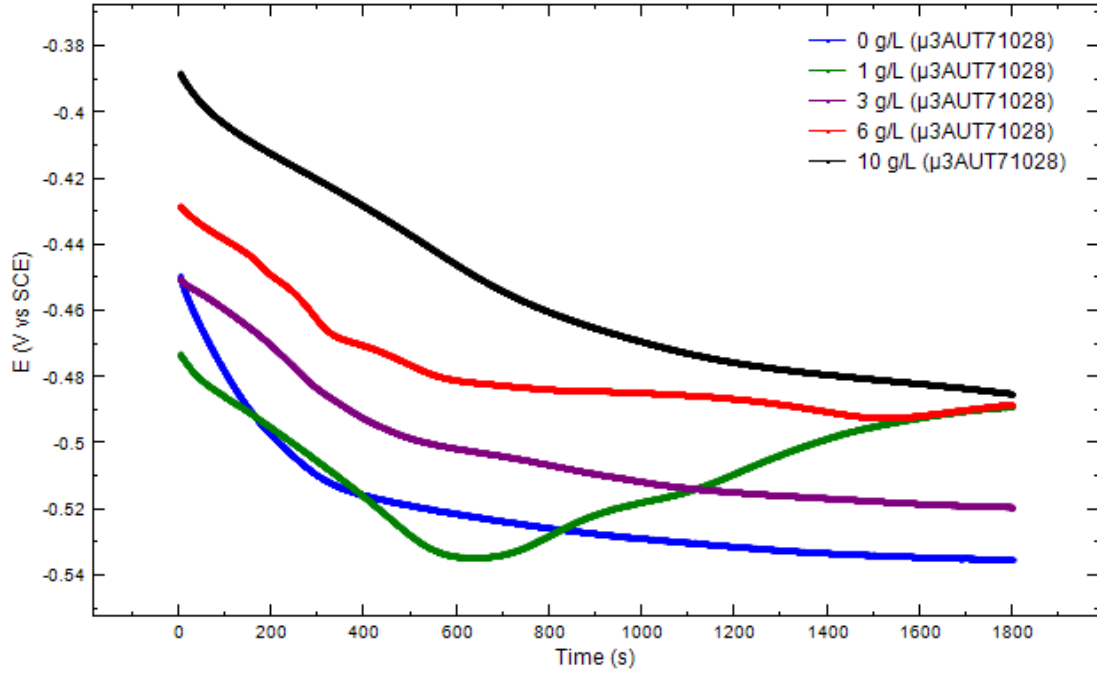


Fig. 3-1 Variation of the open-circuit potential with the immersion time in 3.5 wt% NaCl solution.

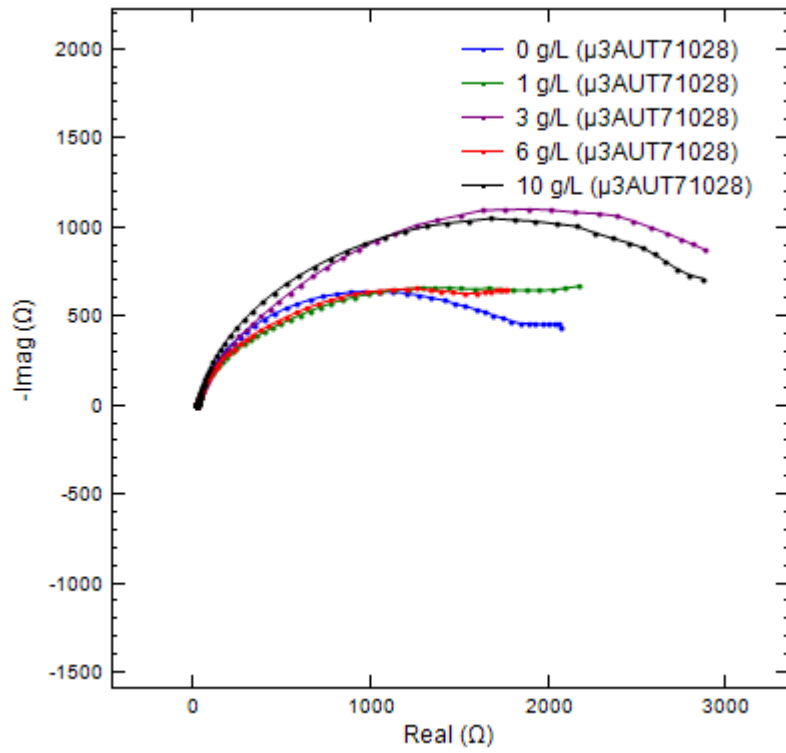


Fig. 3-2 Electrochemical impedance Nyquist plots of the composite coatings.

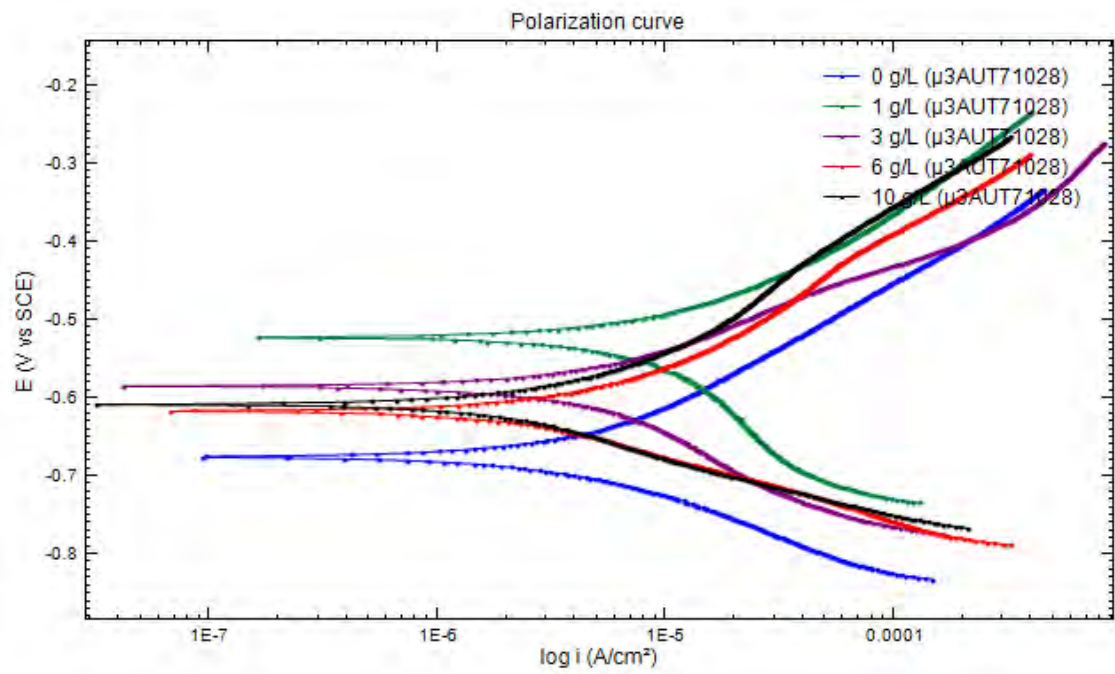


Fig. 3-3 Polarization curves of the composite coating in 3.5 wt% NaCl solution.

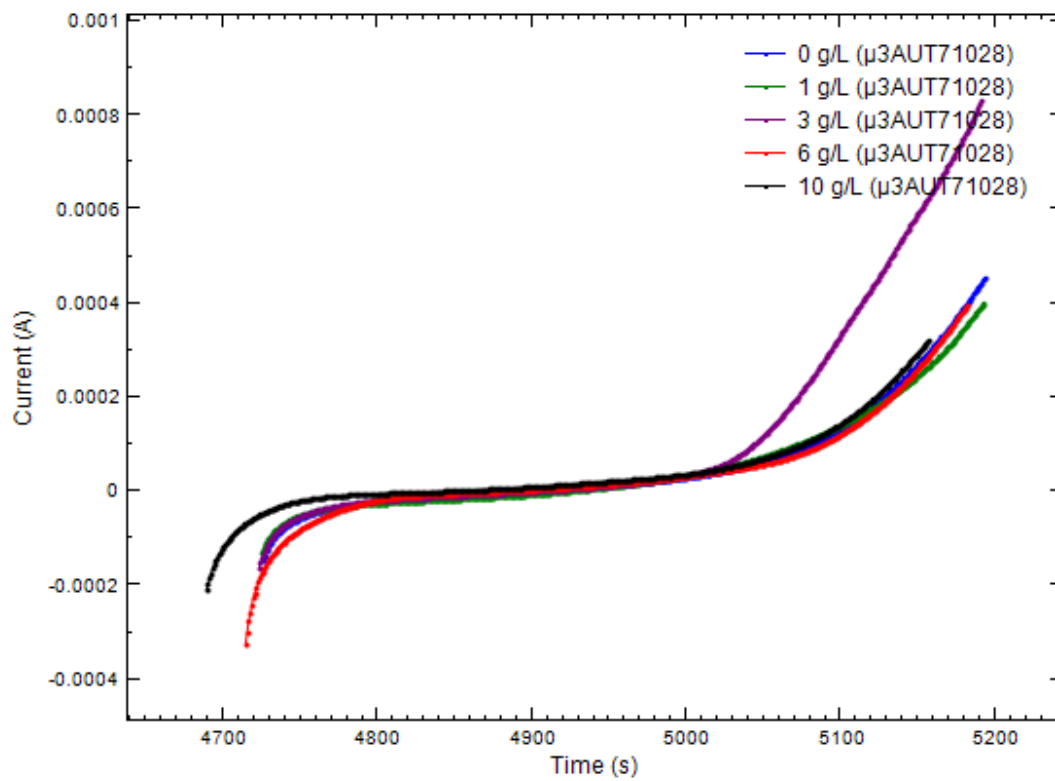


Fig. 3-4 Variation of the current vs time with composite coating

Table 3-1 Corrosion potential and corrosion current densities of the composite coating containing various concentration of boron.

Deposits (g/L)	OCP vs SCE (V)	E_{corr} vs SCE (V)	i_{corr} ($\mu A/cm^2$)	Corrosion rate (mm/year)
0	-0.535	-0.675	4.13	0.0480
1	-0.489	-0.522	13.14	0.1527
3	-0.519	-0.584	2.65	0.0308
6	-0.490	-0.616	3.18	0.0370
10	-0.485	-0.608	2.00	0.0232

From the present work, the potentiodynamic polarization studies indicated that the corrosion resistance of the Ni-W/B composite coatings was much better than the Ni-W alloy coatings. The better corrosion resistance of the composite coatings could be attributed to the boron particles acting as physical barriers against the corrosion process by filling in crevices, gaps and micron holes in the composite coatings.

4) Ni-W-B alloy coating

Electroless deposition has been used to prepare the Ni-B alloy particles or films [24-28]. In this process, dissolving reducing agents such as borohydride, release electrons which are received by metal cations, forming a metal thin film on substrates. Electrodeposition is also well-known as a typical coating method of metal or alloy thin films. The electrodeposition is simple, low cost, and easy to control growth rate. Recently, researchers reported that Ni-B films can be prepared from electrodeposition of Ni, in the presence of trimethylamine borane (TMAB) and dimethylamine borane (DMAB) which acts as boron sources [29-32]. Furthermore, Ogihara, et al., [33] prepared Ni-B films by electrodeposition method using a conventional Ni plating bath containing dimethylamine borane (DMAB) or trimethylamine borane (TMAB) as boron sources, under various plating conditions, and discuss the factors determining film hardness based on their crystalline structure and boron content. In this project, Ni-W-B alloy coating was also designed and prepared by electrodeposition method using Ni-W plating bath containing TMAB as boron source. The electrolyte is shown in Table 4-1.

Table 4-1 Chemical composition of the electrodeposition bath.

Chemicals	
Nickel(II) sulphate (NiSO ₄)	18 g/l
Sodium tungstate	53 g/l
Tri-Sodium citrate	168 g/l
Ammonium chloride (NH ₄ Cl)	31 g/l
Sodium Bromide (NaBr)	18 g/l
TMAB	1 g/L, 3 g/L, 5 g/L, 10 g/L

Table 4-2 Operating conditions

Parameters	
Temperature	40, 50, 60, 75 °C
Current Density	0.01-0.2 A/cm ²
Stirring Speed	200 RPM
pH	2-9

4.1. Surface morphology

Ni-W-B alloy coatings were successfully electrodeposited from the Ni-W plating bath, in the presence of TMAB. The surface morphology of Ni-W-B alloy coating was investigated by SEM. Fig. 4-1 and Fig. 4-2 show the SEM images of Ni-W-B alloy coatings prepared at current density of 0.1 A/cm² and bath temperature of 40, 50, 60, and 75 degree Celsius, respectively. From these figures, it can be seen that the surface becomes smooth with the bath temperature increasing. Further, the crack is easily formed at high bath temperature. Fig. 4-3 and Fig. 4-4 show the SEM images of Ni-W-B alloy coatings prepared at bath temperature of 50 degree Celsius and current density of 0.05, 0.1, 0.15, and 0.2 A/cm², respectively. The surface morphology is very different with different current density. At lower current density of 0.05 A/cm², it is dense and much flat. While the higher current density of 0.15 and 0.2 A/cm², it can form some cracks and holes on the surface of Ni-W-B alloy coating. This special crack and hole morphology may have some interesting application in industry.

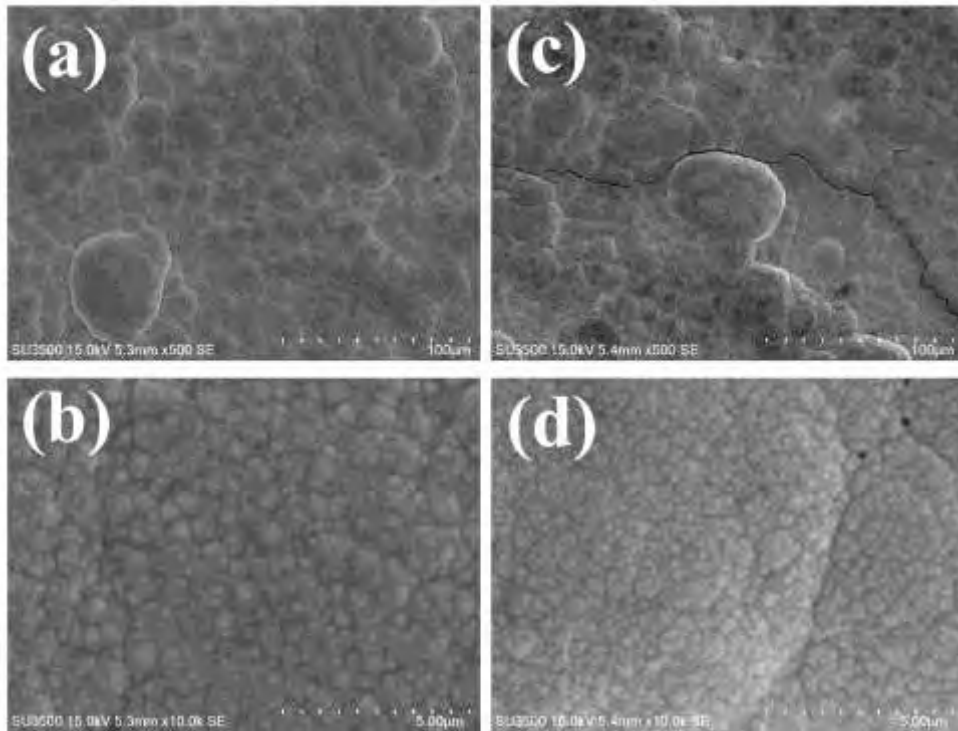


Fig. 4-1. SEM images of Ni-W-B coatings prepared at current density of 0.1 A/cm^2 and different bath temperature, (a, b) 40 degree Celsius, (c, d) 50 degree Celsius.

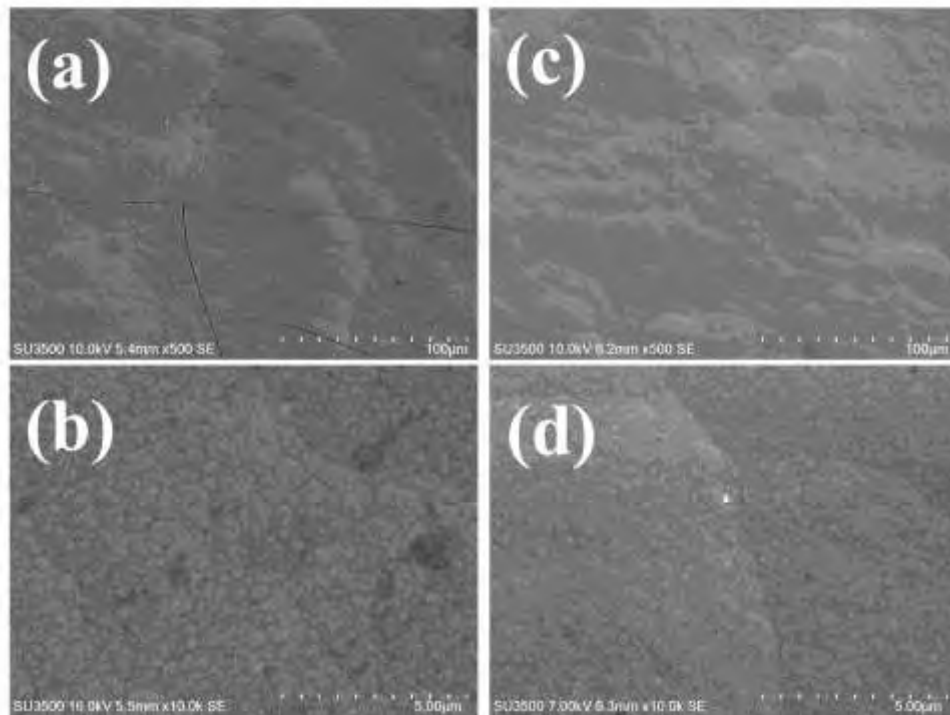


Fig. 4-2. SEM images of Ni-W-B coatings prepared at current density of 0.1 A/cm^2 and different bath temperature, (a, b) 60 degree Celsius, (c, d) 75 degree Celsius.

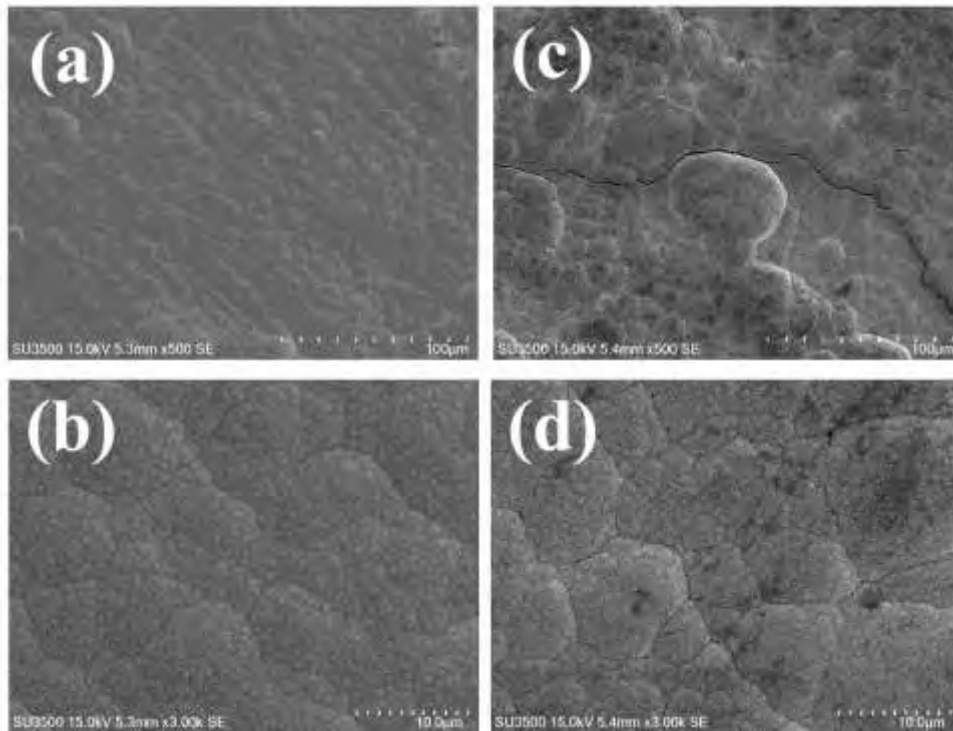


Fig. 4-3. SEM images of Ni-W-B coatings prepared at bath temperature of 50 degree Celsius and different current density, (a, b) 0.05 A/cm², (c, d) 0.1 A/cm².

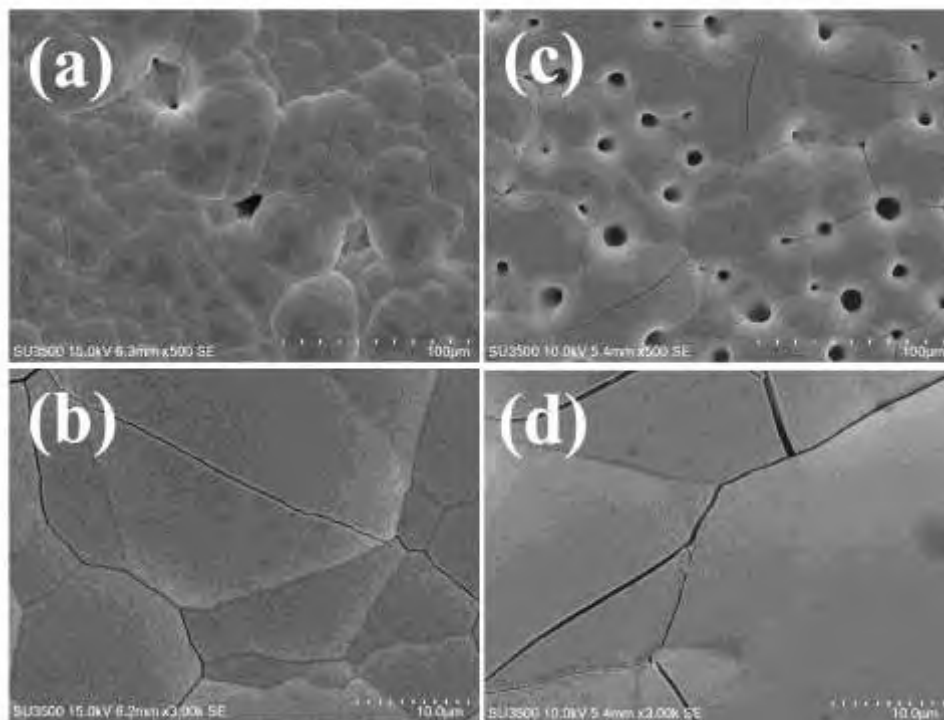


Fig. 4-4. SEM images of Ni-W-B coatings prepared at bath temperature of 50 degree Celsius and different current density, (a, b) 0.15 A/cm², (c, d) 0.2 A/cm².

Reference

- [1] A.J. Detor, C.A. Schuh, *Acta Materialia*, 55 (2007) 371-379.
- [2] C.A. Schuh, T.G. Nieh, H. Iwasaki, *Acta Materialia*, 51 (2003) 431-443.
- [3] N. Sunwang, P. Wangyao, Y. Boonyongmaneerat, *Surface and Coatings Technology*, 206 (2011) 1096-1101.
- [4] X. Zhang, J. Qin, T. Perasinjaroen, W. Aeksen, M.K. Das, R. Hao, B. Zhang, P. Wangyao, Y. Boonyongmaneerat, S. Limpanart, M. Ma, R. Liu, *Surface and Coatings Technology*, 276 (2015) 228-232.
- [5] K.-H. Hou, T. Han, H.-H. Sheu, M.-D. Ger, *Applied Surface Science*, 308 (2014) 372-379.
- [6] X. Zhang, J. Qin, M.K. Das, R. Hao, H. Zhong, A. Thueploy, S. Limpanart, Y. Boonyongmaneerat, M. Ma, R. Liu, (Submitted), (2015).
- [7] Y. Boonyongmaneerat, K. Saengkiattiyut, S. Saenapitak, S. Sangsuk, *Surface and Coatings Technology*, 203 (2009) 3590-3594.
- [8] K.-H. Hou, Y.-C. Chen, *Applied Surface Science*, 257 (2011) 6340-6346.
- [9] Y. Wang, Q. Zhou, K. Li, Q. Zhong, Q.B. Bui, *Ceramics International*, 41 (2015) 79-84.
- [10] J. Qin, T. Irifune, H. Dekura, H. Ohfuji, N. Nishiyama, L. Lei, T. Shinmei, *Physical Review B*, 85 (2012) 014107.
- [11] J. Qin, N. Nishiyama, H. Ohfuji, T. Shinmei, L. Lei, D. He, T. Irifune, *Scripta Materialia*, 67 (2012) 257-260.
- [12] A. Robin, J.C.P. de Santana, A.F. Sartori, *Surface and Coatings Technology*, 205 (2011) 4596-4601.
- [13] S.H. Yeh, C.C. Wan, *Materials Science and Technology*, 11 (1995) 589-593.
- [14] C. Müller, M. Sarret, M. Benballa, *Surface and Coatings Technology*, 162 (2003) 49-53.
- [15] K. Krishnaveni, T.S.N. Sankara Narayanan, S.K. Seshadri, *Journal of Alloys and Compounds*, 466 (2008) 412-420.
- [16] H. Ogiwara, M. Safuan, T. Saji, *Surface and Coatings Technology*, 212 (2012) 180-184.
- [17] U. Lagerpusch, E. Nembach, *Scr Mater*, 42 (2000) 615-619.
- [18] M.G. Hosseini, M. Abdolmaleki, H. Ebrahimzadeh, S.A. Seyed Sadjadi, *Int. J. Electrochem. Sci.*, 6 (2011) 1189-1205.
- [19] M.G. Hosseini, M. Abdolmaleki, S.A. Seyed Sadjadi, *Protection of Metals and Physical Chemistry of Surfaces*, 46 (2010) 117-122.
- [20] C.P. Steffani, J.W. Dint, J.R. Groza, A. Palazoglu, *Journal of Materials Engineering and Performance*, 6 (1997) 413-416.
- [21] F.-Z. Yang, Z.-H. Ma, L. Huang, S.-K. Xu, S.-M. Zhou, *Chinese Journal of Chemistry*, 24 (2006) 114-118.
- [22] G. Graef, K. Anderson, J. Groza, A. Palazoglu, *Materials Science and Engineering: B*, 41 (1996) 253-257.
- [23] T. Nagai, K. Hodouchi, H. Matsubara, *Surf. Coat. Tech.*, 253 (2014) 109-114.

- [24] A.R. Di Giampaolo, J.G. Ordoñez, J.M. Gugliemacci, J. Lira, Surface and Coatings Technology, 89 (1997) 127-131.
- [25] D. Xue, J.-F. Deng, Materials Letters, 47 (2001) 271-275.
- [26] S. Ziyuan, W. Deqing, D. Zhimin, Applied Surface Science, 221 (2004) 62-68.
- [27] M. Anik, E. Körpe, E. Şen, Surface and Coatings Technology, 202 (2008) 1718-1727.
- [28] B. Oraon, G. Majumdar, B. Ghosh, Materials & Design, 29 (2008) 1412-1418.
- [29] K.H. Lee, D. Chang, S.C. Kwon, Electrochimica Acta, 50 (2005) 4538-4543.
- [30] K. Krishnaveni, T.S.N. Sankara Narayanan, S.K. Seshadri, Materials Chemistry and Physics, 99 (2006) 300-308.
- [31] H. Zhou, Q. Yu, Q. Peng, H. Wang, J. Chen, Y. Kuang, Materials Chemistry and Physics, 110 (2008) 434-439.
- [32] Y.N. Bekish, S.K. Poznyak, L.S. Tsybul'skaya, T.V. Gaev'skaya, Electrochimica Acta, 55 (2010) 2223-2231.
- [33] H. Ogihara, K. Udagawa, T. Saji, Surface and Coatings Technology, 206 (2012) 2933-2940.

3. การดำเนินงานในช่วงต่อไป

- Study the effect of deposition parameters on Ni-W-B alloy coating, e.g., TMAB concentration, current density, bath temperature, pH, heat treatment.
- Wear resistance of Ni-W-B/B composite coatings, e.g., Weight loss, SEM, EDS, etc. of the wear track.
- Heat treatment of the Ni-W-B/B composite coatings, e.g., XRD, SEM, Cross-section, Wear resistance.

4. อุปสรรคในการดำเนินงานและแนวทางแก้ไข

-

ลงชื่อ 

Dr. Jiaqian Qin

วันที่ 17 January 2560

Electrodeposition and Mechanical Properties of Ni-W Matrix Composite Coatings with Embedded Amorphous Boron Particles

Jiaqian Qin^{1,2,*}, Xinyu Zhang^{2,*}, Kamontorn Umporntheep³, Vasin Auejitthavorn³, Rongxia Li², Panyawat Wangyao^{3,*}, Yuttanant Boonyongmaneerat¹, Sarintorn Limpanart¹, Mingzhen Ma², Riping Liu²

¹ Metallurgy and Materials Science Research Institute, Chulalongkorn University, Bangkok 10330, Thailand

² State Key Laboratory of Metastable Materials Science and Technology, Yanshan University, Qinhuangdao 066004, P.R. China

³ Metallurgical Engineering Department, Faculty of Engineering, Chulalongkorn University, Bangkok 10330, Thailand

*E-mail: jiaqianqin@gmail.com, xyzhang@ysu.edu.cn, panyawat@hotmail.com

Received: 18 August 2016 / Accepted: 10 September 2016 / Published: 10 October 2016

Hard nickel-tungsten/boron (Ni-W/B) composite coatings were designed and successfully prepared on the surface of low carbon steel by direct current electrodeposition. The effect of boron concentration in the solution on the amount of boron contents in the deposits and mechanical properties were investigated. SEM and EDS elemental mapping show a uniform dispersion of boron particles into the Ni-W matrix could be observed. ICP results reveal that high boron content (~21.7 wt.%) of composite coatings can be achieved at boron concentration of 5 g/L. High hardness of 1266 HK was obtained from the Ni-W/B composite coatings with higher boron contents. This method is much easier to obtain a high hardness of Ni-W/B coatings which is comparable to that of hard chromium plated coatings. Furthermore, the wear resistance is also enhanced for the Ni-W coatings with incorporation of boron particles.

Keywords: Composite coatings; Electrodeposition; Boron; Hardness; Wear resistance

1. INTRODUCTION

Metal matrix composite coatings containing dispersed particles usually exhibit some good properties such as dispersion hardening, self-lubricity, improved wear and corrosion resistance [1-4]. In order to enhance the properties of materials surface, coatings are usually coated onto the materials

by using dry processes (e.g., chemical or physical vapour deposition methods) or wet processes (electrodeposition or electroless plating). The dry process can provide high-quality, super-hard coatings, but it needs extreme reaction conditions and precise control of gas flow. In contrast, the wet process is a simple method. For example, plating (i.e., electrodeposition), which is one of the most important techniques for fabricating nanocomposite and nanocrystal hard coatings [5-10].

The electrodeposited films show excellent functional properties and decorative applications and improve its operating properties subjected to external hazards. Recently, the developed Ni-W coatings exhibit higher hardness, higher heat resistance and also a better corrosion behaviour compared to Ni coatings [9-11]. However, the hardness of Ni-W still can't compare to the traditional chromium coating, which exhibits high hardness of ~ 10 GPa[10]. Incorporation of hard particles to the Ni-W nanocoatings could further enhance the hardness and wear resistance of Ni-W coating. The Ni-W/hard particles composite coatings which have been investigated and fabricated successfully include Ni-W/diamond [7, 12, 13], Ni-W/WC[14], Ni-W/ Al_2O_3 [15], and Ni-W/ SiO_2 [16]. Boron, the elemental neighbour to carbon in the periodic system of elements, which is also known to be superhard material [17, 18]. The high hardness of boron could also improve the nanostructured Ni-W coatings. However, there is no report on the effect of boron on the microstructure and mechanical properties of nanostructured Ni-W coating.

In this work, the Ni-W/B composite coatings were prepared by electrodeposition in a Ni-W plating bath containing amorphous boron particles. Afterwards, surface and cross-section morphology of those composites were observed to determine the effect of the incorporation of boron particles. The microhardness and wear performance of the composites was studied to determine the influence of boron particles. In particular, we measured the boron content in the coatings and determined the relationship between boron content and microhardness of the composite coatings. The strengthening mechanism for the coatings was also discussed according to the experimental evidences.

2. EXPERIMENTAL DETAILS

The Ni-W/B composite coatings were fabricated by a direct current electrodeposition method in a Ni-W plating bath with boron particles suspension. The Ni-W plating bath can be prepared using the following chemicals: 18 g/L $\text{NiSO}_4 \cdot 6\text{H}_2\text{O}$, 53 g/L $\text{Na}_2\text{WO}_4 \cdot 2\text{H}_2\text{O}$, 168 g/L $\text{Na}_3\text{C}_6\text{H}_5\text{O}_7 \cdot 2\text{H}_2\text{O}$, 31 g/L NH_4Cl , 18 g/L NaBr . Amorphous boron particles with concentration of 1 g/L, 3 g/L, 5 g/L, and 10 g/L were used. The received boron powder was examined by scanning electron microscopy (Fig. 1(a)). The particle size was analysed by software as shown in Fig. 1(b). The results show that the boron particles have the size ~ 0.03 - 1.27 μm , and mean size ~ 0.14 μm . All specimens were deposited onto low carbon steel substrates of commercial purity. The steel substrates were masked with insulated tape to leave 20×20 mm^2 of exposed area. The platinum mesh was applied as counter electrode with a spacing of approximately 5 cm between the two electrodes. The basic electrodeposition parameters were the direct current density of 0.1 A/cm^2 , a depositing time of 120 min, an electrolyte stirring speed of 100 rpm, an electrolyte temperature of 75 $^\circ\text{C}$, and a pH value of 8.9. All chemicals were the analytic grade reagents (CARLO). Before electrodeposition, the electrolyte with suspending the boron particles

was stirred at 400 rpm for 1 h and sonicated for 30 min to prevent the particle agglomeration. Prior to each experiment, the steel plates were pre-treated in alkaline sodium hydroxide solution (60 °C), hydrochloric acid (14%) solution, and then rinsed in distilled water. The direct current was applied to the system by a rectifier (SMD-10P, Dashun, Handan, China).

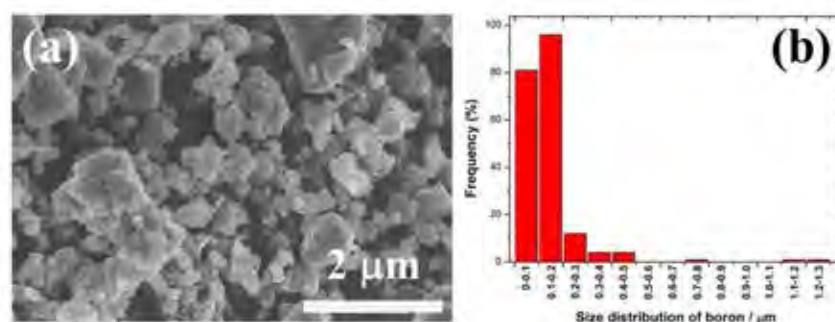


Figure 1. (a) SEM images of amorphous boron particles (b) size distribution of boron particles.

The surface morphology and the composition (Ni and W contents) were studied by scanning electron microscopy (SEM, Hitachi, S4800) and energy-dispersive spectroscopy (EDS), respectively. To determine the boron content in the deposits, the samples were measured using an inductively coupled plasma emission spectrometer (ICP-MS, Thermo Scientific). The phases of the composite coatings were analysed by X-ray diffraction (XRD) using an X'Pert Pro diffractometer (Panalytical). The surface profilometer (Gauges, Ambs, US) was carried out to measure the surface roughness. Knoop microhardness for the surface of coatings was calculated by using a microhardness tester under an indentation load of 100 gf for 15 s after seven different measurement points.

The wear performance was tested by using a CSM reciprocating-sliding tribometer. During the wear testing, the dynamic coefficient of friction was monitored by the connected computer. Si_3N_4 ball, with a load of 10 N, was set to run at 100 mm/s with reciprocation amplitude of 10 mm and without lubrication at room temperature of 20-25 °C. Because the Si_3N_4 ball is harder than the obtained coatings, the ball can wear the coatings, and lower wear resistance will generate the larger surface area of wear track. Therefore, in this study, the wear performance is evaluated using the surface area of wear track.

3. RESULTS AND DISCUSSION

The Ni-W/B composite coatings were successfully prepared by co-deposition of boron particles with Ni-W alloy under magnetic stirring. Figure 2 shows the SEM images of the typical surface morphology of the as-deposited Ni-W and Ni-W/B composite coatings. It can be seen that all samples exhibit the columnar structure. With the boron incorporation, the columnar size becomes smaller. The Ni-W/B composite coatings (Fig. 2 (b-d)) are much more uniform, smooth, and compact surface

structure compared to Ni-W coatings (Fig. 2(a)). Furthermore, the addition of boron particles in the Ni-W matrix decreases the surface roughness and alters the chemical composition. The average surface roughness (R_a) of electrodeposited Ni-W coatings is $1.58 \pm 0.1 \mu\text{m}$, while R_a of electrodeposited Ni-W/B composite coatings is $1.26 \pm 0.07 \mu\text{m}$, $0.93 \pm 0.04 \mu\text{m}$, $1.13 \pm 0.08 \mu\text{m}$, and $1.19 \pm 0.06 \mu\text{m}$, for boron concentration in the plating bath of 1 g/L, 3 g/L, 5 g/L, and 10 g/L, respectively. The surface roughness further reveals that the addition of boron can smooth the surface. This behavior has been reported by previous researchers for Cu-Si₃N₄ composite coatings [19]. Moreover, the surface roughness increases with the increasing concentration of boron above 3 g/L, this may be caused by the boron particles cohering and forming secondary particles in the solution when the boron concentration is larger than 3 g/L. The similar result was also obtained for the composite coatings of Ni-W/MWCNT[4].

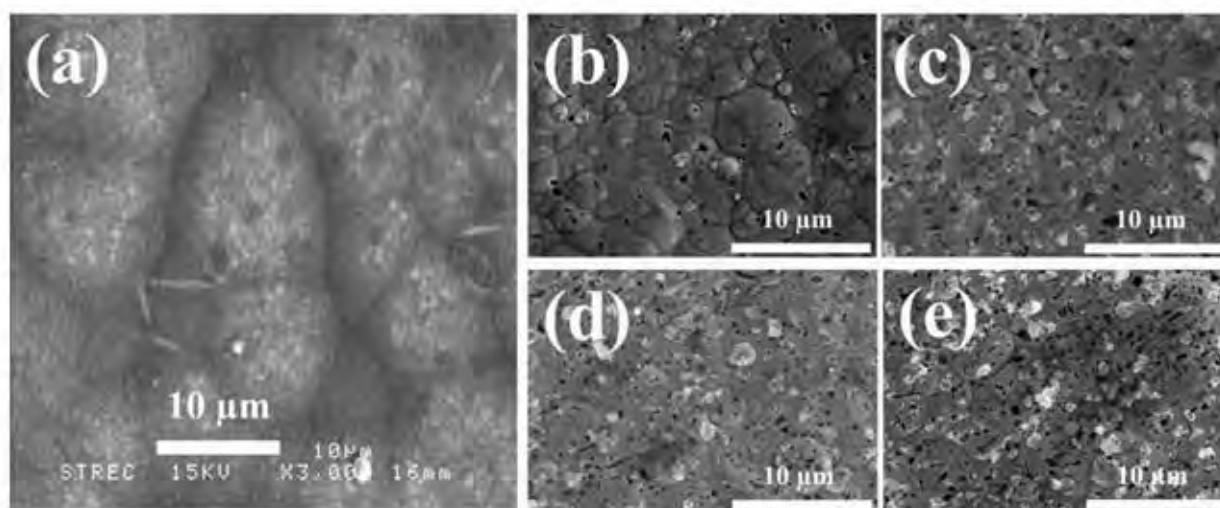


Figure 2. SEM images of Ni-W coating (a), Ni-W/B composite coatings with different boron concentration in the plating bath, (b) 1 g/L, (c) 3 g/L, (d) 5 g/L, (e) 10 g/L.

The EDS elemental mapping was also carried out to study the element distribution of as-deposited Ni-W/B composite coatings obtained with different concentration of boron in solution. Figure 3(a, b) show the Ni and W elemental mapping, respectively, for the Ni-W/B composite coatings. Figure 3(c-f) present the boron elemental mapping images of Ni-W/B composite coatings prepared with 1g/L, 3 g/L, 5 g/L, and 10 g/L, respectively. The boron EDS mapping shows that boron particles are uniformly distributed in the Ni-W alloy matrix. The boron EDS mapping also indicates that the boron content increases with concentration of boron particles in bath from 1 to 5 g/L, while above 5 g/L, the boron content slightly decreases.

The boron content in the composite coatings was further determined by ICP. Fig. 4 shows the relationship between boron concentration in solution and boron content in deposits. From the results presented in Fig. 4, it is interesting to find that the amount of embedded boron particles in the deposits increases sharply with boron concentration in the bath from 1 to 5 g/L, while above 5 g/L, the boron content slightly decreases. The maximum boron content in deposits ($\sim 21.7 \text{ wt.}\%$) can be obtained

according to the ICP results. Moreover, the cross-section morphology and the distribution of boron particles in the Ni-W matrix were also investigated.

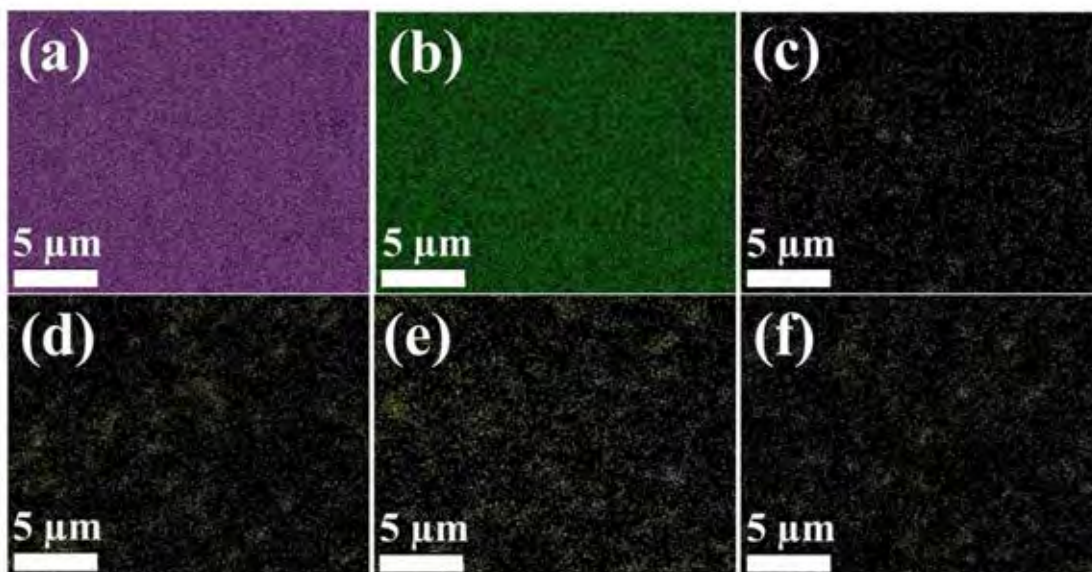


Figure 3. EDS elemental mapping images, (a) Ni, (b) W, and B in the Ni-W/B composite coatings prepared at different boron concentration in plating bath, (c) 1 g/L, (d) 3 g/L, (e) 5 g/L, (f) 10 g/L.

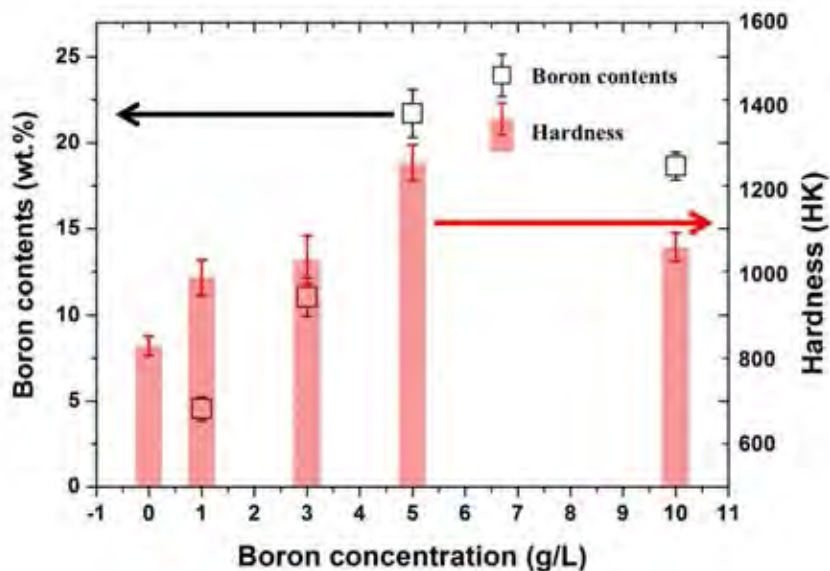


Figure 4. (a) The effect of boron concentration in the bath on boron content (left axis) and hardness of coatings (right axis).

Figure 5(a-d) show cross-sectional SEM images of the Ni-W/B composite coatings fabricated with 1 g/L, 3 g/L, 5 g/L, and 10 g/L, respectively. The thickness of Ni-W/B composite coatings was measured (~47-49 μm) from the cross-sectional SEM images, as shown in Fig. 5. It further implies that

boron particles of sub-micron sizes ($< 1 \mu\text{m}$) are uniformly co-deposited into the Ni-W matrix, and many boron particles are embedded in Ni-W deposition matrix. Moreover, from the cross-sectional SEM images, the volume percentages of boron particles in coating could be estimated by image analysis software (ImageJ). The image analysis results show that the volume percentage of incorporated boron particles into Ni-W matrix is 7 vol.%, 15 vol.%, 20 vol.%, and 18 vol.%, for boron concentration in the bath of 1 g/L, 3 g/L, 5 g/L, and 10 g/L, respectively. This trend of boron content in the coatings is in good agreement with the ICP measurement and EDS elemental mapping.

In the current study, the deposited surface area is $20 \times 20 \text{ mm}^2$, and the thickness of all composite coatings is $\sim 47\text{--}49 \mu\text{m}$ (Fig. 5), then the volume of all composite coatings is almost same. Therefore, the volume percentage of deposited Ni-W matrix is 93 vol.%, 85 vol.%, 80 vol.%, and 82 vol.%, for boron concentration in the bath of 1 g/L, 3 g/L, 5 g/L, and 10 g/L, respectively. This result demonstrated that the amount of Ni-W in the coating that was deposited in the electrolyte declined as the boron concentration increased. In the Ni-W and boron particles co-electrodeposition system, there is competition between boron and metals during the co-deposition process, boron particles can be absorbed onto the surface of the cathode. The boron particles would shield the growth of crystals, resulting in decelerating the Ni-W deposition rate, yielding smaller and better grain sizes of Ni-W coating, finally forming a compact and uniform coating structure.

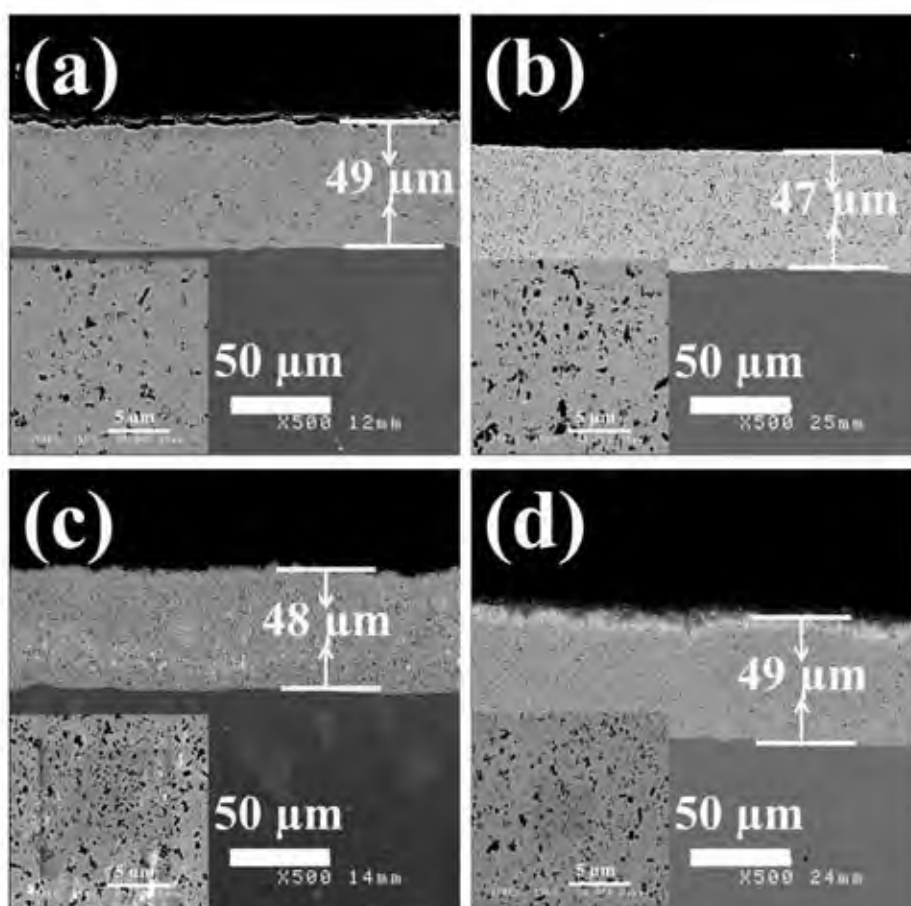


Figure 5. Cross-sectional SEM images of Ni-W/B composite coatings with different boron concentration in bath, (a) 1 g/L, (b) 3 g/L, (c) 5 g/L, (d) 10 g/L.

According to the results from EDS mapping observation, ICP measurement, and ImageJ software analysis, the boron content in the coatings increases sharply with boron concentration in the bath from 1 to 5 g/L, while above 5 g/L, the B content slightly decreases. Here, we can explain the mechanism of incorporation of boron particles in the electrodeposited Ni-W matrix by Guglielmi's model[20]. According to Guglielmi's two step adsorption model, the increase in the boron content in the deposits observed up to 5 g/L is attributed to the increase in the number of particles in the plating bath. The higher concentration can improve the adsorption rate of boron particles on the growing coatings. Thus, a higher percentage of boron particles in Ni-W matrix could be obtained according to Yeh and Wan results[20]. While the boron concentration in bath reached at 10 g/L, the boron content is lower than that of coating prepared at 5 g/L. Thus it might be due to the agglomerate of boron particles with much higher boron concentration in the plating bath. Similar results were also reported by the other researchers [13, 21-23]. At the high boron concentration of 10 g/L, some boron particles in the deposition bath might aggregate together. Therefore, the boron content might decrease at 10 g/L of boron concentration in the plating bath because their size increases due to aggregation. In the current study, the boron concentration of 5 g/L is an optimized value in the Ni-W plating bath to prepare the maximum boron content in coating.

The chemical composition was also determined by EDS. The effect of boron concentration in the plating bath on the W content in the deposits is plotted in Fig. 6. The results reveal that the W content in the coatings decreases slightly with boron concentration in the plating bath increasing. From the Fig. 6, the boron concentration in the plating bath was increased from 0 to 10 g/L, the W content in the deposits decreased from ~42 wt.% to ~38 wt.%. Hou et al. [13] also reported a similar tendency in Ni-W/diamond electrodeposition system. The boron particles in the plating bath could absorb hydrogen ions near the cathode and inhibit the reduction reaction of hydrogen ion to hydrogen. The W content in the deposits decreasing might be caused by the hydrogen ions absorbed by boron particles in the plating bath [24, 25].

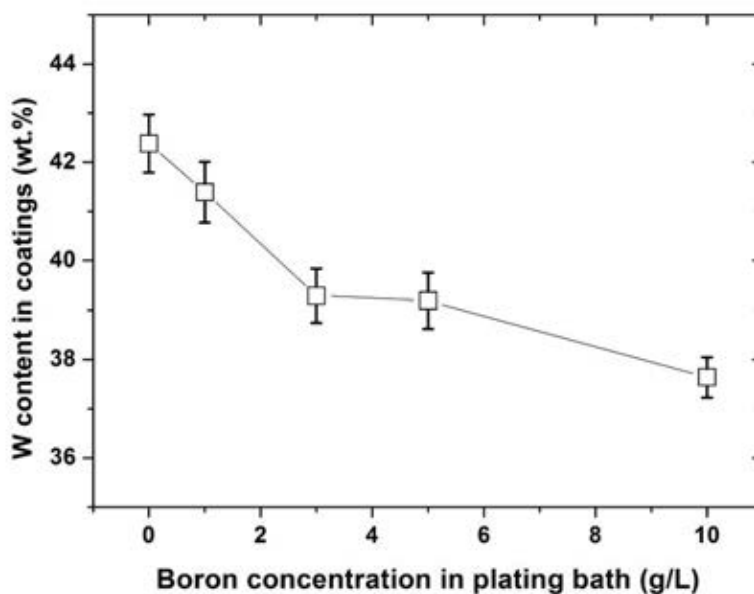


Figure 6. The dependence of W content in Ni-W and Ni-W/B coatings on the boron concentration in the plating bath.

The XRD patterns of coatings with different boron concentration in solution is shown in Fig. 7. From the XRD results, the phase for all the obtained coatings appears to be similar. Ni(W) solid solution can be identified for all the as-deposited films. The incorporation of boron particles to the Ni-W coating does not affect the coatings in terms of phase and their texture. Furthermore, the grain size of Ni-W and Ni-W/B coatings was also estimated from the width of the Ni (111) peaks. The grain size is 2.8 nm, 2.4 nm, 2.3 nm, 2.2 nm, and 2.3 nm, for 0 g/L, 1 g/L, 3 g/L, 5 g/L, and 10 g/L of boron concentration in bath, respectively.

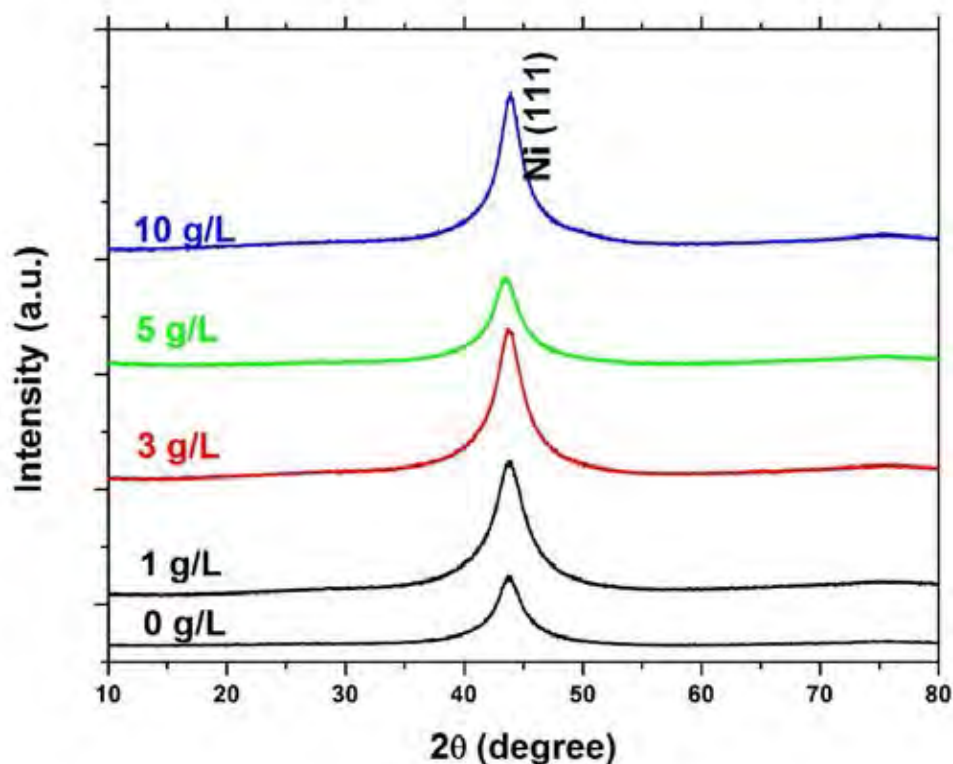


Figure 7. XRD patterns of coatings with different boron concentration in the plating bath.

The microhardness of Ni-W and Ni-W/B coatings was measured by Knoop Hardness Tester, as shown in Fig. 4. Without incorporation of boron particles, the electrodeposited Ni-W coating exhibits the hardness of 835 HK at current density of 0.1 A cm^{-2} , which is little higher than that of the reported vickers microhardness value[10]. The incorporations of boron particles of 1, 3, 5, and 10 g L^{-1} , have the hardness of 994, 1037, 1266, and 1067 Hk, respectively (Fig. 4). The hardness results indicate that the incorporation of boron in coatings can result in a marked enhancement of hardness. The hardness increases with the increase in boron concentration in the plating bath from 1 to 5 g/L, while above 5 g/L, the hardness decreases.

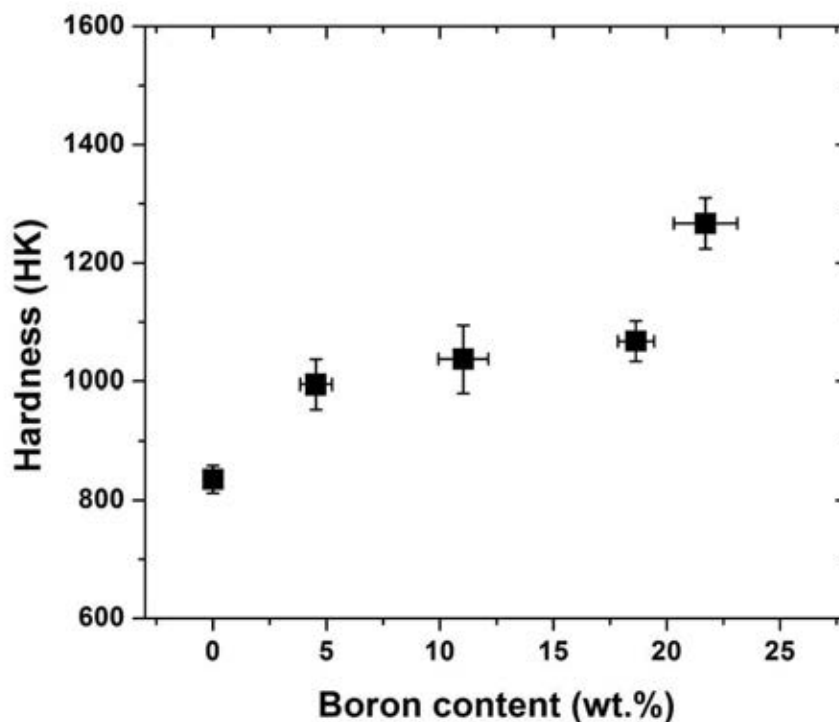


Figure 8. Hardness of Ni-W coating and Ni-W/B nanocomposite coatings presented as a function of the boron content in the deposits.

To better understand the mechanism of hardness enhanced for the obtained coatings, the relationship between boron content in coatings and hardness is shown in Fig. 8. From Fig. 8, it can be seen that the hardness depended on the boron content: composite coatings with higher boron content shows higher hardness. For the hardness of composite coatings, it is controlled by the percentage of incorporated particles and hardness of the matrix. In the current study, the incorporation of boron does not strongly affect the grain size and deposition rate of electrodeposited Ni-W matrix. The incorporated boron particles decrease the W content in deposits. As the previous results [10], the W is the grain refining element and can improve the hardness of Ni-W coatings. However, the current results reveal that hardness of composite coatings increase with the decrease in W content in the deposits, and the increase in boron incorporation in the coatings. Therefore, the hardness of Ni-W/B composite coatings is mainly contributed by the amounts of boron incorporation. The improvement mechanism of hardness for composite can be defined two different kinds of hardening mechanism according to the amount and size of particles, i.e., dispersion strengthening and particle strengthening [22, 26]. From the cross-sectional SEM images, the incorporation of boron particles have the sub-micron size ($<1 \mu\text{m}$), both the particle and dispersion strengthening are the mechanism in enhancing the hardness of the Ni-W/B composite coatings.

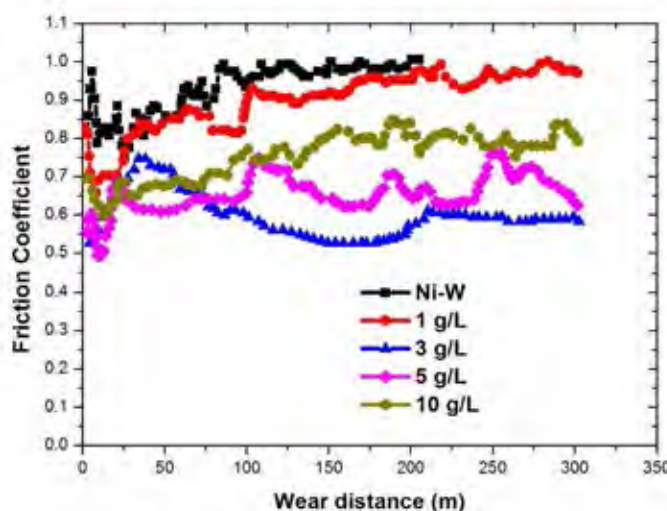


Figure 9. The friction coefficients of the Ni-W coatings and Ni-W/B composite coatings prepared with different boron concentration in solution.

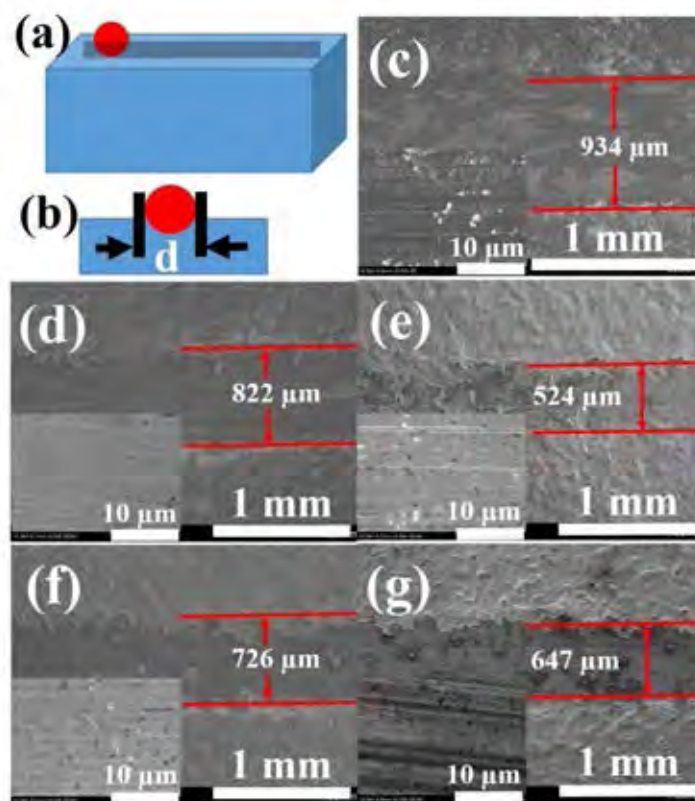


Figure 10. (a) and (b) The schematic graph of wear testing, and the general view of wear track and inside of the wear track of SEM morphology for worn surface, (c) Ni-W coatings, (d-g) Ni-W/B composite coatings prepared with different boron concentration in solution, (d) 1 g/L, (e) 3 g/L, (f) 5 g/L, (g) 10 g/L.

The wear performance was also investigated using the ball-on-disc method. The friction coefficient curves for Ni-W alloy and Ni-W/B composite coatings with boron concentration of 1, 3, 5,

and 10 g/L, are shown in Fig. 9. From the friction coefficient results, it can be clearly seen that the friction coefficient of Ni-W/B composite coatings is lower than that of Ni-W coatings. Furthermore, the lowest friction coefficient is obtained for the Ni-W/B composite coating with boron concentration of 3 g/L. These results can indicate that the Ni-W/B composite coatings would be better wear performance than that of Ni-W coatings.

The schematic graph of wear testing and SEM images of wear track are presented in Fig. 10. Fig. 10(a, b) shows the schematic graph for the wear testing. Since the hardness of Si_3N_4 ball is higher than those of coatings, the ball can easily scratch the surface of coatings, resulting the wear track. The wear resistance means the coatings for resistance to damage from normal wear or usage, thus the lower wear resistance of coatings would be generated large wear track. The wear track can be seen in Fig. 10 (c-g), and the surface area of wear track can be calculated to be 18.68, 16.44, 10.48, 14.52, and 12.94 mm^2 , for Ni-W and Ni-W/B composite coatings with boron concentration in solution 1, 3, 5, and 10 g/L, respectively. It indicates that the wear resistance of Ni-W coatings is lower than those of all Ni-W/B composite coatings, and the best wear performance can be obtained for the Ni-W/B composite coatings prepared at boron concentration in solution of 3 g/L.

In addition, the SEM images of inside wear tracks of Ni-W coatings and Ni-W/B composite coatings are inserted in the corresponded SEM images of Fig. 10 (c-g). For the Ni-W coatings, the worn morphology implies that the wear mechanism is mainly contributed by the abrasive and adhesive wear (Fig. 10(c)). Furthermore, the worn morphologies of Ni-W/B composite coatings show that a smoother surface than that of Ni-W coatings can be obtained. The abrasive grooves on these enlarged SEM images of Ni-W/B composite coatings were almost disappeared. This result could be attributed by the polishing effect of the boron particles grinding the frictional surface of Ni-W/B coatings.

The current work developed one efficient method to prepare Ni-W/B hard coatings with high boron content. The electroplating conditions applied in the present study show that Ni-W/B composite coatings could be deposited from Ni-W plating bath with amorphous boron particles suspension. The higher boron content in the deposits can be easily obtained (~21.7 wt.%) than those of Ni-W-B coatings prepared from sodium borate (~1.86 wt.%) [27, 28] (~1 wt.%) [29], and dimethylamino borane (~1 wt.%) [30, 31], (~3 wt.%) [32]. Several works have also reported the hardness of as-deposited Ni-W-B coatings. For example, Ni-W-B coatings could get a hardness of around 600-875 Hv[27, 28], 600-850 Hv[30-32], prepared from sodium borate, and dimethylamine borane, respectively. While in the present work, the higher hardness (994-1266 HK) of Ni-W/B composite coatings can be easily obtained from Ni-W plating bath with amorphous boron suspension. Furthermore, the previous study also demonstrated that the Ni-W-B coatings contain 1 wt.% boron can be chromium replacement alloys[29], the current results are much higher than that of boron content. Therefore, the developed method can be potential alternative chromium coatings.

4. CONCLUSIONS

In summary, electrodeposited Ni-W/B composite coatings were successfully prepared by dispersing the boron particles in the Ni-W bath. With boron incorporation, the W content in the

deposits decreases and grain size of coatings slight changes. The boron content in the composite coatings increases with the increase in its concentration in the bath up to 5 g/L, beyond which it decreases. The maximum boron content in the electrodeposited Ni-W matrix is about 21.7 wt.%. The Ni-W/B coatings consist of a hard metal matrix and hard boron particles, and thus exhibit high hardness. The hardness of Ni-W/B composite coatings is mainly contributed by the boron content in deposits. A high hardness of 994-1266 HK was obtained in Ni-W/B composite coatings which is comparable to that of hard chromium plated coatings.

ACKNOWLEDGEMENTS

This research is supported by the **Thai Government Budget (2016), Chulalongkorn University (GRB_BSS_105_59_62_03)**. J.Q. would like to acknowledge the support from Thailand Research Fund (TRG5780222), Ratchadaphisek somphoch Endowment Fund, Chulalongkorn University (CU-58-028-AM), and Key Laboratory of Metastable Materials Science and Technology, Yanshan University. X.Z., M.M. and R.L. would like to thank the support from NBRPC (grant 2013CB733000), NSFC (grants 51571174/51531005).

References

1. A. Grosjean, M. Rezrazi, J. Takadoum, P. Berçot, *Surf. Coat. Tech.* 137 (2001) 92.
2. A.F. Zimmerman, G. Palumbo, K.T. Aust, U. Erb, *Mater. Sci. Eng. A* 328 (2002) 137.
3. W.X. Chen, J.P. Tu, L.Y. Wang, H.Y. Gan, Z.D. Xu, X.B. Zhang, *Carbon* 41 (2003) 215.
4. H. Li, Y. He, Y. Fan, W. Xu, Q. Yang, *RSC Advances* 5 (2015) 68890.
5. H. Ogihara, M. Safuan, T. Saji, *Surf. Coat. Tech.* 212 (2012) 180.
6. J. Qin, X. Zhang, Y. Xue, M. Kumar Das, A. Thueploy, S. Limpanart, Y. Boonyongmaneerat, M. Ma, R. Liu, *Surf. Interface. Anal.* 47 (2015) 331.
7. X. Zhang, J. Qin, M.K. Das, R. Hao, H. Zhong, A. Thueploy, S. Limpanart, Y. Boonyongmaneerat, M. Ma, R. Liu, *Sci. Rep.* 6 (2015) 22285.
8. T.J. Rupert, C.A. Schuh, *Acta Mater.* 58 (2010) 4137.
9. N. Sunwang, P. Wangyao, Y. Boonyongmaneerat, *Surf. Coat. Tech.* 206 (2011) 1096.
10. C.A. Schuh, T.G. Nieh, H. Iwasaki, *Acta Mater.* 51 (2003) 431.
11. A.J. Detor, C.A. Schuh, *Acta Mater.* 55 (2007) 371.
12. X. Zhang, J. Qin, T. Perasinjaroen, W. Aeksen, M.K. Das, R. Hao, B. Zhang, P. Wangyao, Y. Boonyongmaneerat, S. Limpanart, M. Ma, R. Liu, *Surf. Coat. Tech.* 276 (2015) 228.
13. K.-H. Hou, T. Han, H.-H. Sheu, M.-D. Ger, *Appl. Surf. Sci.* 308 (2014) 372.
14. Y. Boonyongmaneerat, K. Saengkiattiyut, S. Saenapitak, S. Sangsuk, *Surf. Coat. Tech.* 203 (2009) 3590.
15. K.-H. Hou, Y.-C. Chen, *Appl. Surf. Sci.* 257 (2011) 6340.
16. Y. Wang, Q. Zhou, K. Li, Q. Zhong, Q.B. Bui, *Ceram. Int.* 41 (2015) 79.
17. J. Qin, T. Irifune, H. Dekura, H. Ohfuji, N. Nishiyama, L. Lei, T. Shinmei, *Phys. Rev. B* 85 (2012) 014107.
18. J. Qin, N. Nishiyama, H. Ohfuji, T. Shinmei, L. Lei, D. He, T. Irifune, *Scripta Mater.* 67 (2012) 257.
19. A. Robin, J.C.P. de Santana, A.F. Sartori, *Surf. Coat. Tech.* 205 (2011) 4596.
20. S.H. Yeh, C.C. Wan, *Mater. Sci. Tech-lond.* 11 (1995) 589.
21. C. Müller, M. Sarret, M. Benballa, *Surf. Coat. Tech.* 162 (2003) 49.
22. K. Krishnaveni, T.S.N. Sankara Narayanan, S.K. Seshadri, *J. Alloy. Compd.* 466 (2008) 412.

23. H. Ogihara, M. Safuan, T. Saji, *Surf. Coat. Tech.* 212 (2012) 180.
24. O. Younes, L. Zhu, Y. Rosenberg, Y. Shacham-Diamand, E. Gileadi, *Langmuir*. 17 (2001) 8270.
25. M.-C. Chou, M.-D. Ger, S.-T. Ke, Y.-R. Huang, S.-T. Wu, *Mater. Chem. Phys.* 92 (2005) 146.
26. U. Lagerpusch, E. Nembach, *Scripta Mater.* 42 (2000) 615.
27. M.G. Hosseini, M. Abdolmaleki, H. Ebrahimzadeh, S.A. Seyed Sadjadi, *Int. J. Electrochem. Sci.* 6 (2011) 1189.
28. M.G. Hosseini, M. Abdolmaleki, S.A. Seyed Sadjadi, *Protection of Metals and Physical Chemistry of Surfaces* 46 (2010) 117.
29. C.P. Steffani, J.W. Dint, J.R. Groza, A. Palazoglu, *J. Mater. Eng. Perform.* 6 (1997) 413.
30. F.-Z. Yang, Z.-H. Ma, L. Huang, S.-K. Xu, S.-M. Zhou, *Chin. J. Chem.* 24 (2006) 114.
31. G. Graef, K. Anderson, J. Groza, A. Palazoglu, *Mat. Sci. Eng. B* 41 (1996) 253.
32. T. Nagai, K. Hodouchi, H. Matsubara, *Surf. Coat. Tech.* 253 (2014) 109.

© 2016 The Authors. Published by ESG (www.electrochemsci.org). This article is an open access article distributed under the terms and conditions of the Creative Commons Attribution license (<http://creativecommons.org/licenses/by/4.0/>).

Effect of Sodium Dodecyl Sulphate and Sodium Bromide Additives on Ni–W Nanocoatings

Malay Kumar Das^{1,2}, Jiaqian Qin^{2,*}, Xinyu Zhang^{3,*}, Rongxia Li³, Adisak Thueploy², Sarintorn Limpanart², Yuttanat Boonyongmaneerat², Mingzhen Ma³, and Riping Liu³

¹International Graduate Program of Nanoscience and Technology, Chulalongkorn University, Bangkok 10330, Thailand

²Metallurgy and Materials Science Research Institute, Chulalongkorn University, Bangkok 10330, Thailand,

³State Key Laboratory of Metastable Materials Science and Technology, Yanshan University, Qinhuangdao 066004, P.R. China

Nickel-tungsten (Ni–W) coatings were fabricated by electrodeposition method with varying quantities of sodium dodecyl sulphate and sodium bromide to examine the effects of the aforesaid additives on the coatings. The obtained nanocoatings were studied by X-ray diffraction, scanning electron microscopy, energy dispersive X-ray spectroscopy, and hardness tester. The hardness, tungsten content and grain size attained a maximum value at current density of 0.15 A/cm², 0.1 A/cm² and 0.1 A/cm², respectively. There was a pronounced impact of both the additives on the microstructure and morphology of the coatings. According to results, there are considerable difference in terms of the impact caused by the additives to the tungsten content, hardness and grain size of the coatings. The obtained results suggest that hardness of coatings is mainly contributed by W content in the deposits.

Keywords: Ni–W Nanocoatings, Electrodeposition, SDS, Sodium Bromide.

1. INTRODUCTION

Nanocrystalline nickel tungsten (Ni–W) alloys have a wide array of applications such as fabricating the alloys in some sort of barrier/capping layers for ultra large scale integration applications in copper metallization, potential applications in microelectromechanical systems, various allied applications in mold inserts, magnetic heads and relays, bearings, resistors, electrodes accelerating hydrogen evolution from alkaline solutions, environmentally safe substitute for hard chromium plating in the aerospace industry, etc.¹ Hard-chrome plating has been used as a surface finishing technique in various engineering industries because it has good advantages such as high hardness, corrosion resistance, wear resistance, aesthetic qualities and durability. However, hard-chrome plating solutions are toxic, carcinogenic and hazardous to human health,² so to substitute chromium; the new alternate surface finishing method must maintain hard-chrome's advantages. One very important and sustainable prospect is to substitute hard-chrome plating with metal alloy plating. In various industrial applications (for example boilers) it has been documented that

the surface of the equipment and components involved in the running of the plant are highly prone to mechanical stress, corrosion and damage by wear. This in turn leads to plant closures and subsequent loss in revenue and operations in related industries like mining, mineral processing etc. Hence it becomes imperative to work upon strategies to enhance the surface properties rather than bulk properties^{3–5} in a wide scope of engineering materials and components used in industries.

There has been fairly substantial amount of study on the effect of surfactants on various metal alloys and composites. Wu et al.⁶ investigated the effect of boric acid on electrodepositing processes and structure of Ni–W alloy coatings and reported that the boric acid acts as a surfactant in the solution causing an increase in both the current efficiency and W content. The boric acid impeded the proton reduction, resulting in the formation of a certain complex with tungstate which in turn aided the co-deposition of tungsten leading to an increase in the tungsten content in the deposits. Hamid et al.⁷ investigated the effect of various surfactants on the electroless deposition of Ni–W–P alloys. The surfactants influenced the tungsten content of the deposits along with enhancing

*Authors to whom correspondence should be addressed.

hardness, corrosion resistance and crystalline refinement.⁷ Le et al.⁸ synthesized Ni–W sulfide hydro-treating catalysts under various methodologies of preparation with the influence of organic surfactants as one of the preparation methods. They subsequently studied the effects of the variations in the fabrication methods on the Ni–W hydro-treating catalysts.⁸ It is evident by the study of past as well as contemporary researchers that incorporation of suitable surfactants (cationic or anionic) into a metal alloy or alloy composites coatings tends to have an impact on the surface properties of the deposits. The study of the effect of surfactants on various other metal alloys has also been a field of significant interest for various researchers.^{6–17} However, there have been almost negligible studies on the effects of sodium dodecyl sulphate (SDS) and sodium bromide (NaBr) on Ni–W alloy in terms of microstructure, hardness, crystalline size, tungsten content and faradaic efficiency. The aforesaid fact along with the quest for further investigation and enhancement of the surface properties of electrodeposited Ni–W alloy was the prime motivation behind this work. In this paper the effect of additives and current density of Ni–W alloys has been discussed. The results that were reported threw up certain useful facts which could be used to develop optimal use of additional additives on the Ni–W alloy.

2. EXPERIMENTAL DETAILS

Ni–W coating was fabricated on a stainless steel substrate by means of electrodeposition from an ammonia-citrate bath. The bath composition were nickel sulphate 18 g/l, sodium tungstate 53 g/l, tri-sodium citrate 168 g/l, ammonium chloride 31 g/l, sodium bromide 18 g/l and 25 g/l, SDS 0.1 g/l, 0.5 g/l and 0.8 g/l respectively. The operating temperature was 75 °C, the pH value, stirring speed and the deposition time was kept constant at 8.9, 200 RPM and 2 hours, respectively. The current density was varied between 0.05–0.2 A/cm².

The substrate was subjected to pre-treatment before deposition by means of washing it with soap solution, keeping it immersed in 10% NaOH solution and 14% HCl. Prior to insertion of the electrodes in the plating bath, the substrate was activated by 14% HCl. Except the deposition area the other undesirable parts of the substrate was covered with polymer tape.

X-Ray diffraction (XRD) technique was employed to analyze the phases of the deposits along identification and analysis of the grain size of the coatings. Brookner D8 advance X-ray diffractometer operated at Cu K α radiation at a rating of 40 kV, 20 mA was used. The scan rate was 0.02° per step and the measuring time 0.5 second/step. Scherer's equation was employed for the calculation of the grain size of the coatings:

$$D = \frac{0.9\lambda}{\beta \cos \theta} \quad (1)$$

where, D is the grain size, λ is the incident radiation (1.5418 Å), β is the corrected peak width at half maximum intensity and θ is the angular position.

The samples were characterized in terms of morphology and microstructure by JEOL JSM-6400 scanning electron microscope (SEM) with energy dispersive X-ray spectroscopy (EDS) capability embedded into it. The coating hardness was measured on the surface using Mitutoyo hardness tester with a Vickers's diamond indenter under a load of 100 g (0.98 N). The dwell time for each indentation was 15 s and the values reported represent the average and standard deviation of a minimum of seven measurements. The Vickers hardness can be calculated in accordance with the formula:

$$H_v = 1854 \frac{L}{d^2} \quad (2)$$

where, H_v is the hardness in Vickers's and L is the applied load and d is the diagonal of the indentation.

The Faradaic efficiency (FE) was calculated from the charge passed, the weight gained, and the chemical composition of the deposit as determined by EDS, using the following equation mentioned below. Each sample was weighed before and after deposition and the coating weight was found by calculating the difference in weight. The faradaic efficiency was determined for each specimen using the difference in weights before and after plating. The faradaic efficiency of the alloy is calculated as equation below:

$$FE = \frac{w}{It} \sum \frac{c_i n_i F}{BM_i} \times 100 \quad (3)$$

where, FE is the faradaic efficiency, w is the measured weight of the deposit (g), I is the current passed (A), t is the deposition time (h), c_i is the weight fraction of the element (either nickel or tungsten) in the binary alloy deposit, n_i is the number of electrons transferred in the reduction of 1 mol atoms of that element ($n_i = 2$ for nickel and 6 for tungsten), M_i is the atomic weight of that element (g mol⁻¹), F is the Faraday constant (96,485.3 C mol⁻¹) and B is a unit conversion factor (3600 C A⁻¹h⁻¹).¹⁸

3. RESULTS AND DISCUSSION

3.1. Effect of Current Density

The samples were fabricated at temperature of 75 °C, pH value of 8.9, and current densities ranging from 0.05 A/cm² to 0.2 A/cm². X-ray diffraction patterns for the Ni–W alloy deposits for different current densities are shown in Figure 1. The analysis of the peaks revealed a face centered cubic (FCC) structure of deposits. No W peaks were found. The grain size of the deposits as obtained from the Scherer's equation is 1.9 nm, 1.8 nm, 2.6 nm and 2.7 nm for current density of 0.05 A/cm², 0.1 A/cm², 0.15 A/cm² and 0.2 A/cm², respectively (Fig. 2). The XRD results are consistent with the findings of Yamasaki et al.¹⁹ for Ni–W alloys fabricated by electrodeposition. For all the samples, the appearance of Ni

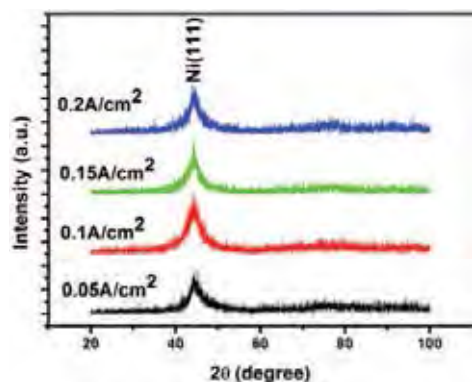


Figure 1. XRD pattern with peak value for different current densities in Ni–W alloy coatings fabricated at temperature of 75 °C, and pH value of 8.9.

peak was related to (111) plane as the major and significant peak in the deposits. The development of this texture was associated with the preferred growth along (111) orientation because of the lower strain associated.²⁰ The grain size of the deposits prepared at current density of 0.1 A/cm² is smaller than those of Ni–W coatings fabricated at other current densities.

The hardness as reported on the Vicker's scale by the Mitutoyo hardness tester is 607, 751, 755 and 722 for the coatings prepared at current density of 0.05 A/cm², 0.1 A/cm², 0.15 A/cm² and 0.2 A/cm², respectively (Fig. 2).

Upon analysis of the SEM images in Figure 3, the deposits are inconsistent for lower current densities. The W content of Ni–W coatings prepared at current density of 0.05 A/cm², 0.1 A/cm², 0.15 A/cm², 0.2 A/cm² is reported to be 20.07 at.%, 21.96 at.%, 20.37 at.%, and 18.86 at.%, respectively (Table I). At current density of 0.1 A/cm², a remarkable refinement of the surface quality with reduced cracks is observed. It might be due to reduced internal stress (in the deposits) as compared to higher current densities.²¹ Also, at current density of 0.1 A/cm², the grain

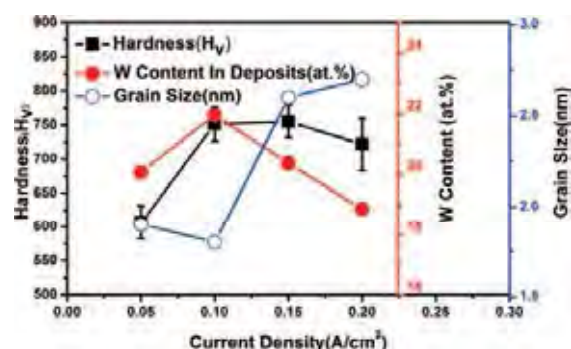


Figure 2. Effect of current densities on the hardness, W content and crystalline size of the Ni–W alloy deposits fabricated at temperature of 75 °C, and pH value of 8.9.

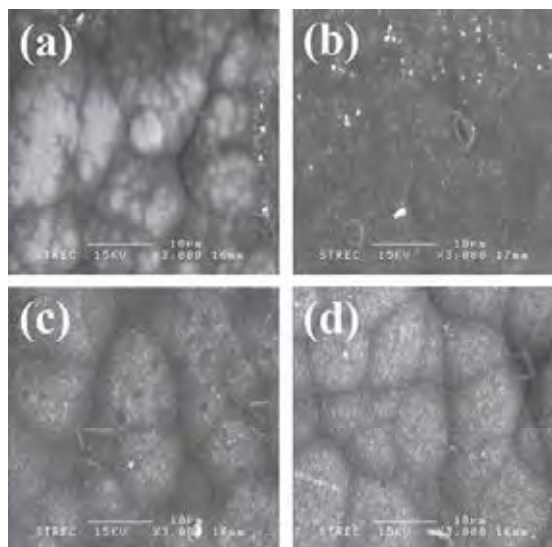


Figure 3. SEM images for the Ni–W coatings prepared at temperature of 75 °C, and pH value of 8.9 for various current densities (a) 0.05 A/cm² (b) 0.1 A/cm² (c) 0.15 A/cm² (d) 0.2 A/cm².

boundaries appear finer and relatively less conspicuous or pronounced in appearance. The tungsten content is found to be maximum at current density of 0.1 A/cm². Owing to optimized tungsten content, high hardness, a relatively smaller grain size and a fairly better morphology as per SEM results; current density of 0.1 A/cm² has been chosen as the operating current density for the subsequent studies on the effects of various additives on our coatings.

The faradaic efficiency is 12.32%, 29.31%, 40.12% and 51.48% for current density of 0.05 A/cm², 0.1 A/cm², 0.15 A/cm², 0.2 A/cm², respectively. The faradaic efficiency is continuously increasing with increasing in current density as reported in Figure 4. At lower current densities, the faradaic efficiency tends to exhibit an decreasing trend which in turn causes the hydrogen evolution become more prominent.¹ The increased hydrogen evolution leads to additional agitation in the solution. It is imperative to maintain an optimal current density during electrodeposition process to minimize hydrogen evolution and agitation in the plating bath. Contemporary researchers have also suggested that with the gradual increase in current density there is a relative increase in Ni ion concentration in the deposits.²² Since, Ni is deposited easily

Table I. Elemental composition of the Ni–W coating prepared at temperature of 75 °C, pH value of 8.9, and different current density.

Current density (A/cm ²)	Nickel (at.%)	Tungsten (at.%)
0.05	79.93	20.07
0.1	78.04	21.96
0.15	79.63	20.37
0.2	81.14	18.86

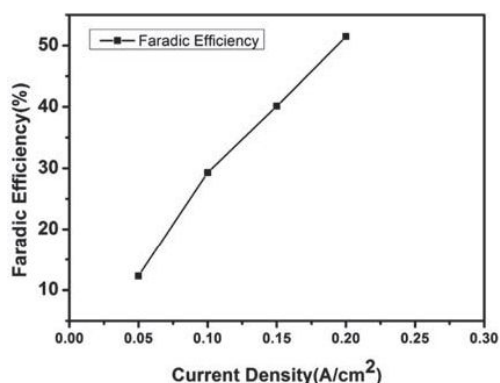


Figure 4. Effect of current density on the faradaic efficiency of the coatings fabricated at temperature of 75 °C, and pH value of 8.9.

as compared to tungsten,¹ a higher value of faradaic efficiency results in higher concentration and distribution of Ni on the coatings which is undesirable as per the research goals. Various contemporary researchers in the metal alloys electrodeposition field have also reported an increase in residual stress with an increase in current density and faradaic efficiency.²¹ Therefore, an optimum pair of current density and faradaic efficiency would lead to reduced residual stress and relatively higher tungsten content in the deposits.

The effect of current density on the grain size, tungsten content, and hardness is plotted in Figure 2. Considerably high value of the hardness coincides with high tungsten content and a reduced grain size. This suggests that the increase in tungsten content and the successive reduction in grain size tend to affect the hardness of the samples in a positive manner.²³ Therefore, a strong dependency of hardness values on both the grain size and W content of the coatings for variations in current density is established.

3.2. Effects of SDS on the Coatings

Various quantities of SDS were added to the plating bath during the course of fabrication of the coatings to study its effects on the Ni–W coatings. The amounts of SDS added were 0.1, 0.5 and 0.8 g/l, respectively. XRD patterns of Ni–W coatings for different quantities of SDS are shown in Figure 5. The diffraction pattern revealed a FCC structure of Ni deposits. Similar to the case of XRD peaks for different current densities no W peaks were found. The grain size is 1.8, 1.8, 2 and 2.1 nm for 0, 0.1, 0.5 and 0.8 g/l of SDS, respectively (Fig. 6). For all the samples a single high intensity Ni peak was reported at (111) plane. The development of the texture was associated with the preferred growth along (111) orientation because of the lower strain associated. The grain size increases with increasing in the amount of SDS in the plating bath beyond 0.1 g/l.

The calculated hardness for various quantity of SDS is 751, 655, 667, and 716 for 0, 0.1, 0.5 and 0.8 g/l of SDS, respectively (Fig. 6). The hardness value has been found

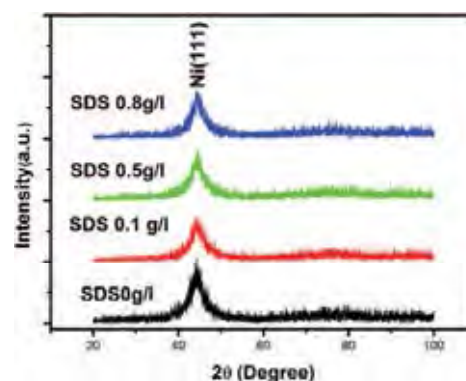


Figure 5. XRD pattern for different quantities of SDS in the plating bath for Ni–W alloy coatings fabricated at current density of 0.1 A/cm², temperature of 75 °C, and pH value of 8.9.

to be maximum for the Ni–W coating prepared without SDS. However, the effect of SDS has been further studied in terms of SEM and EDS analysis to compare the microstructure and elemental composition in the coatings respectively. The microhardness of the coatings increases upon successive increase in the content of SDS up to a typical value of micelle concentration¹⁶ beyond which it would be rather stabilized or not shows any such profound effects.

The samples were also analyzed by SEM (Fig. 7); it is revealed that the addition of SDS significantly alters the composition of the coatings, surface morphology and crack density of the microstructure.¹⁶ The EDS results for the variation in the quantity of SDS in the plating bath are shown in Table II. There seems to be an impact of SDS additions on the tungsten content, marginal impact on hardness, grain size and also the faradaic efficiency of the coatings. Moreover, the SEM images (Fig. 7) suggest wide variations in the surface morphology, crack density and film quality and structure on the coatings with SDS as compared to samples without SDS.

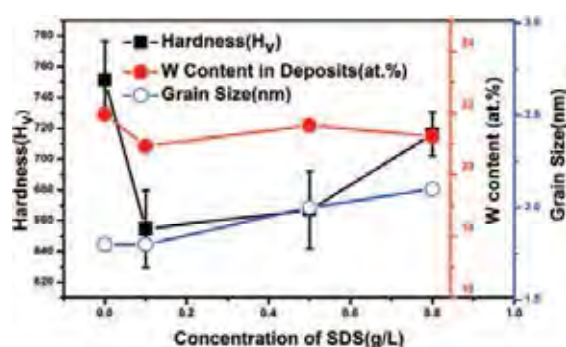


Figure 6. Effect of SDS on the hardness, W content and crystalline size of the Ni–W alloy deposits fabricated at current density of 0.1 A/cm², temperature of 75 °C, and pH value of 8.9.

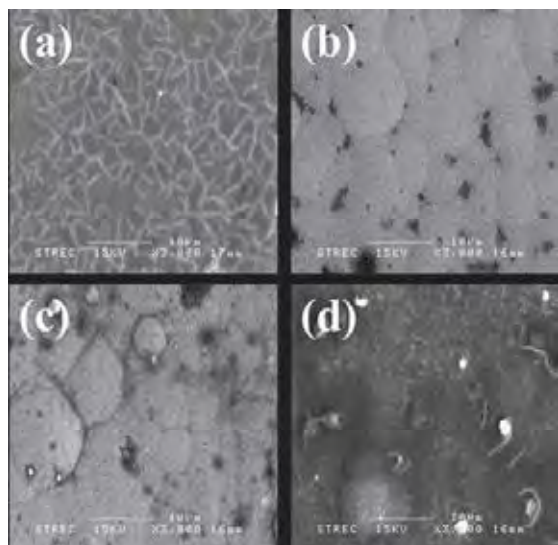


Figure 7. SEM images for the coatings deposited at current density of 0.1 A/cm², temperature of 75 °C, and pH value of 8.9 for various quantities of SDS in the plating bath (a) 0 g/l (b) 0.1 g/l (c) 0.5 g/l (d) 0.8 g/l.

The SEM image of Ni–W coatings prepared without SDS clearly shows numerous cracks on the surface in Figure 7(a), whereas smoother boundaries and reduction of cracks is observed as SDS is added in small quantity in Figure 7(b). This is because of reduction of internal strain and increase in ultimate tensile strength upon addition of SDS which acts as a surfactant.^{9–16} The increase in the ultimate tensile strength due to the addition of SDS surfactant is primarily responsible for the reduced crack density and smoother boundaries in the deposits. The tungsten content of Ni–W coatings prepared at different SDS concentration keeps almost constant, and the hardness of the obtained coatings decreases quickly from 751 Hv to 655 Hv with addition of 0.1 g/L of SDS. From 0.1 g/L to 0.8 g/L SDS, the hardness slightly increases from 655 Hv to 716 Hv. The grain size as reported is increased with increasing in SDS concentration. The above results especially in respect of the change in morphology as per SEM data and EDS results for tungsten content establishes that the effects of the surfactant tends to attain a maximum critical point of influence which is due to attaining a critical micelle concentration¹⁶ beyond which it tends not

Table II. Elemental composition of the Ni–W coatings deposited at temperature of 75 °C, pH value of 8.9, and current density 0.1 A/cm², with different SDS concentration.

Amount of SDS (g/l)	Nickel (at.%)	Tungsten (at.%)
0	78.04	21.96
0.1	79.07	20.93
0.5	78.40	21.60
0.8	78.75	21.25

to have a considerable effect on the aforesaid parameters. The tungsten content and a suitable microstructure are quite important in order to attain good hardness and film quality. Surfactants are important contributors towards reducing the surface tension forces in the coatings which subsequently results in a better and uniform surface with considerably reduced cracks and as in an almost pit free microstructure as observed in Figures 7(b and c).¹⁶ However, the Figure 7(c) depicts sharper boundaries as compared to Figure 7(b).

The variation of the faradaic efficiency with varying amounts of SDS is shown in Figure 8. There is a marked decrease in the values of faradaic efficiency up to a critical minimum value. Beyond 0.5 g/l of SDS the faradaic efficiency shows an increasing trend at 0.8 g/l. This is due to the fact that beyond a critical micelle concentration¹⁶ the effect of SDS ceases to be more conspicuous in terms of decreasing the efficiency of the current to cause electrodeposition.

The effect of the grain size and tungsten content on the micro hardness has been shown in Figure 6. For different amounts of SDS the hardness is maximum at a point where both the crystalline size and tungsten content are relatively higher. As the grain size and tungsten content drop relatively, their effect on hardness is observed in terms of decreasing hardness. For the Ni–W coating prepared without SDS, the hardness is comparatively higher despite a lower value crystalline size suggesting a more pronounced impact of the tungsten content on the hardness than that of the grain size when the amount of SDS is varied in the plating bath.

3.3. Effect of Sodium Bromide

XRD patterns of Ni–W alloy deposits with different amounts of sodium bromide in the plating bath are shown in Figure 9. The XRD patterns show only nickel in the coatings. No W peaks are found. For all the samples the appearance of Ni-peak as suggested by the various values

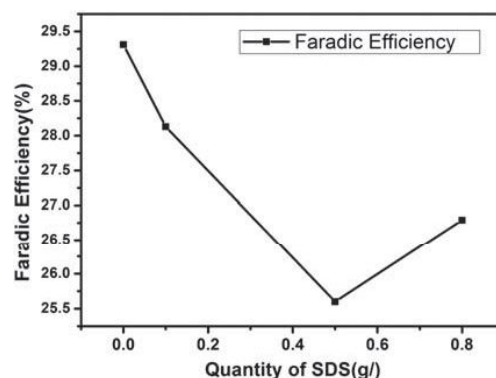


Figure 8. Effect of SDS on the faradaic efficiency of the coatings fabricated at current density of 0.1 A/cm², temperature of 75 °C, and pH value of 8.9.

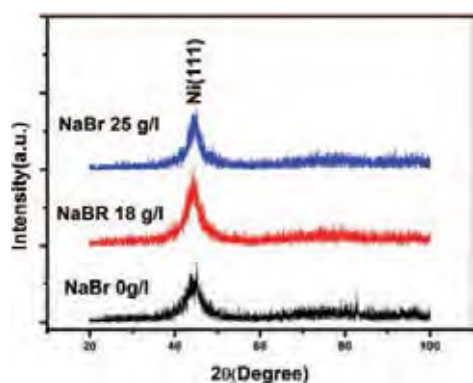


Figure 9. XRD pattern for different quantities of NaBr in the plating bath for Ni–W alloy coatings fabricated at current density of 0.1 A/cm², temperature of 75 °C, and pH value of 8.9.

in the diffractograms was related to (111) plane as the only major and significant peak. The development of this texture was associated with the preferred growth along the (111) orientation because of the lower strain associated with that plane.²⁰ The grain size is 1.6, 1.8 and 2.9 nm for obtained coatings prepared at sodium bromide concentration of 0, 18 and 25 g/l, respectively (Fig. 10). The analysis of the grain size reveals continuous increase upon increasing the quantity of the sodium bromide in the bath.

The hardness is 784, 751 and 718 for 0, 18 and 25g/l of sodium bromide, respectively (Fig. 10). Moreover, with the decrease in the grain size a corresponding increase in the hardness of the alloy deposits is observed. The hardness data as reported corroborates with the Hall-petch analogy^{23–27} suggesting increase in surface toughness/hardness upon decrease in the grain size. The reduced hardness for 25 g/l of NaBr is due to substantially reduced internal stress and crack density in the deposits.

SEM analysis was carried out for deposits with NaBr concentration of 0 g/l, 18 g/l and 25 g/l, respectively (Fig. 11). The sharp difference in cracks and film quality could be seen in Figures 11(b and c), which demonstrates

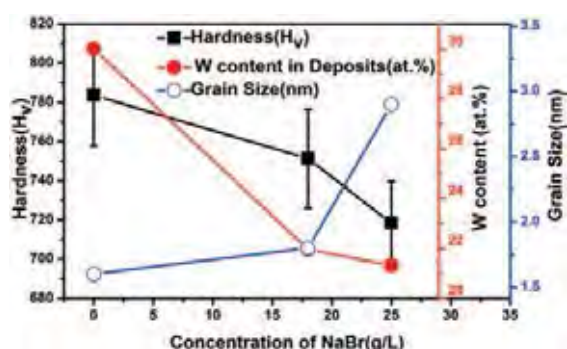


Figure 10. Effect of NaBr on the hardness, W content and crystalline size of the Ni–W alloy deposits fabricated at current density of 0.1 A/cm², temperature of 75 °C, and pH value of 8.9.

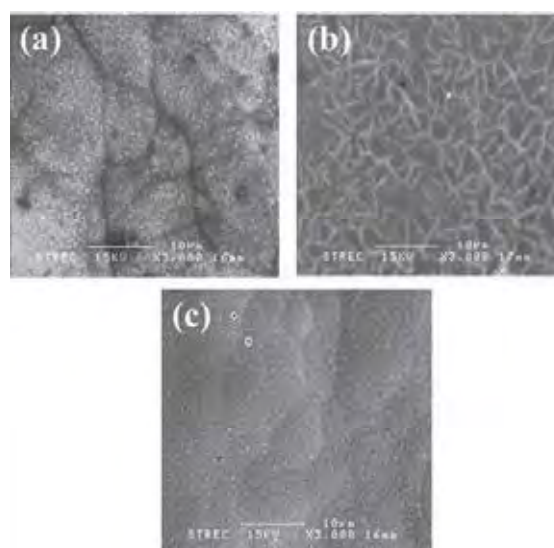


Figure 11. SEM images for the coatings prepared at current density of 0.1 A/cm², temperature of 75 °C, and pH value of 8.9 for various quantities of NaBr in the bath (a) 0 g/l (b) 18 g/l (c) 25 g/l.

that suitable amounts of NaBr has strong impact on the morphology of the deposits in terms of crack reduction and improvement/refinement of the film quality. Figure 11(c) as compared with the Figures 11(a and b) in terms of cracks and film quality exhibits a profound effect of NaBr on the coatings. The effect of NaBr has thus been proven to be detrimental towards enhancing the film quality. There seems to exist almost no cracks in Figure 11(c) corresponding to 25 g/l of NaBr as compared to Figure 11(b) (18 g/l NaBr) and even Figure 11(a) (no NaBr). There is neither deep crack existent nor any fissures or pits formation in the surface of the deposits in Figure 11(c). This suggests a positive impact of NaBr on the coatings. There is a sharp drop in the tungsten content in the deposits (Table III) upon increasing the quantity of NaBr. The faradaic efficiency of the deposition decreases with increasing in the concentration of NaBr in the plating bath (Fig. 12).

The hardness as presented in Figure 10 shows that the hardness of the deposits decreases with increasing in the concentration of NaBr. The highest hardness is observed at 0 g/l of NaBr concentration when the grain size is the minimum and the tungsten content maximum. The lower grain

Table III. Elemental composition of the Ni–W coatings fabricated at temperature of 75 °C, pH value of 8.9, and current density 0.1 A/cm², with different NaBr concentration.

Sodium bromide (g/l)	Nickel (at.%)	Tungsten (at.%)
0	70.00	30.00
18	78.69	21.31
25	78.04	21.96

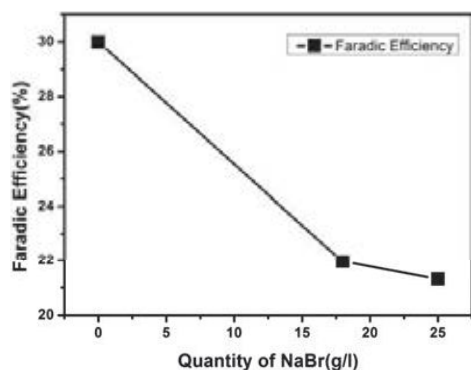


Figure 12. Effect of NaBr on the faradaic efficiency of the coatings fabricated at current density of 0.1 A/cm², temperature of 75 °C, and pH value of 8.9.

size returns a high hardness in the deposits whereas, upon successive increase in the grain size, the hardness tends to decrease as per the hall-petch analogy.²³ The hardness also decreases with the relative decrease in the tungsten content which suggests that the tungsten content in the deposits is also a major factor contributing to the hardness of the deposits. Hence, for the NaBr additive the hardness depends both on the tungsten content and the crystalline size of the deposits.

The effect of W content and the grain size on the hardness of the Ni–W coatings is analyzed for various quantities of SDS and NaBr in the plating bath as shown in Figure 13. It is observed that the hardness is maximum for the highest value of tungsten content in the deposits whereas, the corresponding value for the grain size was reported to be minimum. The increase in hardness and a corresponding increase in W content therefore, establish the enhanced effect of the W content on the hardness as compared to the grain size of the deposits.

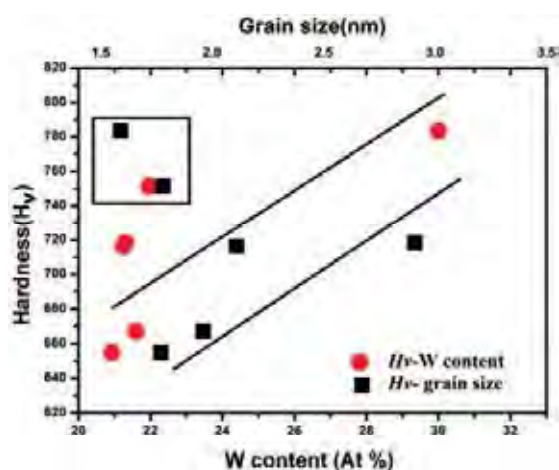


Figure 13. Effect of the W content and crystalline size on the hardness of the Ni–W coatings.

Most of the values of grain size follow inverse hall-petch relationship^{23–27} by means of an increasing value of hardness upon the successive increase in grain size except for the lower values of grain size enclosed in the rectangular box in the graph which report a corresponding high value of W content and hardness. The obtained results further suggest that hardness of coatings is mainly contributed by W content in the deposits.

4. CONCLUSIONS

The investigations for the Ni–W alloy revealed profound and marked differences in the effect of various additives on the coatings as well as established the pivotal role of the applied current density in the nature and attributes of the deposits. SDS and NaBr both have a significant impact on the coatings in terms of the hardness, tungsten content, faradaic efficiency and grain size of the coatings. However, proper NaBr concentration (25 g/l) in the plating bath offers better film quality enhancement and reduction of internal cracks with higher hardness (718 H_v), high tungsten content (21.31 at.%), moderate grain size (2.9 nm) and optimal value of faradaic efficiency (29.31%) as compared to SDS where for 0.1 g/l of SDS though the SEM results is quite better as compared to other samples with different quantities of SDS but the other vital parameters namely hardness (655 H_v), tungsten content (20.93 at.%), grain size (1.8 nm) and faradaic efficiency (28.13%) are not as desirable as per the research objectives of obtaining a high hardness, high tungsten content deposits with relatively refined microstructure, enhanced film quality and lower crack density. The effect of NaBr tends to be the more pronounced towards obtaining an enhanced microhardness and suitable SEM results with low crack density and a refined film structure.

Acknowledgments: This research is supported by **National Research Council of Thailand (NRCT, 183299)**. Jiaqian Qin would like to acknowledge the support from Thailand Research Fund (TRG5780222), Ratchadaphisek somphoch Endowment Fund (2013), Chulalongkorn University (CU-56-805-FC), and Key Laboratory of Metastable Materials Science and Technology, Yanshan University. Malay Kumar Das would like to acknowledge the support from the 100th Anniversary Chulalongkorn University Doctoral Scholarship. Xinyu Zhang, Mingzhen Ma and Riping Liu would like to thank the support from NBRPC (grant 2013CB733000), NSFC (grants 51571174/51434008).


References and Notes

1. N. Eliaz, T. Sridhar, and E. Gileadi, *Electrochim. Acta* 50, 2893 (2005).
2. T. Nagai, K. Hodouchi, and H. Matsubara, *Surf. Coat. Tech.* 253, 109 (2014).
3. Y.-L. Shang, L. Huo, Y.-L. Jia, F.-H. Liao, J.-R. Li, M.-X. Li, and S.-H. Zhang, *Colloid. Surface A* 325, 160 (2008).

4. Y.-L. An, H.-Y. Du, Y.-H. Wei, N. Wang, L.-F. Hou, and W.-M. Lin, *Mater. Design.* 46, 627 (2013).
5. G. Krauss, *J. Heat Treat.* 9, 81 (1992).
6. Y. Wu, D. Chang, D. Kim, and S.-C. Kwon, *Surf. Coat. Tech.* 173, 259 (2003).
7. Z. A. Hamid, *Surf. Interface. Anal.* 35, 496 (2003).
8. Z. Le, P. Afanasiev, D. D. Li, X. G. Long, and M. Vrinat, *Catal. Today* 130, 24 (2008).
9. S. Mohajeri, A. Dolati, and S. Rezagholibeiki, *Mater. Chem. Phys.* 129, 746 (2011).
10. L. Chen, L. Wang, Z. Zeng, and J. Zhang, *Mater. Sci. Eng. A* 434, 319 (2006).
11. M.-D. Ger, *Mater. Chem. Phys.* 87, 67 (2004).
12. N. K. Shrestha, M. Masuko, and T. Saji, *Wear* 254, 555 (2003).
13. C. Guo, Y. Zuo, X. Zhao, J. Zhao, and J. Xiong, *Surf. Coat. Tech.* 202, 3385 (2008).
14. Q. Feng, T. Li, H. Teng, X. Zhang, Y. Zhang, C. Liu, and J. Jin, *Surf. Coat. Tech.* 202, 4137 (2008).
15. E. Rudnik, L. Burzyńska, Ł. Dolasiński, and M. Misiak, *Appl. Surf. Sci.* 256, 7414 (2010).
16. J. Sudagar, J. Lian, Q. Jiang, Z. Jiang, G. Li, and R. Elansezhian, *Prog. Org. Coat.* 74, 788 (2012).
17. P. K. Sahoo, S. S. K. Kamal, M. Premkumar, T. J. Kumar, B. Sreedhar, A. K. Singh, S. K. Srivastava, and K. C. Sekhar, *Int. J. Refract. Met. H.* 27, 784 (2009).
18. A. Subramania, A. R. Sathya Priya, and V. S. Muralidharan, *Int. J. Hydrogen Energ.* 32, 2843 (2007).
19. T. Yamasaki, P. Schloßmacher, K. Ehrlich, and Y. Ogino, *Nanostruct. Mater.* 10, 375 (1998).
20. M. Zemanová, M. Krivosudská, M. Chovancová, and V. Jorík, *J. Appl. Electrochem.* 41, 1077 (2011).
21. W. Huang, Y. Zhao, and X. Wang, *Surf. Coat. Tech.* 235, 489 (2013).
22. F. Ebrahimi and Z. Ahmed, *J. Appl. Electrochem.* 33, 733 (2003).
23. T. J. Rupert and C. A. Schuh, *Acta Mater.* 58, 4137 (2010).
24. G. J. Fan, H. Choo, P. K. Liaw, and E. J. Laverna, *Mater. Sci. Eng. A* 409, 243 (2005).
25. M. A. Meyers, A. Mishra, and D. J. Benson, *Prog. Mater. Sci.* 51, 427 (2006).
26. S. Takeuchi, *Scripta Mater.* 44, 1483 (2001).
27. H. W. Song, S. R. Guo, and Z. Q. Hu, *Nanostruct. Mater.* 11, 203 (1999).

Received: 13 October 2015. Accepted: 8 December 2015.

SCIENTIFIC REPORTS



OPEN

Co-electrodeposition of hard Ni-W/diamond nanocomposite coatings

Xinyu Zhang¹, Jiaqian Qin², Malay Kumar Das^{2,3}, Ruru Hao¹, Hua Zhong¹, Adisak Thueploy², Sarintorn Limpanart², Yuttanant Boonyongmaneerat², Mingzhen Ma¹ & Riping Liu¹

Received: 30 November 2014

Accepted: 11 February 2016

Published: 29 February 2016

Electroplated hard chrome coating is widely used as a wear resistant coating to prolong the life of mechanical components. However, the electroplating process generates hexavalent chromium ion which is known carcinogen. Hence, there is a major effort throughout the electroplating industry to replace hard chrome coating. Composite coating has been identified as suitable materials for replacement of hard chrome coating, while deposition coating prepared using traditional co-deposition techniques have relatively low particles content, but the content of particles incorporated into a coating may fundamentally affect its properties. In the present work, Ni-W/diamond composite coatings were prepared by sediment co-electrodeposition from Ni-W plating bath, containing suspended diamond particles. This study indicates that higher diamond contents could be successfully co-deposited and uniformly distributed in the Ni-W alloy matrix. The maximum hardness of Ni-W/diamond composite coatings is found to be 2249 ± 23 Hv due to the highest diamond content of 64 wt.%. The hardness could be further enhanced up to 2647 ± 25 Hv with heat treatment at 873 K for 1 h in Ar gas, which is comparable to hard chrome coatings. Moreover, the addition of diamond particles could significantly enhance the wear resistance of the coatings.

Composite plating is a technique involving co-electrodeposition of inert particles with metal/alloy in order to promote the hardness, wear and corrosion properties of the coatings, which has a great application in the industries. The composite coatings are prepared by co-electrodeposition of second-phase particles into a metal/alloy matrix, which show excellent higher hardness, lubricity, and wear properties^{1–5}. The content of particles incorporated into a coating may fundamentally affect its properties. While deposition coatings fabricated using traditional co-deposition techniques have relatively low particles content⁶, the use of low-cost composite electroplating methods continues to expand and addresses the major challenge of achieving high levels of co-deposited particles. On the other hand, the hardness of composite coatings are controlled not only by the content of incorporated particles, but also by the hardness of the matrix⁷. Ogihara *et al.*⁷ reported that the hardness of Ni-B/diamond coatings was 1940 Hv. The hardness of the composite coating increased from 1940 Hv to 2494 Hv by heat treatment at 673 K for 1 h in air, comparable to hard chrome coatings and hard coatings prepared by dry processes. For example, the hardness of hard chrome coating is 850–1100 Hv⁸, and the hardness of TiN coatings deposited by dry process sputtering or supersonic plasma spraying is 2000–2700 Hv. Furthermore, Ogihara *et al.*⁹ also prepared the hard Ni-B/diamond composite coatings (micro-hardness 1248 Hv) by one-step electrodeposition. The hardness of composite coatings was further enhanced up to 2310 Hv by heat treatments, comparable to electroplated hard chrome coating, TiN coatings prepared by dry process and Ni-B/diamond composite coatings prepared by two-step wet process.

Electrodeposited Ni-W alloys were recently developed as a candidate to replace the environmentally hazardous hexavalent hard chromium coatings. The hardness of Ni-W can reach up to 700 Hv by controlling their grain size into the nanocrystalline regime¹⁰. Furthermore, the hardness of Ni-W coatings can be enhanced from 700 Hv to 1050 Hv by heat treatment¹¹. According to these results, it is suggested that Ni-W alloys could be good candidate of matrix for diamond composite coatings. Hou *et al.*¹² and Wang *et al.*¹² successfully prepared the Ni-W/diamond composite coatings by electrodeposition. The microhardness reached a maximum (1205 Hv) after annealing at 600 °C due to the precipitation of the Ni₄W phase. Zhang *et al.*¹³ also prepared Ni-W/diamond composite coatings using pulse current electrodeposition. The maximum hardness of as-deposited coatings was

¹State Key Laboratory of Metastable Materials Science and Technology, Yanshan University, Qinhuangdao 066004, P.R. China. ²Metallurgy and Materials Science Research Institute, Chulalongkorn University, Bangkok 10330, Thailand. ³International Graduate Program of Nanoscience & Technology, Chulalongkorn University, Bangkok 10330, Thailand. Correspondence and requests for materials should be addressed to J.Q. (email: jiaqian.q@chula.ac.th) or R.L. (email: riping@ysu.edu.cn)

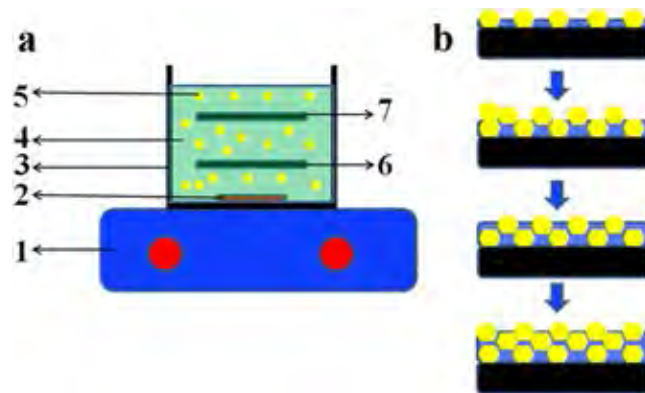


Figure 1. Schematic representation of the Ni-W-diamond composite coatings formation process through SCD method. (a) The deposition setup, 1-magnetic hot plate, 2- stirrer, 3-beaker, 4-electrolyte, 5-diamond particles, 6-steel cathode, 7-anode. (b) The schematic representation of composite coatings formation process through SCD method.

Chemicals/Parameters	
NiSO ₄ ·6H ₂ O	18 g L ⁻¹
Na ₂ WO ₄ ·2H ₂ O	53 g L ⁻¹
Na ₃ C ₆ H ₅ O ₇ ·2H ₂ O	168 g L ⁻¹
NH ₄ Cl	31 g L ⁻¹
NaBr	18 g L ⁻¹
Diamond	0, 1, 2, 5, 10, 20 g L ⁻¹
Current density	0.05, 0.10, 0.15, and 0.20 A cm ⁻²
Temperature	75 °C
pH	8.9

Table 1. Bath compositions and deposition conditions.

988 Hv. The hardness of Ni-W/diamond, however, cannot be compared to the Ni-B/diamond composite coatings, which could be caused by the relatively low diamond particles content in the deposits. Consequently, in the present study, we report a simple one-step sediment co-electrodeposition (SCD) process for preparing hard Ni-W/diamond composite coatings.

Results and Discussions

Synthesis of the Ni-W/diamond coatings. Ni-W and Ni-W/diamond coatings have been conventionally prepared by the electrodeposition method^{12,14}. However, it is difficult to co-deposit diamond particles into the formed matrix with the conventional electrodeposition method. Therefore, the diamond content in Ni-W/diamond composite coatings prepared using the conventional electrodeposition is low, so that the hardness of diamond particles would make only a minor contribution to the hardness of the obtained coatings. We have previously demonstrated the preparation of composite coatings using SCD method¹⁵. Figure 1(a) shows the setup of SCD. Figure 1(b) shows the schematic representation of the Ni-W-diamond composite coatings formation process through SCD method. In the typical process, diamond particles will be suspended in the electrolyte solution during the deposition. Therefore, diamond particles could be easily co-electrodeposited with metal ions on the substrate because of the gravity of diamond particles. This SCD fabrication process can significantly improve the content of diamond particles in the deposits. In this study, the co-electrodeposition of Ni-W and diamond was conducted in a 200 mL plating bath with aqueous bath chemistry. The bath composition and plating conditions are listed in Table 1. Analytical reagents and deionized water were used to prepare the plating solution. The diamond particles of mean size of 0.8 and 3 μm were chosen to be co-deposited with nickel in the present experiments. Carbon steel was employed as a cathode. Prior to plating, steel substrates were successively washed in soap, rinsed in NaOH, HCl, and distilled water, and activated in 14% HCl. The steel substrates were masked with insulating tape with 4 cm² of exposed area left. The steel substrate and Pt coated-Fe mesh plate with a distance of 35 mm in between were horizontally immersed into 200 ml of the electrodeposition baths. Electrodeposition was carried out under constant current density (0.05, 0.1, 0.15, and 0.2 A cm⁻²) and Ni-W/diamond composite coatings were successfully electrodeposited on the steel plates.

Microstructure of the Ni-W/diamond coatings. The scanning electron microscopy (SEM) images of Ni-W/diamond composite coatings are shown as Fig. 2, where Fig. 2(a–e) show the surface morphology of a Ni-W/diamond coatings fabricated via sediment co-deposition technique with current density of 0.1 A cm⁻², bath temperature 75 °C, and different diamond concentration in bath, 1 g L⁻¹, 3 g L⁻¹, 5 g L⁻¹, 10 g L⁻¹, and 20 g L⁻¹,

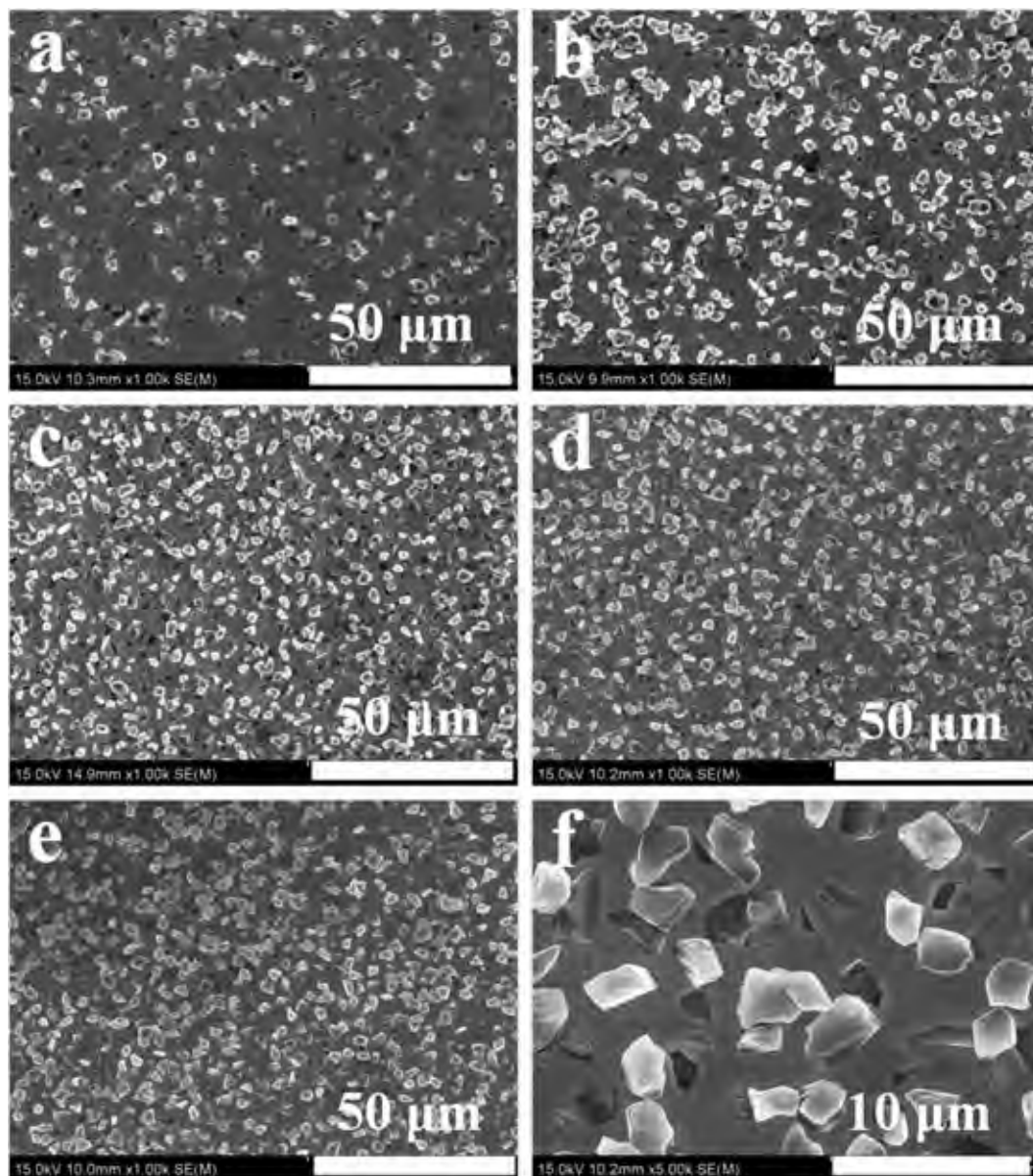


Figure 2. SEM images of Ni-W/diamond composite coatings. The coatings prepared under deposition current density of 0.1 A/cm^2 , bath temperature of 75°C , and different diamond concentration in solution, (a) 1 g L^{-1} , (b) 2 g L^{-1} , (c) 5 g L^{-1} , (d) 10 g L^{-1} , (e) 20 g L^{-1} . (f) the enlarged area of (d).

respectively. The particles in Fig. 2 represent the co-deposited diamond in Ni-W matrix. It can be seen that the diamond particles are embedded into the Ni-W matrix, and they are uniformly and finely present, indicating that the diamond particles were co-deposited into the Ni-W matrix one by one. This can be seen clearly in Fig. 2(f), which is the enlarged area of Fig. 2(d). Furthermore, it can be seen that more diamond particles were co-deposited in the matrix presented in Fig. 2(c–e) than in those shown in Fig. 2(a,b). These SEM micrographs indicate that the uniform distribution of diamond particles throughout the deposits, and the diamond content in deposits increased with the diamond concentration in bath from 1 to 5 g L^{-1} , while above 5 g L^{-1} the diamond content in deposits kept almost constant.

Cross-sectional SEM images of Ni-W/diamond coatings prepared by the SCD method are also shown in Fig. 3. Figure 3(a–d) present the cross-section of a Ni-W/diamond coatings fabricated via SCD technique with current density of 0.1 A cm^{-2} , bath temperature 75°C , and different diamond concentration in bath, 1 g L^{-1} , 5 g L^{-1} , 10 g L^{-1} , and 20 g L^{-1} , respectively. The results reveal that the thickness of coatings is strongly affected by the diamond concentration in bath. As the diamond concentration is increased, the thickness of coatings decreases. The thickness of coatings for different current density (0.05 A cm^{-2} , 0.1 A cm^{-2} , and 0.2 A cm^{-2}) was also examined, as shown in Fig. 3(b,e,f), respectively. It can be seen that the thickness increases with the current density. The thickness of the coating is *ca.* $25\text{--}70 \mu\text{m}$ with different deposition conditions. The inserted images show the enlarged cross section SEM images, which suggest that the coating is composed of dense diamond particles with

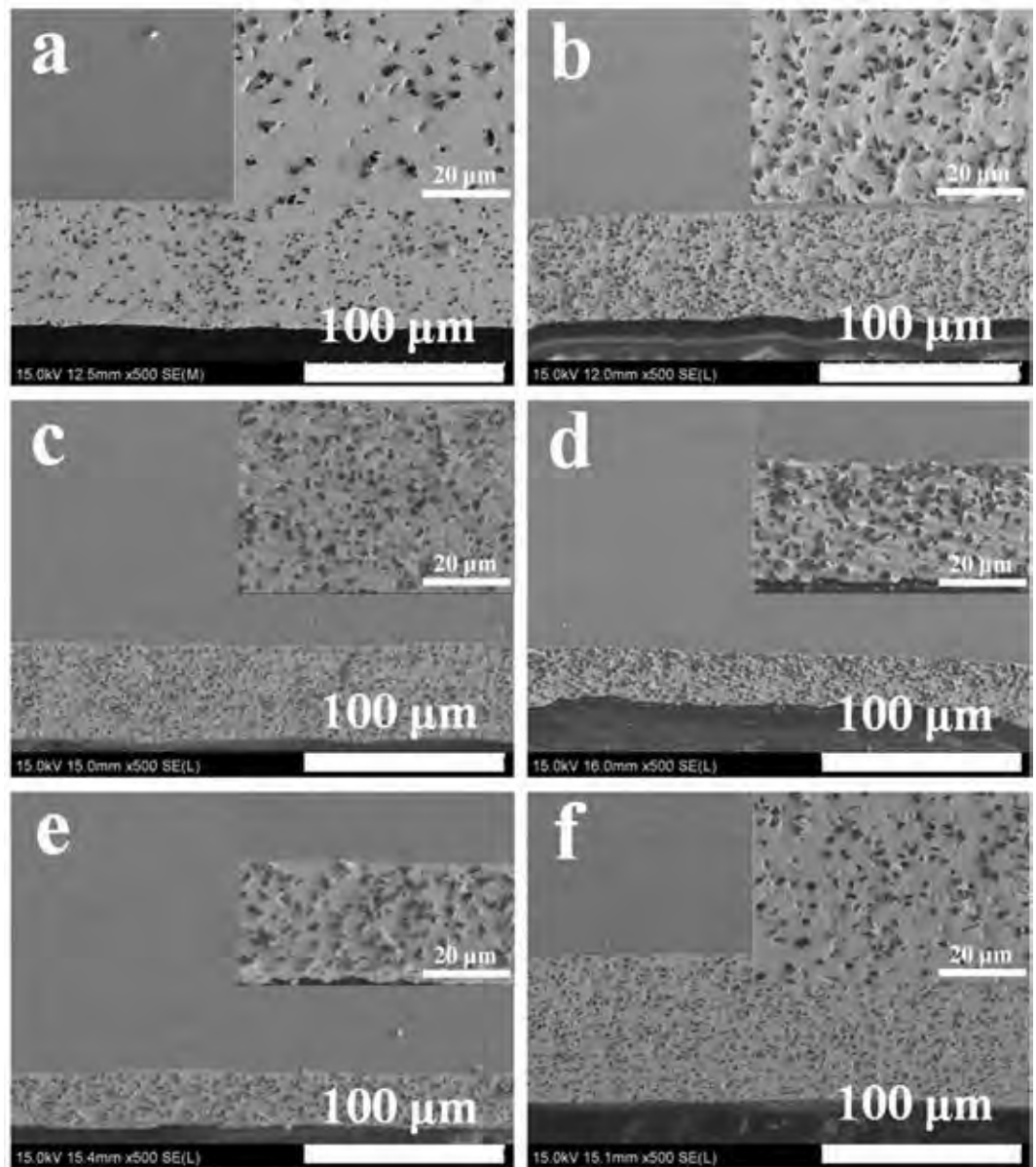


Figure 3. SEM image for cross-section of Ni-W/diamond composite coating under bath temperature of 75 °C. (a) diamond concentration of 1 g L⁻¹ and current density of 0.1 A cm⁻², (b) diamond concentration of 5 g L⁻¹ and current density of 0.1 A cm⁻², (c) diamond concentration of 10 g L⁻¹ and current density of 0.1 A cm⁻², (d) diamond concentration of 20 g L⁻¹ and current density of 0.1 A cm⁻², (e) current density of 0.05 A cm⁻² and diamond concentration of 5 g L⁻¹. (f) current density of 0.2 A cm⁻² and diamond concentration of 5 g L⁻¹.

diameters of ca. 2–4 μm. The results confirm that diamond particles are distributed uniformly in the Ni-W matrix, as expected.

The chemical composition of the as-deposited composite coatings was examined by energy dispersive X-ray spectroscopy (EDS) analysis. The W content is ~41–45 wt.%, as shown in Table 2. To determine the interface of chemical bonding and composition distribution between diamond particles and Ni-W matrix, the line EDS and X-ray elemental mapping were also carried out, as presented in Fig. 4. Figure 4(a,b) show the EDS analysis for the surface and cross section, respectively. Here, line scan EDS through the diamond particles zone and Ni-W matrix was performed. The results imply that Ni-W matrix showed the Ni and W spectrum and diamond particles zone that only presented the carbon spectrum. Thus, it indicates that diamond particles embedded into the Ni-W matrix by mechanical interlocking with Ni-W electroplating. Furthermore, the X-ray elemental mappings of Ni, W, and C along with the SEM image of the Ni-W/diamond composite coatings are shown in Fig. 4(d–f). The X-ray elemental mapping of C further confirms the uniform distribution of the diamond particles in the Ni-W matrix.

The diamond contents in the composite coatings was evaluated using the gravimetrically method. Figure 5(a) shows the diamond contents in the coatings prepared with different diamond concentration, particles size, and

Deposition conditions			As-deposited		After heat treatment
Diamond size (μm)	Concentration (g L^{-1})	Current density (A dm^{-2})	Grain size (nm)	W content (wt.%)	Grain size (nm)
3	5	5	1.1	41.6	8.6
3	5	10	1.1	42.8	8.5
3	5	15	1.1	42.0	5.2
3	5	20	1.7	41.4	6.2
3	1	10	1.1	44.4	10.7
3	2	10	1.2	43.4	5.7
3	10	10	1.1	42.6	9.1
3	20	10	1.1	43.0	9.8
0.8	1	10	1.1	42.3	–
0.8	5	10	1.4	41.7	6.8
0.8	10	10	1.1	40.8	–
–	0	10	2.8	44.8	9.4

Table 2. Grain size and W content in the Ni-W/diamond nanocomposite coatings with different deposition conditions.

current density. The results reveal that, as the diamond concentration in bath is increased from 0 to 5 g L^{-1} , the diamond particles content in deposits increased quickly, while the diamond concentration in bath is above 5 g L^{-1} , the diamond content in coatings kept almost constant. This could be caused by the blocking effect of the powder on the surface area available for plating¹⁶. Furthermore, the larger diamond particles embedded into the Ni-W matrix is better than that of smaller diamond particles (Fig. 5(a)). During the SCD process, particles are adsorbed onto the growing film surface in two successive steps and then are embedded within the electrodeposited metal matrix. Probably, diamond particles of $0.8 \mu\text{m}$ were too light to drop off on the substrate surface, resulting that the less of smaller diamond particles embedded into the metal matrix. In contrast, $3 \mu\text{m}$ of diamond particles were uniformly co-deposited into the Ni-W matrix, which is associated with the conditions that the diamond particles were dispersed uniformly in the bath and constantly dropped off and adsorbed on the cathode surface well.

The surface roughness of Ni-W and Ni-W/diamond coatings was examined by surface profilometer as shown in Fig. 5(b). The surface roughness (R_a) of Ni-W coatings is $1.06 \mu\text{m}$. While the R_a of Ni-W/diamond ($3 \mu\text{m}$) coatings increases from 1.19 to $2.09 \mu\text{m}$ with the diamond concentration in bath from 1 to 20 g L^{-1} . Moreover, as the diamond concentration in bath is 5 g L^{-1} , the R_a of Ni-W/diamond coatings is 1.41, 1.54, 1.34, and $1.34 \mu\text{m}$ with current density of 0.05, 0.10, 0.15, and 0.20 A cm^{-2} , respectively. Although R_a is 1–2 μm , the composite coatings have relatively flat surface.

The X-ray diffraction (XRD) patterns of Ni-W/diamond composite coatings were presented as Fig. 6, where Fig. 6(a) shows the XRD of Ni-W/diamond composite coatings obtained at diamond concentration of 1, 2, 5, 10, 20 g L^{-1} , in their as-plated condition. Three peaks occurred at 2θ angle of $\sim 44^\circ$, $\sim 75.3^\circ$, and $\sim 91.5^\circ$ which are indexed to diamond (JCPDS File No. 06-0675). And the broadened peaks at centre $\sim 44^\circ$ and $\sim 76^\circ$ could be matched with the Ni (JCPDS File No. 04-0850). This signifies the formation of solid solution of W in Ni and the peaks can be ascribed to (111) and (200) of the face-centered cubic (FCC)-Ni. Furthermore, the XRD patterns of Ni-W and Ni-W/diamond composite coatings with diamond concentration of 5 g L^{-1} at current density of 0.1 A cm^{-2} were shown in Fig. 6(b). It can be seen that the sharp diamond (111) peak appears in a XRD diffractogram of Ni-W/diamond composite coatings (Fig. 6(a,b)). XRD results could further demonstrate that the Ni-W/diamond composite coatings were successfully fabricated by using SCD method.

It has been reported that the properties of Ni-W coatings can be enhanced by heat treatment^{11,17}. The heat treatment can change the amorphous structure into a crystalline alloy structure, such as Ni_4W , NiW, as shown in Fig. 6(c), which have higher hardness than the amorphous Ni-W coatings. Wang *et al.*¹² reported that heat treatment can improve the hardness of Ni-W/diamond, which can reach up to 1205 Hv from 800 Hv (as deposited). In the present work, heat treatment was also performed under 873 K in Ar gas. Figure 6(c) shows the XRD patterns of Ni-W/diamond coating fabricated at current density of 0.10 A cm^{-2} , with diamond size $3 \mu\text{m}$ and 5 g L^{-1} . The as-prepared coating has a broad diffraction peak at around $2\theta = 30\text{--}55^\circ$ (Fig. 6(a)), which indicates an amorphous structure. The sharp peaks occurred at 2θ angle of $\sim 44^\circ$ which is indexed to diamond (JCPDS File No. 06-0675). After heat treatment at 873 K for 1 h in Ar gas, the broad peak has disappeared and diffraction peaks corresponding to Ni, diamond, WC, Ni_4W , and NiW appear¹². It also implies that the growth and coarsening of grain are promoted with an increase in heat treatment temperature. The grain size of obtained coatings was calculated from the width of the Ni (111) peaks observed in the XRD patterns using Scherrer's equation. The grain sizes before and after heat treatment for Ni-W alloy and Ni-W/diamond composite coating are displayed in Table 2. We note that in the present alloy and composite coatings system W is a grain refining element, owing to its subtle tendency for grain boundary segregation^{18–20}; accordingly, across the samples in Table 2, grain size is in agreement with the previous work²⁰.

Mechanical properties of Ni-W/diamond composite coatings. Figure 7 presents the hardness measurement results of Ni-W and Ni-W/diamond coatings. As is seen, without diamond additions, the

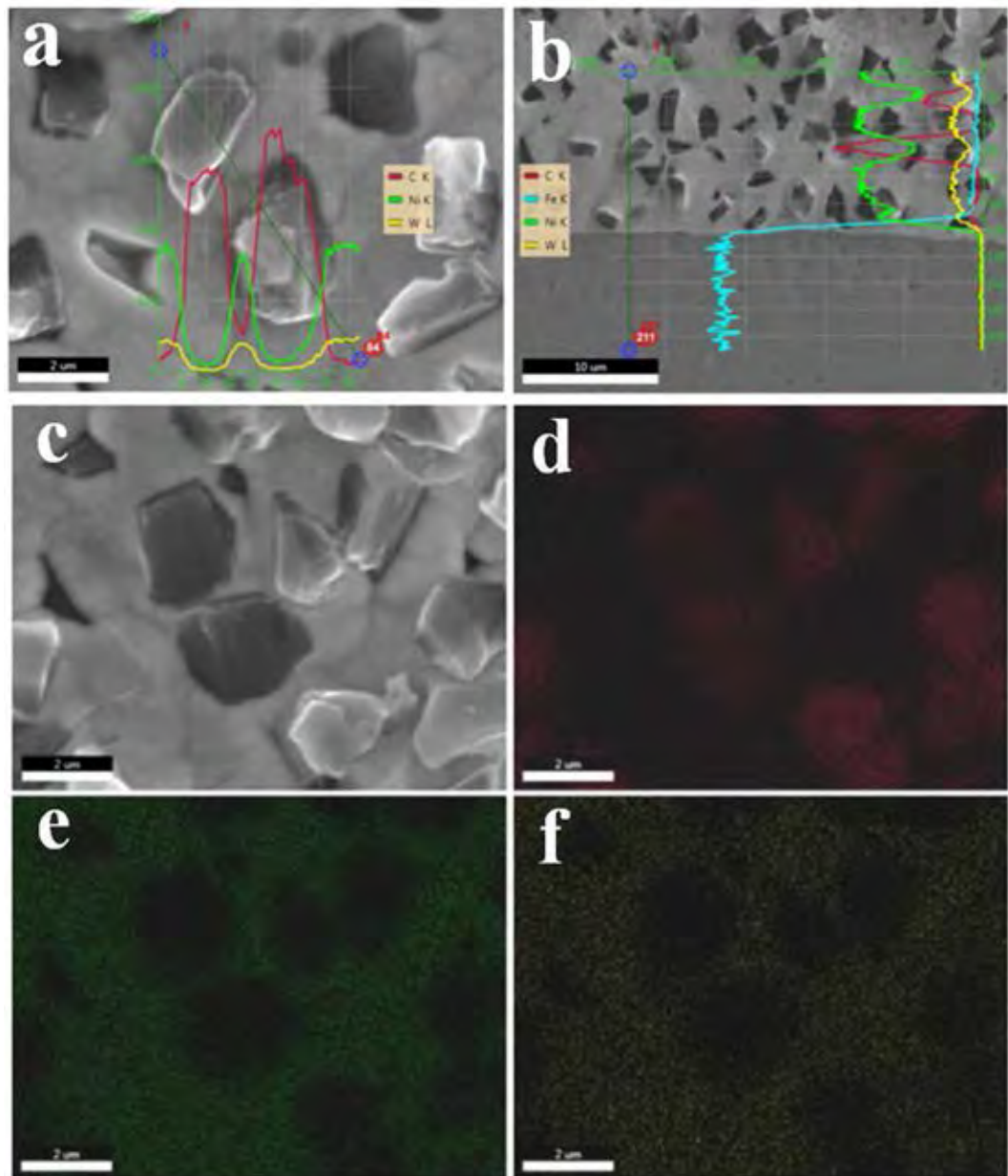


Figure 4. EDS analysis. (a) line EDS through diamond particles and Ni-W matrix on surface, (b) line EDS through diamond particles and Ni-W matrix on cross-section, (c) SEM image area of elemental mapping, (d) C element mapping, (e) Ni element mapping, (f) W element mapping.

electrodeposited Ni-W alloys fabricated with current density of 0.1 A cm^{-2} , exhibit the hardness of $810 \pm 32 \text{ Hv}$, which is in good agreement with the reported value²¹. The composite coatings prepared with diamond particles concentrations in bath of 1, 2, 5, 10, 20 g L^{-1} , exhibit the hardness of 916 ± 20 , 1370 ± 41 , 2060 ± 52 , 2076 ± 59 , and $2249 \pm 23 \text{ Hv}$, respectively. From Fig. 7(a), it can be seen that the incorporations of diamond can result in a marked improvement of hardness. The hardness increased with the concentration of diamond particles in the bath from 0 to 5 g L^{-1} , while above 5 g L^{-1} , the hardness did not cause significant differences. From the SEM (Fig. 2) and diamond content results (Fig. 5(a)), the diamond content in deposits increased quickly with increasing in the diamond concentration from 0 to 5 g L^{-1} , while the diamond content was very stable above 5 g L^{-1} . The results may be due to the blocking effect of the powder on the surface area available for plating¹⁶. Considering the mechanical properties of materials, the hardness of Ni-W/diamond composite coatings is controlled by three factors: co-deposition of diamond particles, the W content and grain size of metal matrix. According to the EDS and XRD results (Table 2), the W content ($\sim 40\text{--}44 \text{ wt.}\%$) and grain size of metal matrix ($\sim 1.1 \text{ nm}$) did not have a significant change. Thus, the hardness of Ni-W/diamond composite coatings is mainly contributed by diamond content in deposits. In order to understand how the diamond content in deposits affects the hardness of coatings, it is therefore useful to represent the hardness of diamond-free and diamond incorporated Ni-W alloys as a function

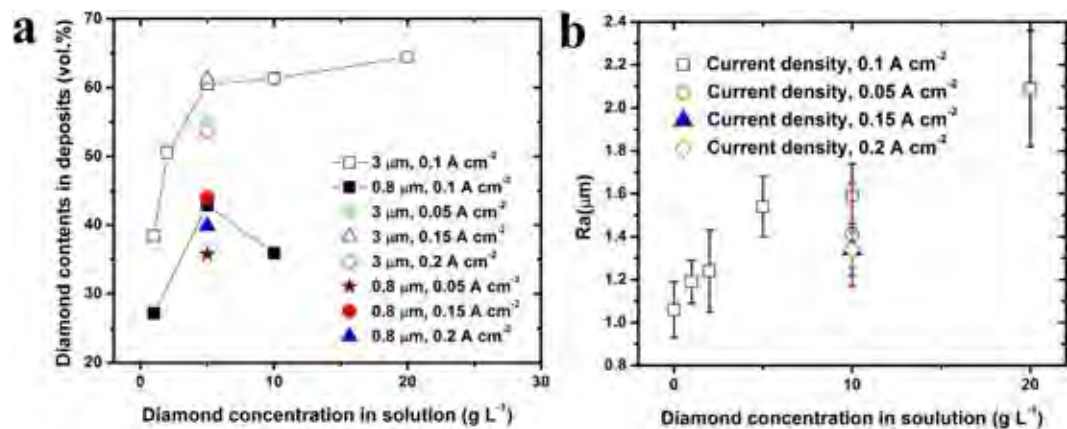


Figure 5. Diamond contents and surface roughness of Ni-W/diamond composite coatings. (a) The diamond particles content in deposits increased quickly with increasing in diamond concentration from 0 to 5 g L⁻¹, while above 5 g L⁻¹, the diamond content kept constant, (b) Surface roughness (Ra) increases with diamond concentration increasing, while the Ra is almost same for the composite coatings deposited at different current density.

of the diamond content in the deposits, which was shown in Fig. 7(b). From this figure, it can be observed that the diamond content in deposits strongly influences the hardness. The hardness increased quickly with the diamond content. Figure 7(a) also shows the effect of diamond size and current density on the hardness of Ni-W/diamond composite coatings. The hardness of Ni-W/diamond (3 μm) composite coatings is about 2.5 times higher than those of Ni-W/diamond (0.8 μm) coatings, which follows the same trend as the diamond contents in the deposits (Fig. 5(a)). The diamond content of Ni-W/diamond (0.8 μm) coatings were lower than those of Ni-W/diamond (3 μm) coatings. We consider that sedimentation contributes to these results. As sedimentation has a strong influence on large particles, therefore, the larger particles could be easily dropped off and co-deposited into the Ni-W alloy, which results in a reduction of the diamond content at diamond particles of 0.8 μm. With the current density increasing, the hardness of Ni-W/diamond increased from 1663 ± 19 to 2193 ± 46 Hv, while the hardness slightly decreased above 0.15 A cm^{-2} . A similar tendency was also observed in another electrodeposition system (Ni-B/diamond)²². To the best of our knowledge, the Ni-W/diamond coating is the hardest among coatings fabricated by wet chemical process. Moreover, the hardness of Ni-W/diamond coatings is higher than that of hard chrome coating (850–1100 Hv)⁸ and Ni-B/diamond coating (1940 Hv, load 50 gf)^{7,9}, which is even in the same range as the hard coatings prepared by dry process (e.g. TiN, 2000–2700 Hv).

The hardness with different deposition conditions after heat treatment was also examined, as shown in Fig. 7a. The results imply that the hardness of the Ni-W/diamond coatings increased from 2060 ± 52 , 2076 ± 59 , and 2249 ± 23 Hv to 2263 ± 37 , 2437 ± 41 , 2647 ± 25 Hv with diamond concentration 5, 10, 20 g L⁻¹, respectively, with heat treatment at 873 K for 1 h in Ar gas. In order to examine the structural change of Ni-W/diamond coatings during heat treatment, XRD patterns were measured, as shown in Fig. 6(c). Heat treatment of the coating resulted in the crystal growth and the formation of WC hard phase and Ni₄W, NiW alloy. Without diamond incorporation, oxide has been detected according to the XRD results, which agreed with the previous work¹⁷. However, the accurate phase identification could not be made but Ni-O, W-O, or Ni-W-O phases could be possible. While XRD results reveal no oxide was formed during the high temperature treatment for Ni-W/diamond composite coatings (Fig. 6(c)). According to the present results, the formation of WC hard phase in the Ni-W matrix and the precipitate of NiW and Ni₄W alloy caused the hardening of the Ni-W/diamond coating.

The performance of many products and engineering components depends critically on tribological properties of surfaces such as wear and friction. Here the wear testing was also performed by using reciprocating-sliding tribometer for Ni-W (prepared at current density of 0.1 A/cm^2) and Ni-W/diamond composite coatings (deposited at current density of 0.1 A/cm^2 and diamond concentration of 2, 5, and 10 g/L). Figure 8 shows the corresponding coefficient of friction (CoF) data for Ni-W and Ni-W/diamond composite coatings, respectively. For Ni-W coating the friction coefficient is always larger than those of Ni-W/diamond composite coatings. During the wear testing, if the maximum friction force is larger than 10 N, i.e. the CoF is larger than 1 in present case with the load of 10 N, the testing will be stopped by the protection function of the equipment. For Ni-W coatings, one test stopped when the sliding distance reached 42 m and it stopped at 200 m again at another test because the CoF became larger than 1. For Ni-W/diamond composite coatings, however, the CoF was kept almost constant ~ 0.2 – 0.45 for sliding distance of 300 m or even longer. For example, the friction coefficient of obtained coatings prepared at diamond concentration of 5 g/L can keep ~ 0.4 until the sliding distance approaching up to 600 m. The CoF reveals that the addition of diamond could significantly reduce the friction coefficient. Observing the wear tracks generated on treated samples can provide information on the wear performance and mechanics of reciprocating ball-on-plate sliding, of particular interest is the changes induced by addition of the diamond.

From the Fig. 8, it can be seen that the friction coefficient decreases sharply during running in and then stabilizes to steady-state. During the wear testing process, it takes place as the two surfaces are moving in relation to each other, and both physical and chemical changes occur. As a function of time the wear process changes in

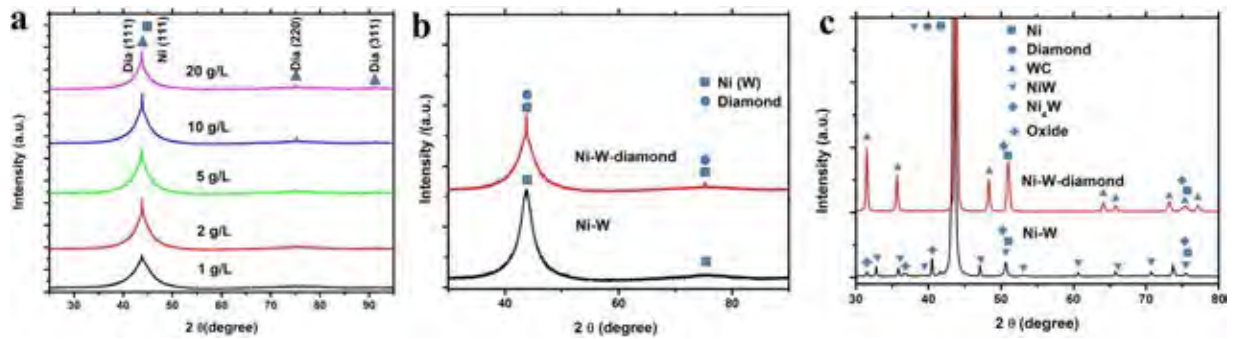


Figure 6. XRD analysis of the obtained samples. (a) XRD patterns of Ni-W/diamond composite coatings obtained at diamond concentration of 1, 2, 5, 10, 20 g L⁻¹, in their as-plated condition, (b) XRD patterns of as-deposited Ni-W and Ni-W-diamond coatings, (c) XRD patterns of heat treatment of Ni-W and Ni-W/diamond coatings.

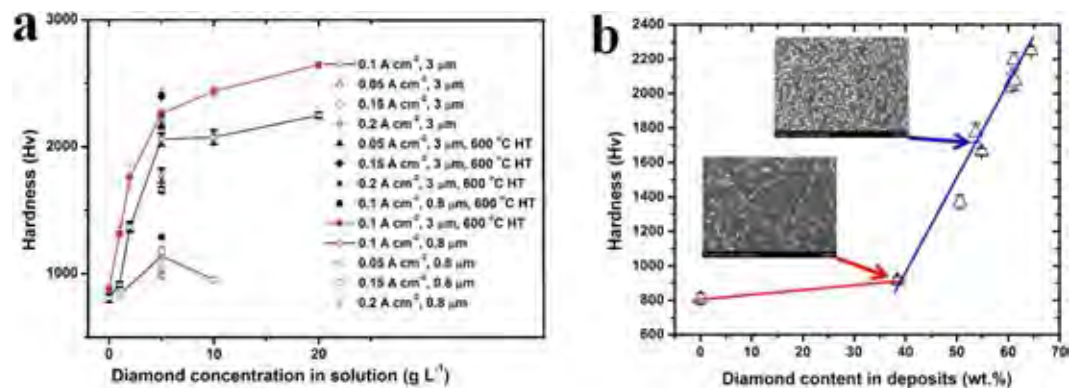


Figure 7. Hardness of coatings. (a) Hardness of the coatings with different deposition conditions and heat treatment, (b) hardness of the Ni-W alloys and Ni-W/diamond composite coatings presented as a function of the diamond content in coatings.

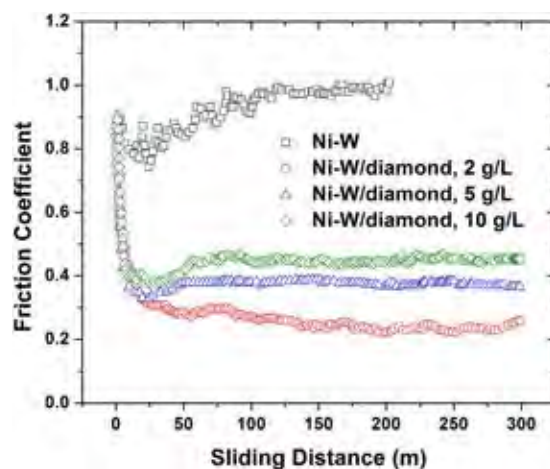


Figure 8. The friction coefficient during wear testing. With diamond incorporation, the friction coefficient decreases.

both geometry and the material composition. For the Ni-W/diamond composite coatings, in the initial phase of wear process, the ball will abrasive both Ni-W matrix and diamond particles, resulting the higher friction coefficient. Then, the diamond particles could be exposed and applied as micro-cutter. Despite being hard, diamond particles are known to have low friction coefficient. Therefore, the friction coefficient decreases and keeps stable in all obtained composite coatings. The reduction of friction coefficients can be explained by the formation of

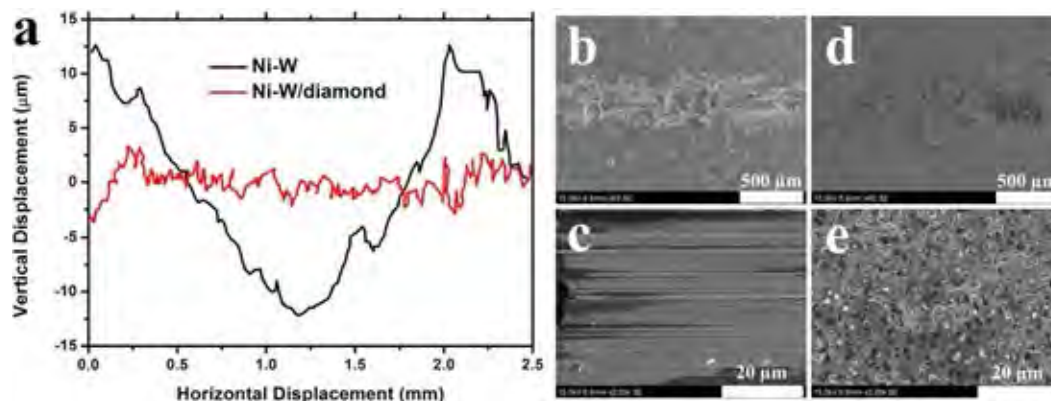


Figure 9. Worn surface observation. (a) Wear track profilometry scans for Ni-W coatings, and Ni-W/diamond composite coatings. (b) general SEM view of wear track of Ni-W coatings, (c) inside of the wear track of Ni-W coatings, (d) general SEM view of wear track of Ni-W/diamond composite coatings, (e) inside of the wear track of Ni-W/diamond composite coatings.

low-shear micro-points on the coating or perhaps only on the asperity tips of the coatings²³. While the Ni-W coatings, the friction coefficient slightly increases and reaches up to 1 at about 40 m (one test) and 200 m (another test) sliding distance.

Figure 9(a) presents the 2D surface profilometry of wear scars. The wear scars can clearly demonstrate that the Ni-W/diamond composite coatings exhibit better wear resistance. From the 2D wear scars, the wear volume could be estimated for Ni-W coatings (0.55 mm³). However, the measurement of wear volume for Ni-W/diamond composite coatings is difficult because of the very less of removed coatings.

SEM was also performed to study the inside wear tracks of the Ni-W (sliding distance 42 m) and Ni-W/diamond composite coatings prepared with diamond concentration of 5 g/L (sliding distance 600 m), as shown in Fig. 9(b–e). From the Fig. 9(b,c) can be observed that the wear track of Ni-W coatings is clear and the smeared appearance of the surface is typical of material spalled, lots of scratching, as well as extensive plastic deformation. The morphology of worn surface of the Ni-W/diamond composite coatings is shown in Fig. 9(d,e). It can be observed that the wear track is not clear. No any diamond particles were peeled off during the wear test from the magnified SEM worn surface of Ni-W/diamond composite coatings (Fig. 9(e)) owing to the strong adherence between diamond particles and Ni-W matrix.

Due to the high hardness of the coatings deposited, balls used for testing were also worn. The SEM wear scar morphology has been attributed in part to adhesion of ball materials to the wear worn surface. This is also confirmed by the elemental mapping, as shown in Fig. 10, which indicates that elemental map showing the distribution of N, Si, C, Ni, W elements in the worn surface of Ni-W/diamond composite coatings. It can be seen that the concentrated position of red spot contain a higher proportion and uniformly of C elements. It shows diamond particles have extensive distribution in the worn surface of Ni-W/diamond composite coatings. The reinforced diamond particles have reduced the direct contact between the Ni-W matrix and the counter ball during the wear test that also reduced the friction coefficient and resulted in the higher wear resistance. Figure 10(b,c) show that the N and Si elements uniformly distribute on the worn surface, it suggests that the hardest diamond particles could easily remove the ball materials during the wear testing, and the removed ball materials adhere onto the worn surface.

In summary, sediment co-electrodeposition was performed to prepare hard Ni-W/diamond composite coatings. These coatings exhibited extreme high hardness and superior wear resistance. The hardness of the composite coatings was increased by increasing the concentration and size of diamond particles in present study because diamond particles with higher concentration and larger sized tend to co-deposit into Ni-W matrix more easily. Furthermore, the hardness was improved by heat treatment of the coatings. The hardest Ni-W/diamond composite coating in the present work was even higher than that of Ni-B/diamond coatings prepared by wet process and comparable to hard coatings prepared by dry processes.

Methods

Chemicals. Nickel(II) sulfate hexahydrate NiSO₄·6H₂O(Carlo), Sodium tungstate dihydrate Na₂WO₄·2H₂O(Carlo), Tri-sodium citrate dihydrate Na₃C₆H₅O₇·2H₂O(Carlo), Ammonium chloride NH₄Cl(Carlo), Sodium bromide NaBr(Carlo) used in the present study were of analytical reagent grade. Diamond powder was from Huanghe Xuanfeng Co. Ltd., China. All aqueous solutions were prepared using double distilled water.

Sample preparation. The co-electrodeposition of Ni-W and diamond was conducted in a 200 mL plating bath with aqueous bath chemistry. The bath composite and plating conditions are listed in Table 1. We have previously demonstrated the preparation of composite coatings using SCD method¹⁵. Figure 1(a) shows the setup of SCD. Figure 1(b) shows the schematic representation of the Ni-W-diamond composite coatings formation process through SCD method. Analytical reagents and deionized water were used to prepare the plating solution. The diamond particles of a mean particles size of 0.8 and 3 μm were chosen to co-deposit with nickel in the present

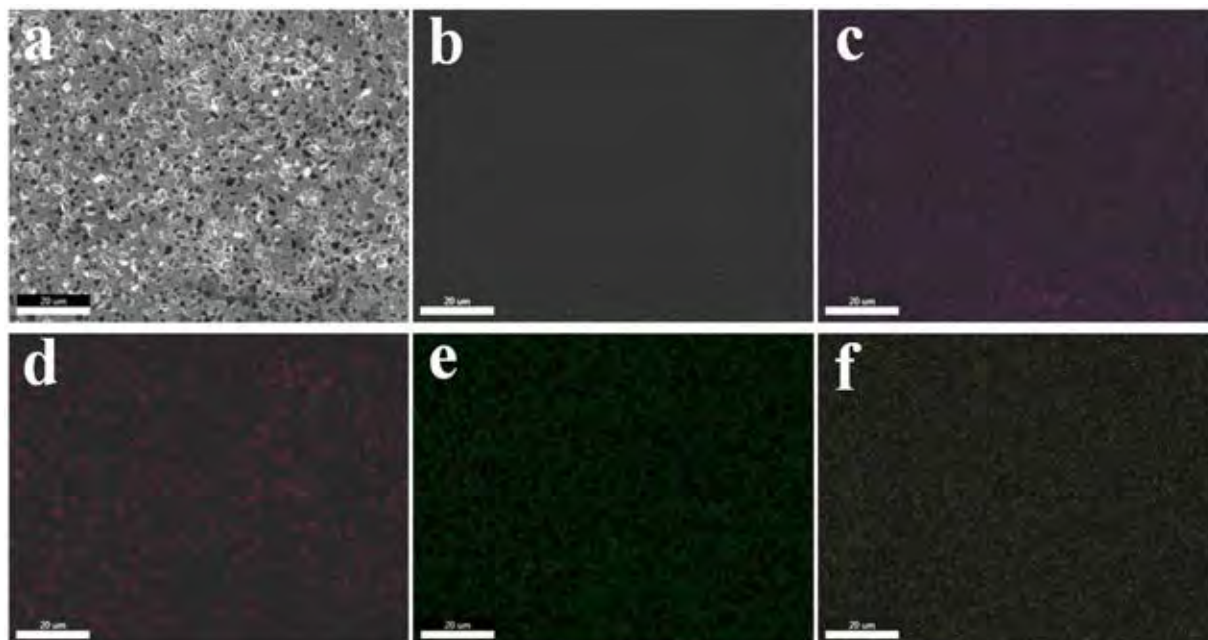


Figure 10. Elemental mapping of worn surface. (a) SEM image, (b) N element mapping, (c) Si element mapping, (d) C element mapping, (e) Ni element mapping, (f) W element mapping.

experiments. The concentration of diamond particles in the bath are 1, 2, 5, 10, 20 g L⁻¹. The bath temperature was maintained at 75 °C. The pH of the electrolyte was 8.9, and it was unaffected by the diamond additions. Carbon steel was employed as a cathode. Prior to plating, steel substrates were washed in soap, rinsed in NaOH, HCl, and distilled water, and activated in 14% HCl. The steel substrates were masked with insulated tape to leave 4 cm² of exposed area.

The steel substrate and Pt coated-Fe mesh plate with a distance of 35 mm were horizontally immersed into 200 ml of the electrodeposition baths. Electrodeposition was carried out under constant current density (0.05, 0.1, 0.15, and 0.2 A cm⁻²). Ni-W/diamond composite coatings were electrodeposited on the steel plates. The coatings were washed with water and dried in air at room temperature. In addition, a Ni-W alloy coating was also obtained by SCD using the developed setup.

Materials characterization. Prior to surface analysis, all coatings were washed in deionized water and ultrasonicated in acetone for 5 min. Optical microscope (OM) was used to determine the thickness of coating. Scanning electron microscopy (SEM, Hitachi, S4800) was performed to observe the surface of the coatings. The particle contents in the composite coatings was evaluated using the gravimetrically method. Deposits were stripped in nitric acid, which was filtered, and the mass of diamond powder in the deposit was estimated gravimetrically. The phases of the composite coatings were detected via X-ray diffraction using an X'Pert Pro diffractometer (Panalytical). The surface profile (Gauges, Ambs, US) was used to measure the surface roughness. Vickers microhardness for the surface of coatings was measured using a microhardness tester under an indentation load of 100 gf for 15 s at seven different locations of a specimen, and the average value of the five measurements (except the maximum and minimum values) is quoted as the hardness of the film.

Wear tests were performed using a CSM reciprocating-sliding tribometer, connected to a computer monitoring the dynamic coefficient of friction (in both sliding directions), relative humidity and temperature. Tests were performed by applying a normal load of 10 N to a stationary ball of diameter 6 mm. The ball materials used were Si₃N₄. The ball-on-plate machine was set to run at 100 mm/s with reciprocation amplitude of 10 mm and without lubrication. The tests performed at temperatures between 20 and 25 °C. Before each test, both the sample and the ball counterface were ultrasonically cleaned in acetone for 10 min, and dried by hot air. The anti-wear performance of the films was estimated from the weight loss of the specimens. After the wear tests, the morphology of each wear scar was observed by SEM. Also the SEM and EDS were used to obtain information regarding the morphology and chemical composition of the wear debris.

References

- Xu, H., Yang, Z., Li, M.-K., Shi, Y.-L., Huang, Y. & Li, H.-L. Synthesis and properties of electroless Ni-P-Nanometer Diamond composite coatings. *Surf. Coat. Tech.* **191**, 161–165 (2005).
- Shrestha, N. K., Takebe, T. & Saji, T. Effect of particle size on the co-deposition of diamond with nickel in presence of a redox-active surfactant and mechanical property of the coatings. *Diam. Relat. Mater.* **15**, 1570–1575 (2006).
- Ger, M.-D. Electrochemical deposition of nickel/SiC composites in the presence of surfactants. *Mater. Chem. Phys.* **87**, 67–74 (2004).
- Grosjean, A., Rezrazi, M., Takadom, J. & Berçot, P. Hardness, friction and wear characteristics of nickel-SiC electroless composite deposits. *Surf. Coat. Tech.* **137**, 92–96 (2001).
- Pavlatou, E. A., Stroumbouli, M., Gyftou, P. & Spyrellis, N. Hardening effect induced by incorporation of SiC particles in nickel electrodeposits. *J. Appl. Electrochem.* **36**, 385–394 (2006).

6. Tomaszewski, T. W. *Trans. Inst. Met. Finish.* **54**, 45–48 (1976).
7. Oghara, H. *et al.* Synthesis of super hard Ni-B/diamond composite coatings by wet processes. *Chem. Commun.* **46**, 442–444 (2010).
8. Kosta, I., Sarret, M. & Müller, C. Structure, microhardness and corrosion behaviour of nanostructured CoP coatings obtained by direct current and pulse plating. *Electrochim. Acta* **114**, 819–826 (2013).
9. Oghara, H., Miyamoto, K., Udagawa, K. & Saji, T. Electrodeposition of Super Hard Ni-B/Diamond Composite Coatings. *Chem. Lett.* **40**, 1072–1073 (2011).
10. Giga, A., Kimoto, Y., Takigawa, Y. & Higashi, K. Demonstration of an inverse Hall–Petch relationship in electrodeposited nanocrystalline Ni–W alloys through tensile testing. *Scripta Mater.* **55**, 143–146 (2006).
11. Sunwang, N., Wangyao, P. & Boonyongmaneerat, Y. The effects of heat treatments on hardness and wear resistance in Ni–W alloy coatings. *Surf. Coat. Tech.* **206**, 1096–1101 (2011).
12. Wang, H.-T., Sheu, H.-H., Ger, M.-D. & Hou, K.-H. The effect of heat treatment on the microstructure and mechanical properties of electrodeposited nanocrystalline Ni–W/diamond composite coatings. *Surf. Coat. Tech.* **259**, Part B, 268–273 (2014).
13. Zhang, X. *et al.* Preparation and hardness of pulse electrodeposited Ni–W–diamond composite coatings. *Surf. Coat. Tech.* **276**, 228–232 (2015).
14. Chianpairot, A., Lothongkum, G., Schuh, C. A. & Boonyongmaneerat, Y. Corrosion of nanocrystalline Ni–W alloys in alkaline and acidic 3.5wt.% NaCl solutions. *Corros. Sci.* **53**, 1066–1071 (2011).
15. Qin, J. *et al.* The high concentration and uniform distribution of diamond particles in Ni–diamond composite coatings by sediment co-deposition. *Surf. Interface. Anal.* **47**, 331–339 (2015).
16. Marlborough, A. E. Small finishing systems: Aubin Co., A. E. Marlborough, Conn. *Metal Finish.* **95**, 22 (1997).
17. Hou, K.-H., Chang, Y.-F., Chang, S.-M. & Chang, C.-H. The heat treatment effect on the structure and mechanical properties of electrodeposited nano grain size Ni–W alloy coatings. *Thin Solid Films* **518**, 7535–7540 (2010).
18. Detor, A. J., Miller, M. K. & Schuh, C. A. Measuring grain-boundary segregation in nanocrystalline alloys: direct validation of statistical techniques using atom probe tomography. *Phil. Mag. Lett.* **87**, 581–587 (2007).
19. Detor, A. J., Miller, M. K. & Schuh, C. A. Solute distribution in nanocrystalline Ni–W alloys examined through atom probe tomography. *Philosophical Magazine* **86**, 4459–4475 (2006).
20. Rupert, T. J. & Schuh, C. A. Sliding wear of nanocrystalline Ni–W: Structural evolution and the apparent breakdown of Archard scaling. *Acta Mater.* **58**, 4137–4148 (2010).
21. Schuh, C. A., Nieh, T. G. & Iwasaki, H. The effect of solid solution W additions on the mechanical properties of nanocrystalline Ni. *Acta Mater.* **51**, 431–443 (2003).
22. Oghara, H., Safuan, M. & Saji, T. Effect of electrodeposition conditions on hardness of Ni–B/diamond composite films. *Surf. Coat. Tech.* **212**, 180–184 (2012).
23. Holmberg, K., Ronkainen, H. & Matthews, A. Tribology of thin coatings. *Ceram. Int.* **26**, 787–795 (2000).

Acknowledgements

This research is supported by Thailand Research Fund (TRG5780222). J.Q. would like to acknowledge the support from National Research Council of Thailand (NRCT, 183299), Ratchadaphisek somphoch Endowment Fund (2013), Chulalongkorn University (CU-56-805-FC), and Key Laboratory of Metastable Materials Science and Technology, Yanshan University. X.Z., M.M. and R.L. would like to thank the support from NBRPC (grant 2013CB733000), NSFC (grants 51571174/51531005).

Author Contributions

J.Q., X.Z. and R.L. designed and coordinated the research. J.Q., X.Z., M.D., R. H., H. Z., A.T., S. L., Y.B. and M.M. did the experiments and analyzed all data. J.Q. and X.Z. wrote the manuscript.

Additional Information

Competing financial interests: The authors declare no competing financial interests.

How to cite this article: Zhang, X. *et al.* Co-electrodeposition of hard Ni–W/diamond nanocomposite coatings. *Sci. Rep.* **6**, 22285; doi: 10.1038/srep22285 (2016).



This work is licensed under a Creative Commons Attribution 4.0 International License. The images or other third party material in this article are included in the article's Creative Commons license, unless indicated otherwise in the credit line; if the material is not included under the Creative Commons license, users will need to obtain permission from the license holder to reproduce the material. To view a copy of this license, visit <http://creativecommons.org/licenses/by/4.0/>



Effect of electrodeposition conditions on structure and mechanical properties of Ni-W/diamond composite coatings



Malay Kumar Das^{a,b}, Rongxia Li^c, Jiaqian Qin^{b,*}, Xinyu Zhang^{c,*}, Kumkumlata Das^d, Adisak Thueploy^b, Sarintorn Limpanart^b, Yuttanat Boonyongmanerat^b, Mingzhen Ma^c, Riping Liu^c

^a International Graduate Program of Nanoscience & Technology, Chulalongkorn University, Thailand

^b Metallurgy and Materials Science Research Institute, Chulalongkorn University, Bangkok, Thailand

^c State Key Laboratory of Metastable Materials Science and Technology, Yanshan University, Qinhuangdao, P.R., China

^d College of Allied and Medical Sciences, Purbanchal University, Nepal

ARTICLE INFO

Article history:

Received 1 February 2016

Revised 26 September 2016

Accepted in revised form 20 November 2016

Available online 30 November 2016

Keywords:

Composite coatings

Electrodeposition

Diamond

Hardness

Wear resistance

ABSTRACT

Ni-W/diamond composite coatings were prepared by electrodeposition from a Ni-W plating bath with diamond particles suspended into the bath. The effect of the plating parameters on microstructure and mechanical properties was investigated. The deposits reported a maximum hardness of 1207 ± 32 Hv. The film hardness is depended on the concentration of diamond particles in the plating bath and also on the size of the co-deposited diamond particles. The sample with diamond concentration of 10 g/L in the bath and co-deposited at current density of 0.15 A/cm² reported the optimized wear resistance and diamond content in the deposit. In this paper the effect of the incorporation of diamond particles into the Ni-W matrix has been discussed in terms of the aforesaid operating conditions and particle size.

© 2016 Elsevier B.V. All rights reserved.

1. Introduction

Composite electrodeposition is a suitable technique of co-depositing various particles of pure metals, ceramics and organic materials in a base matrix of metal/metal alloys to improve the deposits properties such as hardness, wear resistance, surface roughness and uniformity of distribution of co-deposited particles [1–10]. Hardness is an important surface property which relates to the wear resistance and mechanical strength of the material. Hard coatings are used to improve the longevity of products, facilitate the enhancement of performance for cutting tools and other materials which are coated with hard materials such as diamond by various wet and dry processes. However, there are various advantages of wet process of fabrication of coatings over the dry process which involves the use of costly equipment, extreme reaction conditions and higher costs. Electrodeposition is a simple and very commonly used method of wet process deposition of films. It is extensively used to fabricate hard metal and alloy films on materials (for example Cr, Ni-W alloy) [11–14] to name a few.

Electrodeposited Ni-W alloy coatings have been able to serve as a replacement to the hazardous hexavalent chromium coatings [15–17]. Various researchers report that the hardness of the Ni-W alloy is mainly

determined by the W content and grain size of the electrodeposited Ni-W [18–21]. The hardness of the as-deposited Ni-W alloy has been reported to vary between 460 and 670 Hv [18–21]. However, the hardness of the Ni-W alloy is significantly lesser than that of chromium coatings which report high hardness of 1100 Hv [20,22]. Moreover, various literatures have stated that addition of suitable particles (for example diamond, Al₂O₃, WC and SiC) to a hard alloy matrix can significantly enhance mechanical properties such as hardness, wear resistance and corrosion resistance of the deposits [17,23–26]. However, for composite coatings of nanostructured Ni-W matrix reinforced by diamond particles there are only a few publications. Hou et al. [27] prepared Ni-W/diamond composite coatings and investigated its mechanical properties. They reported that the highest level of incorporation of diamond was about 21.1 vol.% at diamond concentration in bath of 1 g/L. In our previous study, Ni-W/diamond composite coatings were also deposited by pulse electrodeposition [10] and sediment co-electrodeposition method [28]. The results demonstrated that the pulse current can affect the diamond incorporation and W content in the deposit. Further, the sediment co-electrodeposition method could significantly improve the diamond content in deposits, resulting high hardness of Ni-W/diamond composite coating. Combined with previous research on Ni-W/diamond [10,27–29], Ni/diamond [3,6], Ni-Co/diamond [2,7], Ni-P/diamond [1,5,30], Ni-B/diamond [4] composite coatings, the electrodeposition parameters and size of diamond particles can strongly affect the properties of composite coating. Therefore, this paper aims to further investigate and

* Corresponding authors.

E-mail addresses: jiaqian.q@chula.ac.th (J. Qin), xyzhang@ysu.edu.cn (X. Zhang).

examine the effect of electrodeposition conditions on microstructure and mechanical properties for the Ni-W/diamond composite coating.

In the present study, co-deposition of Ni-W/diamond composite coating was prepared from Ni-W plating bath containing diamond particles in suspension. The effect of electrodeposition parameters on the hardness, wear resistance and microstructure of the deposits were investigated. Microstructural and mechanical properties of the obtained Ni-W/diamond composite coatings that were directly related to the electrodeposition conditions were also determined.

2. Experimental details

Ni-W/diamond composites were fabricated by means of electrodeposition from an ammonia-citrate bath (200 mL). The bath composition was nickel sulphate 18 g/L, sodium tungstate 53 g/L, tri-sodium citrate 168 g/L, ammonium chloride 31 g/L, sodium bromide 18 g/L. The deposition was carried out. The diamond concentration was varied in the bath (1 g/L, 2 g/L, 3 g/L, 5 g/L, 10 g/L and 20 g/L) and the particle size of diamond used were 0.2, 0.3, 0.9, 3 and 6 μm , respectively. The operating temperature was 75 °C. The pH, stirring speed and the deposition time was kept constant at 8.9, 200 RPM and 2 h, respectively. The current density was varied between 0.05 and 0.2 A/cm².

During the electrodeposition process, Pt mesh was applied as anode, and carbon steel was used as a cathode, and the distance was 35 mm. The coating area was fixed at 2*2 cm². The substrate was rinsed with soap solution before deposition and pre-treated with 10% NaOH and 14% HCl solution for a period of 20 and 10 min, respectively. Prior to insertion of the electrodes in the plating bath, the substrate was activated by 14% HCl. Except the deposition area the other undesirable parts of the substrate was covered with polymer tape.

X-Ray diffraction (XRD) technique was employed to analyze the phases of the deposits along identification and analysis of the crystalline structure of the coatings. Brooker D8 advance X-ray diffractometer operated at Cu K α radiation at a rating of 40 kV, 20 mA. The scan rate was 0.02° per step and the measuring time 0.5 s/step. Scherer's equation [27] was employed for the calculation of the grain size of the electrodeposited coatings.

$$D = \frac{0.9\lambda}{\beta \cos\theta} \quad (1)$$

where, D is the grain size, λ is the X-ray wavelength (1.5418 Å), β is the corrected peak width at half maximum intensity (FWHM) and θ is Bragg angle.

The samples were characterized in terms of morphology and microstructure by JEOL JSM-6400 scanning electron microscope (SEM) with energy dispersive X-ray spectroscopy (EDS) capability embedded into it. The volume percentages of the incorporated diamond particles in the obtained Ni-W/diamond composite coatings were determined from the cross-sectional SEM images by the image analysis software (ImageJ) to estimate the portion of diamond content in the coatings.

The coating hardness was measured on the surface using Mitutoyo hardness tester with a Vickers's diamond indenter under a load of 100 g (0.98 N) at seven different locations of the coating. The dwell time for each indentation was 15 s. The Vickers hardness can be calculated in accordance with the formula:

$$Hv = 1854 \frac{L}{d^2} \quad (2)$$

Here, Hv is the hardness in Vickers's and L is the applied load and d is the diagonal of the indentation. The average value of the five measurements (except the maximum and minimum values) is quoted here as the hardness of the obtained composite coating.

The tribological property of the deposits was analyzed by wear test. The wear test was carried out at an air humidity of 45 \pm 10 RH% and a temperature of 24 \pm 1 °C using a ball-on-disc tribometer with the sample placed horizontally on a turntable. The tests were performed by applying a load of 20 N to a zirconium dioxide ball of diameter 6 mm, a linear speed of 9.42 cm/s for a total sliding distance of 500 m and for the total wear duration of 53 min. The hardness of the zirconium dioxide ball was ~1300 Hv. Before each test, both the sample and the ball counter face were ultrasonically cleaned in acetone for 10 min, and dried by hot air. The anti-wear performance of the films was estimated from the weight loss of the specimens.

3. Results and discussion

Fig. 1 (a–d) shows the SEM image of Ni-W/diamond (NWD) composite deposits fabricated at 1 g/L, 3 g/L, 5 g/L and 10 g/L diamond concentration in plating bath at current density of 0.15 A/cm², respectively. 3 μm diamond particles were used for the fabrication of NWD deposits at 0.15 A/cm² and varying diamond concentration in the plating bath. Fewer diamond particles appear to be co-deposited on the surface for samples fabricated at 1 g/L (Fig. 1 (a)) and 3 g/L (Fig. 1 (b)) diamond concentration in the plating bath. Upon increasing the plating bath diamond concentration to 5 g/L (Fig. 1 (c)) and 10 g/L (Fig. 1 (d)) the

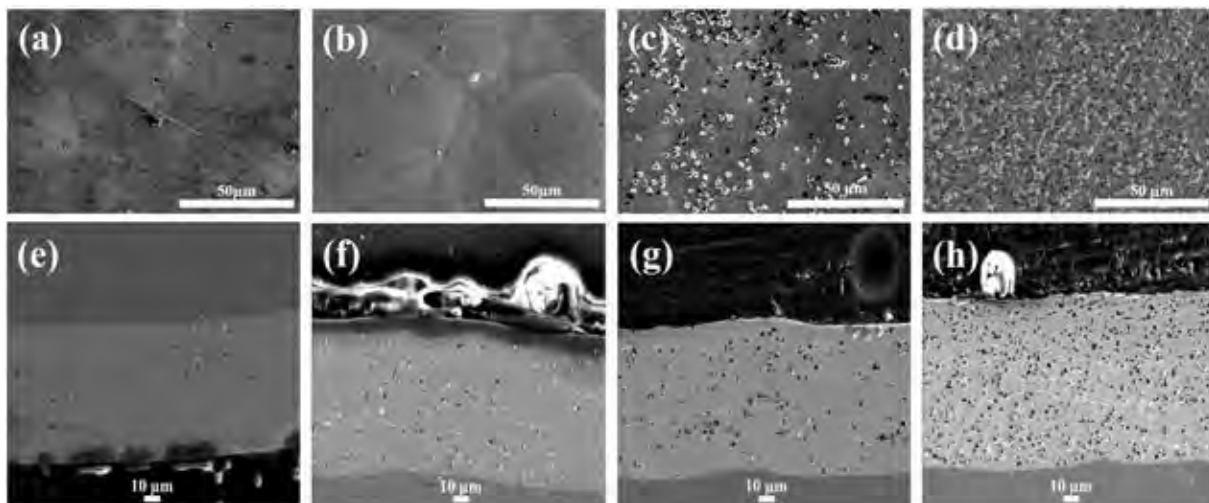


Fig. 1. Effect of diamond concentration in plating solution on morphology of Ni-W/diamond composite coatings prepared at temperature of 75 °C, pH 8.9, and current density of 0.15 A/cm². SEM images, (a) 1 g/L, (b) 3 g/L, (c) 5 g/L, (d) 10 g/L, and cross section SEM images, (e) 1 g/L, (f) 3 g/L, (g) 5 g/L, (h) 10 g/L.

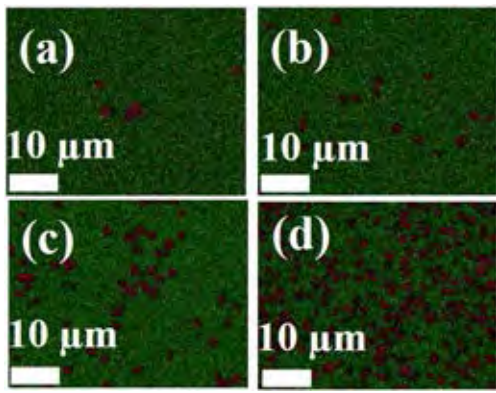


Fig. 2. EDS element mapping images of Ni-W/diamond composite films fabricated at current density of 0.15 A/cm², temperature of 75 °C, pH 8.9, and different diamond concentrations in the plating bath, (a) 1 g/L, (b) 3 g/L, (c) 5 g/L, (d) 10 g/L.

number of diamond particles co-deposited along with the uniformity of distribution of diamond particles appears drastically enhanced.

The increase in the diamond concentration of the deposits also enhances the morphology of the Ni-W matrix in terms of crack reduction and uniform incorporation of diamond particles. The sample fabricated with 10 g/L diamond concentration in the plating bath (Fig. 1 (d)) exhibits the highest level of incorporation and uniformity in distribution of diamond particles throughout the matrix as compared to the samples fabricated with lower values of diamond concentration in the plating bath.

Fig. 1 (e–h) shows the cross-sectional SEM images for the samples with variation in the diamond concentration in the plating bath. The cross-sectional SEM images also suggest an increase in the diamond incorporation and relatively more uniform distribution into the deposits upon increasing the diamond concentration in the plating bath from 1 g/L to 10 g/L (Fig. 1 (e–h)). The increase in the diamond concentration of the bath therefore enhances the co-deposition of the diamond particles in the deposits significantly.

Fig. 2 indicates the EDS elemental mapping of diamond particles co-deposited into the Ni-W matrix. The diamond incorporation in the deposits increases significantly upon increasing the diamond concentration in bath from 5 g/L to 10 g/L. The diamond distribution also seems more uniform for the sample containing 10 g/L diamond concentration in bath as compared to other concentrations.

The hardness of the NWD deposits increases from 734 ± 15 Hv to 1207 ± 32 Hv as the concentration of diamond was increased from 1 g/L to 10 g/L in the NWD plating bath. However, the hardness declined significantly to 989 ± 28 Hv, 832 ± 37 Hv as the diamond concentration was increased to 15 and 20 g/L, respectively. Therefore, upon increasing the diamond particles concentration in the deposits beyond 10 g/L the effect of the diamond particles on the hardness of the NWD deposits isn't as significant as with 10 g/L diamond concentration in the plating bath. Fig. 3 shows the comparison of diamond content (vol.%) in the deposits for various diamond concentrations in the bath and current densities. The diamond content in the deposits increases upon increasing the diamond concentration in bath from 1 g/L to 10 g/L (Fig. 3). The samples with 10 g/L diamond concentration in the plating bath and fabricated at current density 0.15 A/cm² reports the highest value of diamond content in the deposits at 32 vol.%. While the diamond content in the deposits decreased to 30 vol.% and 28 vol.% at the diamond concentration in the bath of 15 g/L and 20 g/L, respectively. Similar results for increase in composite particle concentration in the deposits upon increasing the particles concentration in bath have been reported by Ogihara et al. [26] for Ni-B/diamond composite films and Guglielmi et al. [31] for Ni/silicon carbide composite films. The composite co-deposition process has been explained by Guglielmi et al. [31] when the composite particles are adsorbed onto the alloy surface and then incorporated into the electrodeposited alloy matrix [31]. Upon an increase

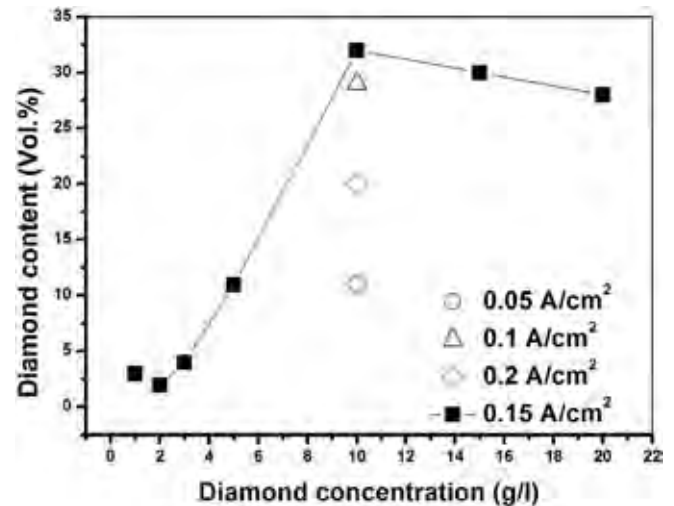


Fig. 3. Effect of diamond concentrations and current density on diamond content of Ni-W/diamond composite deposits fabricated at temperature of 75 °C and pH 8.9.

in the diamond concentration in bath there is a corresponding increase in the number of diamond particles that collide onto the surface of the electrode which in turn results in the increase in the diamond content of the electrodeposited coatings [4,31]. However, at higher diamond concentration in the bath, the aggregation of diamond particles in the solution will cause the co-deposition process difficult, resulting the decreasing in the diamond content in the coatings.

The samples fabricated at various current densities were also investigated (Figs. S1, and 1 (d)). From the Fig. 3, the diamond content in the composite coatings increases initially with the current density and reaches a maximum at 0.15 A/cm², and then the diamond content decreases at current density of 0.2 A/cm². The EDS elemental mapping results further confirm the SEM observation in respect of uniform distribution and incorporation of diamond particles at the aforesaid current densities (Fig. S2). These results can be attributed to the transition from an activation-controlled metal deposition reaction to a diffusion-controlled one of particles transfer. When the current density is smaller than 0.15 A/cm², the co-deposition process is controlled by the adsorption of diamond particles. The increasing of diamond content in coatings can be contributed by the increasing of adsorbed diamond particles to arrive in the cathode surface with the current density increasing, which is consistent with Guglielmi's model [31]. When the current density is higher than 0.15 A/cm², the adsorption of diamond particles on the cathode will be always slower than the metal deposition rate, resulting the decreasing in the incorporation of diamond particles with the current density increasing.

The NWD samples exhibit slight increase in the deposition rate upon increasing the diamond concentration in the plating bath (Fig. S3(a)). The thickness of the deposits varied in the range of ~56–66 μm. The deposition rate was reported to be 28 μm, 30 μm, 30 μm and 33 μm for the samples fabricated with 1 g/L, 3 g/L, 5 g/L and 10 g/L diamond concentration in the plating bath, respectively. It reveals that diamond incorporation doesn't strongly affect the deposition rate (Figs. S3(a) and 1(e–f)). However, the current density can significantly influence the deposition rate (Figs. S4(e–h) and S5(a)). The roughness varies between 0.8 and 2.1 μm for all the samples fabricated with different diamond concentration and current density (Figs. S3(b) and S5(b)). The sample fabricated with 1 g/L diamond concentration at current density 0.05 A/cm² reports the lowest value of surface roughness at 0.8 μm, whereas the sample fabricated with the same diamond concentration at current density 0.2 A/cm² reports the highest value of surface roughness at 2.1 μm. However, the samples with 10 g/L diamond concentration in bath have relatively lower values of surface roughness. This suggests that an increase in the diamond concentration in bath and

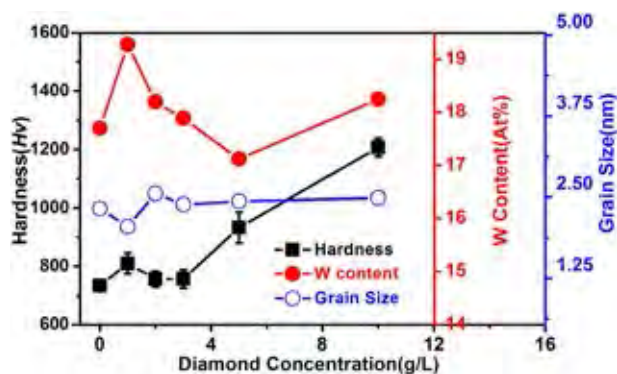


Fig. 4. Effect of diamond concentration in the plating bath on the hardness, W content and grain size of the Ni-W/diamond composite deposits prepared at temperature of 75 °C, pH 8.9 and current density of 0.15 A/cm².

incorporation in the deposits tends to reduce the roughness of the deposits [32].

Fig. 4 compares the effect of diamond concentration in bath on W content, grain size, and hardness of the deposits at 0.15 A/cm² current density. The samples report hardness values of 734 ± 15, 810 ± 36, 756 ± 27, 757 ± 31, 933 ± 53 and 1207 ± 32 Hv for the samples fabricated at current density 0.15 A/cm² with 0 g/L, 1 g/L, 2 g/L, 3 g/L, 5 g/L and 10 g/L diamond concentration in the plating bath, respectively. As per Fig. 4 it is quite evident that the hardness increases sharply upon an increase in the diamond concentration in the plating bath from 3 g/L to 5 g/L and 10 g/L, respectively. The W content of the NWD deposits varies between ~17.7–19 at.% for the samples fabricated with different diamond concentration in the plating bath. The grain size of the deposits varies between 2 and 2.5 nm. The samples exhibit high hardness even for the lower values of the W content in the deposits. However, an increase in the diamond concentration in the plating bath amounts to an increase in the diamond content of the deposits (Fig. 3). The relatively uniform co-deposition of diamond particles at 10 g/L diamond concentration (as shown in Fig. 1 (d)) also has a role in increasing the overall strength of the Ni-W alloy matrix as the hardness increases upon an increase in the diamond content of the deposits. This suggests to the enhanced role of the reinforced and co-deposited composite diamond particles towards enhancing the hardness of the deposits. The maximum hardness reported was 1207 ± 32 Hv, for the sample fabricated at 0.15 A/cm² current density and 10 g/L diamond concentration (Fig. 4).

Fig. 5 shows the effect of current density on the hardness, grain size and W content of coatings prepared at 10 g/L diamond concentration in bath. The hardness tends to increase upon increase in the current density from 0.05 to 0.15 A/cm², and at current density > 0.15 A/cm², the hardness decreases with current density. The values of hardness are 744 ± 49, 1127 ± 29, 1207 ± 32 and 973 ± 28 Hv for the samples fabricated at 0.05 A/cm², 0.1 A/cm², 0.15 A/cm² and 0.2 A/cm², respectively. The grain size of all deposits was reported to be in the range of ~2–2.5 nm, which doesn't have very big difference (Fig. 5). The W content varies between ~18 at.%–21 at.%. There is a marked decrease in the W content of the deposits at current density > 0.1 A/cm² (Fig. 5). The adsorption of diamond particles into the matrix tends to inhibit the deposition of Ni²⁺ and W⁶⁺ ions [27,33]. Various researchers report that absorption of hydrogen ions by the diamond particles near the cathode prevents the hydrogen ions from being reduced to nascent hydrogen. The hydrogen ions that are, thus absorbed by the diamond particles results in a decrease of the W content in the composite deposits [34,35].

The effect of particles size of diamond on the coatings was also investigated. Fig. 6 (a–e) shows the SEM images of the NWD composite coatings fabricated with diamond particles of various sizes (0.2, 0.3, 0.9, 3 and 6 μm). The inserted images depict the higher magnification SEM observation of the corresponded sample. The diamond incorporation and

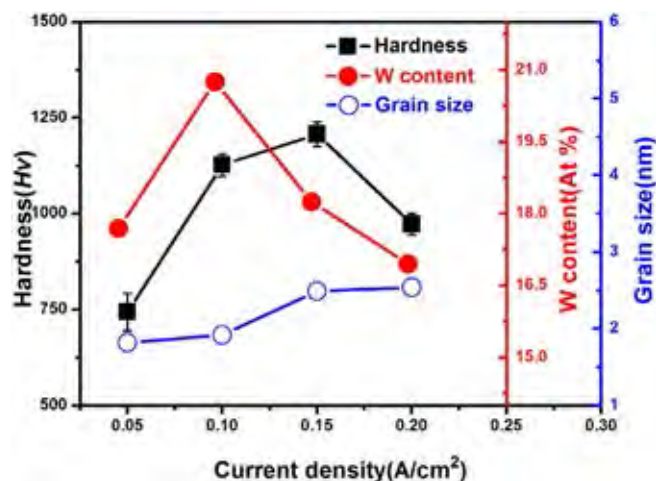


Fig. 5. Effect of the current density on the hardness, W content and grain size of the Ni-W/diamond composite coatings prepared at temperature of 75 °C, pH 8.9, and 10 g/L of diamond concentration in the plating bath.

distribution appears to increase with the increasing particle size of diamond up to 3 μm at which the diamond particles are uniformly distributed and co-deposited into the alloy matrix. However, upon further increasing the diamond size to 6 μm the distribution ceases to be as uniform as in case of 3 μm.

The EDS elemental mapping results for the samples fabricated with diamond particles of different size (fabricated at 10 g/L diamond concentration and current density 0.15 A/cm²) exhibits an increase in the carbon content of the deposits as the size of the diamond particles is increased from 0.2 μm to 3 μm (Fig. S6). However, as the diamond particle size is increased from 3 μm to 6 μm the carbon content and in turn the incorporation of diamond particles appears to be diminished to a large extent.

The diamond content (vol.%) for the NWD samples fabricated with diamond particles of different size (fabricated at 10 g/L diamond concentration and current density 0.15 A/cm²) is reported in Fig. 7. The diamond content of the deposits increases from 2 vol.% to 32 vol.% as the diamond particle size is increased from 0.2 μm to 3 μm, respectively. Upon further increasing the size of diamond particles from 3 μm to 6 μm the diamond particles content in the deposits exhibits a sharp decline. Ogiwara et al. [26] reported that the diamond content in the deposits increases upon increasing the particle size of diamond because the weight change caused by the diamond co-deposition increases and is proportional to the mean particle radius (r^3) of the diamond particles. Therefore, the diamond content decreases as the size of diamond particles increases beyond 3 μm in this study because of the sedimentation of larger diamond particles before being properly incorporated into the matrix.

The surface roughness of the NWD samples fabricated (at 10 g/L diamond concentration and current density 0.15 A/cm²) with different size diamond particles was reported to be 0.3 ± 0.02 μm, 0.4 ± 0.04 μm, 1.5 ± 0.27 μm, 1.1 ± 0.11 μm, 1.2 ± 0.12 μm for the samples fabricated with 0.2 μm, 0.3 μm, 0.9 μm, 3 μm and 6 μm diamond particle size, respectively (Fig. S7(a)). It can be seen that the NWD surface gets rougher upon increasing the diamond particle size from 0.2 μm to 0.9 μm. Beyond 0.9 μm as the diamond particle size is increased to 3 μm and 6 μm there is a slight reduction in the value of surface roughness. The SEM image for different size of diamond particles (Fig. 6) also indicate the larger size diamond particles protruding out of the Ni-W matrix as compared to the sub-micron size diamond particles which are barely noticeable on the base Ni-W matrix. Therefore, it is natural to infer that the deposits fabricated with sub-microns size diamond particles would result in smoother surfaces as compared to samples with larger size diamond particles. Similar dependence of the surface

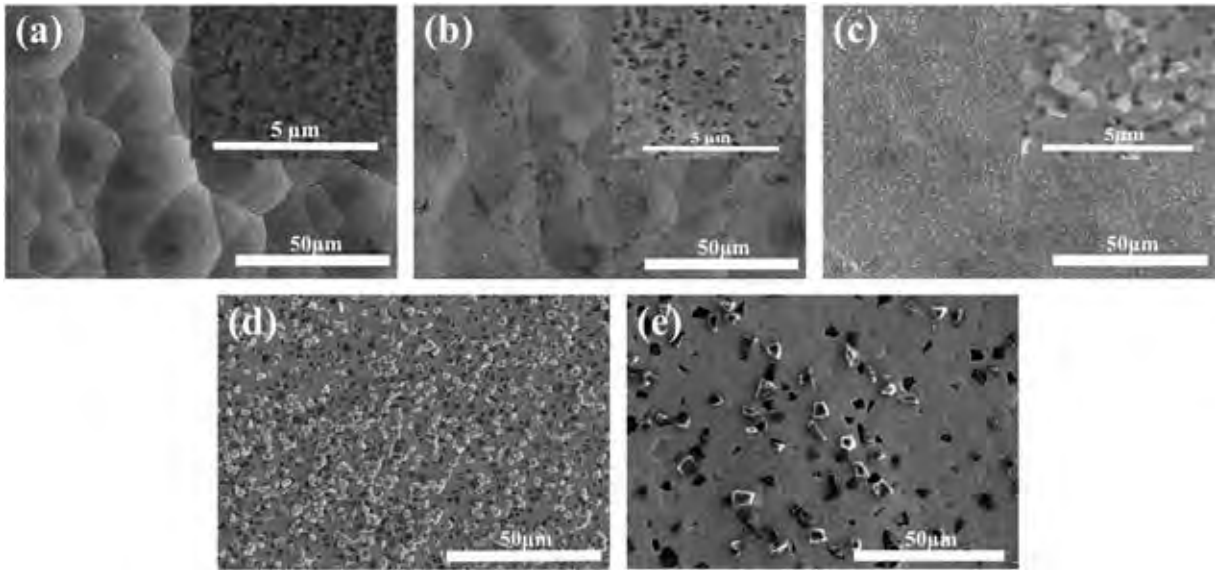


Fig. 6. SEM images of Ni-W/diamond composite coatings fabricated at current density of 0.15 A/cm^2 , diamond concentration of 10 g/L , temperature of 75°C and $\text{pH } 8.9$, for different size of diamond particles, (a) $0.2 \mu\text{m}$, (b) $0.3 \mu\text{m}$, (c) $0.9 \mu\text{m}$, (d) $3 \mu\text{m}$, (e) $6 \mu\text{m}$. The inserted images are the SEM image at higher magnification for (a), (b), and (c), respectively.

roughness on the composite particle size has also been reported by Ogihara et al. [26].

The hardness was reported to be 638 ± 31 , 701 ± 20 , 739 ± 14 , 1207 ± 32 , $879 \pm 68 \text{ Hv}$ for the samples fabricated $0.2 \mu\text{m}$, $0.3 \mu\text{m}$, $0.9 \mu\text{m}$, $3 \mu\text{m}$ and $6 \mu\text{m}$ size of diamond particles, respectively. The hardness of the deposits increased as the size of the diamond particles was increased from $0.2 \mu\text{m}$ to $3 \mu\text{m}$. However, for samples fabricated with $6 \mu\text{m}$ size diamond particles the hardness of the deposits reported a sharp decline of >300 points on the Vicker's scale. The W content of the deposits varied between ~ 11 – $16 \text{ at.}\%$. The W content of the deposits was also reported to be high for the sample fabricated with $3 \mu\text{m}$ size diamond particles, whereas the grain size was in the range of 2 – 3 nm for different sizes of diamond particles. The high diamond content of the deposits for the samples fabricated with $3 \mu\text{m}$ size diamond particles (Fig. 7) coincides with the high value of hardness for the same sample (Fig. 8). This suggests that the diamond content in the coating is a major contributor towards enhancing the hardness of the deposits for the samples fabricated with different size of diamond particles. The high value of hardness also coincides with a higher value of W content in Fig. 8. This indicates that the W content is also a factor in determining the hardness of the deposits for variation in the size of diamond

particles. The hardness value is relatively low for samples fabricated with sub microns size diamond particles as compared to the samples fabricated with $3 \mu\text{m}$ diamond particles. Moreover, the hardness decreases even as the diamond particle size is increased beyond $3 \mu\text{m}$ to $6 \mu\text{m}$.

The electrodeposition parameters and the diamond particle size could affect the composition of the base alloys and the incorporated diamond content in the deposits from this study, and this can influence the hardness of the obtained composite coatings. To further understand the mechanism of hardness enhancement, the hardness of the obtained deposits as a function of the diamond contents in the composite coatings is shown in Fig. 9. The hardness increases with the increase in the diamond content of the deposits. The W content of the NWD deposits does not tend to enhance the hardness of the deposits (Fig. S7(b)) as compared to the diamond content in the deposits which tends to have a direct impact on the hardness of the deposits (Figs. 3 and 4). The samples with high values of W content report a lower value of hardness (Fig. S7(b)), whereas the hardness of the deposits increases significantly as the plating bath diamond concentration and in turn the diamond content in the deposits increases (Figs. 4 and 3). The maximum value of hardness ($1207 \pm 32 \text{ Hv}$) corresponds with the highest value of diamond content in the deposits ($32 \text{ vol.}\%$), whereas the corresponding W

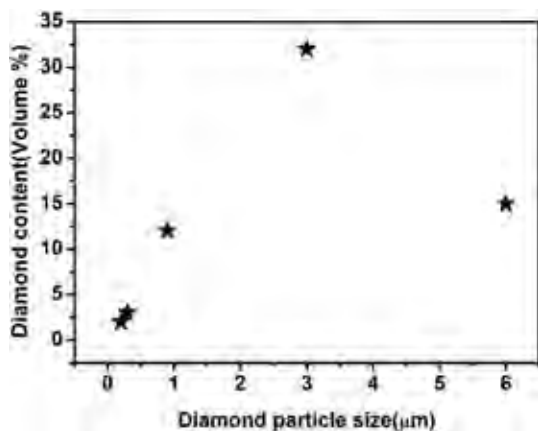


Fig. 7. Diamond content of Ni-W/diamond composite deposits for various size of diamond particles fabricated at diamond concentration of 10 g/L , temperature of 75°C and $\text{pH } 8.9$.

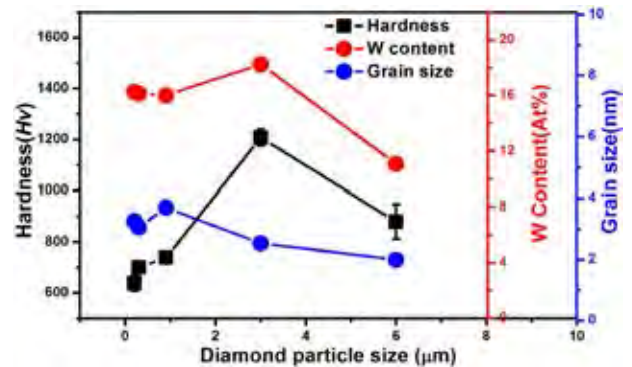


Fig. 8. Effect of the diamond particle size on the hardness, W content and grain size of the Ni-W/diamond composite deposits fabricated at current density of 0.15 A/cm^2 , 10 g/L of diamond concentration, temperature of 75°C and $\text{pH } 8.9$.

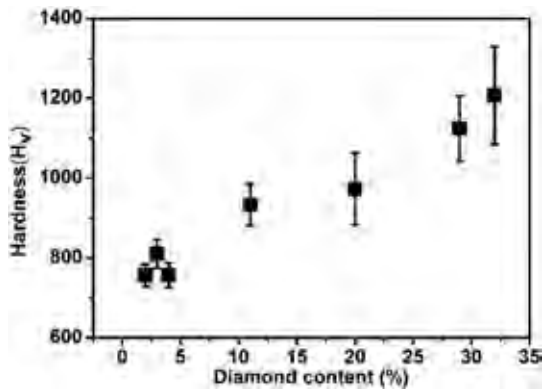


Fig. 9. The hardness of the Ni-W/diamond composite deposits presented as a function of diamond content in the coatings.

content (18.25 at.%) reported for the same isn't the highest value among all samples. Moreover, the hardness is quite high even for samples reporting a lower value of W content (Fig. S7(b)). The hardness reported for samples having lower diamond content is lower and there is a near linear relationship between the diamond content of the deposits and the film hardness (Fig. 9). This indicates that the hardness depends more on the diamond content in the deposits as compared to the W content for the Ni-W/diamond composite coatings.

The wear performance of Ni-W/diamond composite coatings was also performed by using a ball-on-disc tribometer. Fig. 10 shows the wear rate for various diamond concentrations in the plating bath. The wear rate was reported to be 0.15 mg/mm², 0.098 mg/mm², 0.071 mg/mm², 0.067 mg/mm², 0.044 mg/mm², 0.014 mg/mm² and 0.24 mg/mm² for the NWD samples fabricated at current density 0.15 A/cm² and plating bath diamond concentration of 0 g/L, 1 g/L, 2 g/L, 3 g/L, 5 g/L, 10 g/L and 20 g/L, respectively. Moreover, additional comparisons for the friction co-efficient data of the samples with 10 g/L and 2 g/L diamond concentration and the samples with 10 g/L and 20 g/L diamond concentration has been shown in Fig. S8 (a) and (b), respectively. The samples with the high plating bath concentration and content of diamond particles exhibit lower wear rate as compared to samples fabricated from plating baths having lower diamond concentrations and content (Fig. 10). It is evident in Fig. 10 that the wear rate decreases continuously upon increasing the plating bath diamond concentration and reaches a minimum value at 10 g/L beyond which it rises sharply at 20 g/L. This is because at higher plating bath concentration of diamond particles the co-deposition rate is considerably reduced due to aggregation of diamond particles at the electrode [26]. The diamond

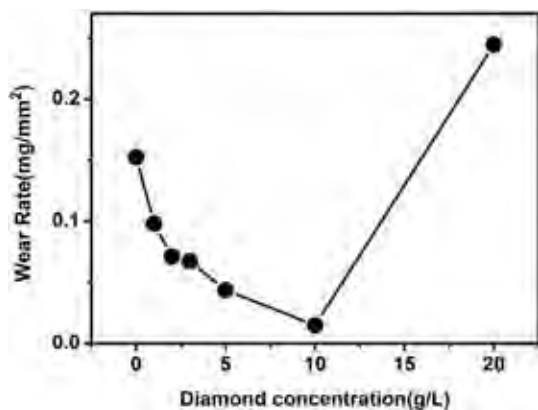


Fig. 10. Effect of diamond concentration in the plating bath on the wear rate of Ni-W/diamond composite coatings fabricated at temperature of 75 °C and pH 8.9.

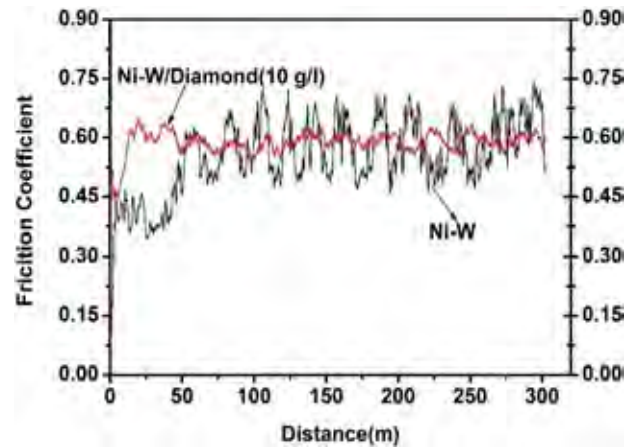


Fig. 11. The friction coefficient of the Ni-W alloy and Ni-W/diamond (10 g/L) composite coatings fabricated at temperature of 75 °C and pH 8.9.

content values for the different diamond concentration in the element mapping images also co-relates to the wear rate data. The samples with the high diamond content (Figs. 2, 3) also report a low wear rate (Fig. 10) compared to samples having lower diamond content. The effect of diamond particles towards enhancing the wear resistance of the NWD deposits is clear by the wear rate results in Fig. 10. The samples having a low wear rate (Fig. 10) also report a lower value of surface roughness (Fig. S3 (b)) and lower values of friction co-efficient (Fig. 11) [36]. The variation in the friction co-efficient also is relatively lower for the samples having low wear rate as in case of sample having 10 g/L diamond concentration in the plating bath compared to pure Ni-W alloy (0 g/L diamond concentration in the bath) (Fig. 11). The friction co-efficient of the Ni-W alloy varied from 0.37 to almost 0.75, whereas the variation was within the range of 0.5 to 0.65 for the NWD sample fabricated with 10 g/L diamond concentration in the plating bath. The variation in friction co-efficient was also higher for the 2 g/L (Fig. S8(a)) and 20 g/L (Fig. S8(b)) NWD samples as compared to the 10 g/L samples.

4. Conclusions

- (1). The diamond content in the deposits increases upon increasing the diamond concentration in the plating bath up to 10 g/L and current density up to 0.15 A/cm². The maximum diamond content in the deposits was reported at 32 vol.%.
- (2). The hardness of the deposits is found to depend more on the diamond content of the deposits as compared to the W content. The deposits with high diamond content report a high value of hardness despite having lower values of W content in them. The maximum value of hardness reported was 1207 ± 32 Hv.
- (3). The samples with high diamond content are relatively smoother and report a lower value of surface roughness. Moreover, the surface roughness varies the least for the sample fabricated at 10 g/L diamond concentration in the plating bath.
- (4). The wear resistance is also improved upon increase in the diamond content in the deposits and the wear rate is the least for the sample fabricated at 10 g/L diamond concentration in the plating bath.

Acknowledgements

This research is supported by the Thai Government Budget (2016), Chulalongkorn University (GRB_BSS_105_59_62_03). J.Q. would like to acknowledge the support from Thailand Research Fund (TRG5780222), Ratchadaphisek somphoch Endowment Fund, Chulalongkorn University

(CU-58-028-AM), and Key Laboratory of Metastable Materials Science and Technology, Yanshan University. M.K.D. would like to acknowledge the support from the 100th Anniversary Chulalongkorn University Doctoral Scholarship. X.Z., M.M. and R.L. would like to thank the support from NBRPC (grant 2013CB733000), NSFC (grants 51571174/51531005).

Appendix A. Supplementary data

Supplementary data to this article can be found online at <http://dx.doi.org/10.1016/j.surfcoat.2016.11.074>.

References

- [1] J.W. Jappes, B. Ramamoorthy, P.K. Nair, Novel approaches on the study of wear performance of electroless Ni–P/diamond composite deposits, *J. Mater. Process. Technol.* 209 (2009) 1004–1010.
- [2] E. Lee, I. Moon, Electrolytic codeposition of diamond particles with nickel and cobalt metals, *Plat. Surf. Finish.* 89 (2002) 55–59.
- [3] E.C. Lee, J.W. Choi, A study on the mechanism of formation of electrocodeposited Ni–diamond coatings, *Surf. Coat. Technol.* 148 (2001) 234–240.
- [4] H. Ogihara, K. Miyamoto, K. Udagawa, T. Saji, Electrodeposition of super hard Ni–B/diamond composite coatings, *Chem. Lett.* 40 (2011) 1072–1073.
- [5] Y. Shi, Z. Yang, H. Xu, M. Li, H. Li, Preparation of electroplated Ni–P-ultrafine diamond, Ni–P–carbon nanotubes composite coatings and their corrosion properties, *J. Mater. Sci.* 39 (2004) 5809–5815.
- [6] N.K. Shrestha, T. Takebe, T. Saji, Effect of particle size on the co-deposition of diamond with nickel in presence of a redox-active surfactant and mechanical property of the coatings, *Diam. Relat. Mater.* 15 (2006) 1570–1575.
- [7] L. Wang, Y. Gao, H. Liu, Q. Xue, T. Xu, Effects of bivalent Co ion on the co-deposition of nickel and nano-diamond particles, *Surf. Coat. Technol.* 191 (2005) 1–6.
- [8] L. Wang, Y. Gao, Q. Xue, H. Liu, T. Xu, Effects of nano-diamond particles on the structure and tribological property of Ni-matrix nanocomposite coatings, *Mater. Sci. Eng. A* 390 (2005) 313–318.
- [9] J. Qin, X. Zhang, Y. Xue, M. Kumar Das, A. Thueploy, S. Limpanart, Y. Boonyongmaneerat, M. Ma, R. Liu, The high concentration and uniform distribution of diamond particles in Ni–diamond composite coatings by sediment co-deposition, *Surf. Interface Anal.* 47 (2015) 331–339.
- [10] X. Zhang, J. Qin, T. Perasinjaroen, W. Aeksen, M.K. Das, R. Hao, B. Zhang, P. Wangyao, Y. Boonyongmaneerat, S. Limpanart, M. Ma, R. Liu, Preparation and hardness of pulse electrodeposited Ni–W–diamond composite coatings, *Surf. Coat. Technol.* 276 (2015) 228–232.
- [11] F.G. Arieta, D.T. Gawne, The wettability and durability of chromium plating, *Surf. Coat. Technol.* 73 (1995) 105–110.
- [12] A.C. Mishra, A.K. Thakur, V. Srinivas, Effect of deposition parameters on microstructure of electrodeposited nickel thin films, *J. Mater. Sci.* 44 (2009) 3520–3527.
- [13] M. Donten, H. Cesiulis, Z. Stojek, Electrodeposition and properties of Ni–W, Fe–W and Fe–Ni–W amorphous alloys. A comparative study, *Electrochim. Acta* 45 (2000) 3389–3396.
- [14] S.C. Kwon, M. Kim, S.U. Park, D.Y. Kim, D. Kim, K.S. Nam, Y. Choi, Characterization of intermediate Cr–C layer fabricated by electrodeposition in hexavalent and trivalent chromium baths, *Surf. Coat. Technol.* 183 (2004) 151–156.
- [15] Y. Wu, D.-y. Chang, D.-s. Kim, S.-c. Kwon, Effects of 2-butyne-1,4-diol on structures and morphologies of electroplating Ni–W alloy, *Surf. Coat. Technol.* 162 (2003) 269–275.
- [16] Y. Boonyongmaneerat, K. Saengkiattiyut, S. Saenapitak, S. Sangsuk, Pulse co-electrodeposition and characterization of NiW–WC composite coatings, *J. Alloys Compd.* 506 (2010) 151–154.
- [17] Y. Boonyongmaneerat, K. Saengkiattiyut, S. Saenapitak, S. Sangsuk, Effects of WC addition on structure and hardness of electrodeposited Ni–W, *Surf. Coat. Technol.* 203 (2009) 3590–3594.
- [18] A.J. Detor, C.A. Schuh, Tailoring and patterning the grain size of nanocrystalline alloys, *Acta Mater.* 55 (2007) 371–379.
- [19] K.R. Sriraman, S. Ganesh Sundara Raman, S.K. Seshadri, Synthesis and evaluation of hardness and sliding wear resistance of electrodeposited nanocrystalline Ni–W alloys, *Mater. Sci. Eng. A* 418 (2006) 303–311.
- [20] C.A. Schuh, T.G. Nieh, H. Iwasaki, The effect of solid solution W additions on the mechanical properties of nanocrystalline Ni, *Acta Mater.* 51 (2003) 431–443.
- [21] C.N. Panagopoulos, G.D. Plainakis, D.A. Lagaris, Nanocrystalline Ni–W coatings on copper, *Mater. Sci. Eng. B* 176 (2011) 477–479.
- [22] C.B. Nielsen, P. Leisner, A. Horsewell, On texture formation of chromium electrodeposits, *J. Appl. Electrochem.* 28 (1998) 141–150.
- [23] S.T. Aruna, V.K. William Grips, K.S. Rajam, Ni-based electrodeposited composite coating exhibiting improved microhardness, corrosion and wear resistance properties, *J. Alloys Compd.* 468 (2009) 546–552.
- [24] T. Tsubota, S. Tani, T. Ishida, M. Nagata, Y. Matsumoto, Composite electroplating of Ni and surface-modified diamond particles with silane coupling reagent, *Diam. Relat. Mater.* 14 (2005) 608–612.
- [25] K.H. Hou, M.D. Ger, L.M. Wang, S.T. Ke, The wear behaviour of electro-codeposited Ni–SiC composites, *Wear* 253 (2002) 994–1003.
- [26] H. Ogihara, M. Safuan, T. Saji, Effect of electrodeposition conditions on hardness of Ni–B/diamond composite films, *Surf. Coat. Technol.* 212 (2012) 180–184.
- [27] K.-H. Hou, T. Han, H.-H. Sheu, M.-D. Ger, Preparation and wear resistance of electrodeposited Ni–W/diamond composite coatings, *Appl. Surf. Sci.* 308 (2014) 372–379.
- [28] X. Zhang, J. Qin, M.K. Das, R. Hao, H. Zhong, A. Thueploy, S. Limpanart, Y. Boonyongmaneerat, M. Ma, R. Liu, Co-electrodeposition of hard Ni–W/diamond nanocomposite coatings, *Sci. Rep.* 6 (2016) 22285.
- [29] H.-T. Wang, H.-H. Sheu, M.-D. Ger, K.-H. Hou, The effect of heat treatment on the microstructure and mechanical properties of electrodeposited nanocrystalline Ni–W/diamond composite coatings, *Surf. Coat. Technol.* 259 (Part B) (2014) 268–273.
- [30] V. Reddy, B. Ramamoorthy, P.K. Nair, A study on the wear resistance of electroless Ni–P/diamond composite coatings, *Wear* 239 (2000) 111–116.
- [31] N. Guglielmi, Kinetics of the deposition of inert particles from electrolytic baths, *J. Electrochem. Soc.* 119 (1972) 1009–1012.
- [32] A. Robin, J.C.P. de Santana, A.F. Sartori, Co-electrodeposition and characterization of Cu–Si₃N₄ composite coatings, *Surf. Coat. Technol.* 205 (2011) 4596–4601.
- [33] Y.W. Yao, S.W. Yao, L. Zhang, Preparation, mechanical properties and wear resistance of Ni–W/SiC nanocomposite coatings, *Mater. Sci. Technol.* 24 (2008) 237–240.
- [34] O. Younes, L. Zhu, Y. Rosenberg, Y. Shacham-Diamand, E. Gileadi, Electroplating of amorphous thin films of tungsten/nickel alloys, *Langmuir* 17 (2001) 8270–8275.
- [35] M.-C. Chou, M.-D. Ger, S.-T. Ke, Y.-R. Huang, S.-T. Wu, The Ni–P–SiC composite produced by electro-codeposition, *Mater. Chem. Phys.* 92 (2005) 146–151.
- [36] A. Riyadh, A. Khairel Rafezi, Y. Al-Douri, Evaluate the effects of various surface roughness on the tribological characteristics under dry and lubricated conditions for Al–Si alloy, *J. Surf. Eng. Mater. Adv. Tech.* 2012 (2012).